Development of Au/TiO_2-coated SCR-DeNOx Catalysts with Increased Elemental Mercury Co-oxidation Activity under Hot and Cold Site Power Plant Flue Gas Conditions

Dissertation

zur Erlangung des

Doktorgrades der Ingenieurwissenschaften (Dr.-Ing.),

des

Zentrums für

Ingenieurwissenschaften

der Martin-Luther-Universität

Halle-Wittenberg,

vorgelegt

von Frau Beatrice-Andreea Esiyok

geb. am 22. November 1981 in Romania

Betreuender Hochschullehrer:

Prof. Dr.-Ing. habil. Heinz Köser, Otto-von-Guericke Universität Magdeburg

External Reviewer

Prof. Dr. techn. Günter Scheffknecht, Universität Stuttgart

Halle (Saale), 27 September 2016

Eidesstattliche Erklärung / Declaration under Oath

Ich erkläre an Eides statt, dass ich die Arbeit selbstständig und ohne fremde Hilfe verfasst, keine anderen als die von mir angegebenen Quellen und Hilfsmittel benutzt und die den benutzten Werken wörtlich oder inhaltlich entnommenen Stellen als solche kenntlich gemacht habe.

I declare under oath that this thesis is my own work entirely and has been written without any help from other people. I used only the sources mentioned and included all the citations correctly both in word or content.

_____ _____

Datum / Date Unterschrift des Antragstellers / Signature of the applicant

Preface and Acknowledgments

This thesis has been submitted in candidacy for the Ph.D. degree in chemical engineering at the Martin Luther University Halle-Wittenberg (MLU), Germany. The majority of the experimental work presented and discussed herein was carried out at the laboratories of Zentrums für Ingenieurwissenschaften (ZIW) in Merseburg, from March 2009 to September 2013 under the supervision of Prof. Dr. Eng. Habil. Heinz Koeser. The research was conducted with the financial support by two Erasmus scholarships for the following periods March – September 2009 and October 2010 – August 2011, as well as the scholarship from Gheorghe Asachi University of Iasi, Romania for the October 2009 – September 2011 period.

First and foremost, I would like to thank my supervisor for the many fruitful discussions, suggestions and observations throughout this project and for being a continuous source of inspiration.

I would further like to express my gratitude to Prof. Dr. Eng. Ion Balasanian from Gheorghe Asachi Technical University of Iasi for his trust, support, useful advices and encouragement of my work. Special thanks to Assoc. Prof. Liliana Lazar for her constant support and many inspiring advices.

Many thanks to Prof. Dr. Herbert Pöllmann from the Institute of Geosciences of Martin Luther University for the X-ray diffraction analysis of the catalysts and the insightful discussions. Warm thanks to Dr. Judith Kuntsche and Mrs. Ute Mentzel from Institute of Pharmacy of Martin Luther University for their help with zeta potential and particle size measurements. I would like to thank Dr. Brandusa Dragoi and Assoc. Prof. Adrian Ungureanu for lending me their vast expertise in diffuse reflectance UV-Vis analysis. Kind thanks to Prof. Dr. Gabriela Carja from Gheorghe Asachi Technical University for the FE-SEM analysis and to Dr. Hempel from Otto-von-Guericke University, Germany for SEM

studies of the catalysts. I would like to thank Dr. Ioana Fechete from Strasbourg University, France for the BET studies and to Dr. Marino from Steag Energy Services, USA for XRF and BET investigations of the catalysts. Many thanks to Daniela Chicet from Gheorghe Asachi University, Romania for EDX investigations.

Furthermore, I would like to thank my colleagues Katharina Zeng and Sebastian Hopf for their technical input and many interesting discussions. Many thanks to Mrs. Heidrun Foerster for performing some of the mercury analysis. Also, I would like to thank the people from the department for their advice, co-work, feedback, and the enjoyable atmosphere.

I have been very fortunate to have the constant support and wise advices of my husband and family throughout this period. Finally, I would like to mention and thank to my cosmopolite Erasmus friends for enjoyable time and many interesting discussions.

ABSTRACT

The present thesis entitled *Developement of Au/TiO_2-coated SCR-DeNOx catalysts with increased elemental mercury co-oxidation activity under hot and cold site power plant flue gas conditions* revolves around the topic of removal of elemental mercury from coal-fired power plant flue gases. Gaseous mercury is an undesired by-product formed during high temperature combustion of different fuels. When emitted in the atmosphere, elemental mercury is subjected to long range transport before being oxidised and deposited in aquatic systems. Mercury emissions abatement in coal-fired power plants depends on the type of mercury species found in the flue gases to be treated. Some basic aspects regarding the formation, catalytic oxidation and removal of elemental mercury from flue gases are discussed in the first part of this thesis.

The experimental investigations presented in this thesis take on the task of developing SCR-DeNOx catalysts with enhanced catalytic activity for the oxidation of elemental mercury.

The commercial monolithic catalyst employed for the selective catalytic reduction (SCR) of nitrogen oxides (NOx) exhibits, to a certain degree, co-oxidation activity for elemental mercury. However, this co-oxidation activity is not enough to meet the stringent regulations imposed on mercury emissions. To develop a monolithic catalyst with increased mercury oxidation activity, a number of catalysts were prepared, characterized and tested in this work. A commercial SCR honeycomb shaped catalyst was selected as support, whereas Au/TiO_2 catalyst powders with different TiO_2 supports and different gold loadings were employed for coating the surface of the monolithic catalyst.

The remainder of the Part Two of the thesis focused on the catalytic activity of the Au/TiO_2-coated SCR catalysts for mercury oxidation, DeNOx and SO_2/SO_3 conversion reactions. The mercury oxidation activity was evaluated with respect to reaction temperature,

gold loadings, coating types and HCl content of the simulated flue gas. Under certain reaction conditions, the Au/TiO_2 coatings increased the mercury oxidation activity of the SCR catalyst by a factor of 2. Catalytic investigations into the DeNOx activity of the prepared catalysts were conducted and the effect of NH_3/NO feed ratio and coating type on the NO reduction efficiency investigated. It was found that the Au/TiO_2 coatings had only a marginal effect on the DeNOx activity of the SCR catalyst. In this work, the undesired side reaction of SO_2/SO_3 conversion was studied and, the obtained results indicate that the conversion rates depend on the coating types and gold loadings.

In conclusion, the Au/TiO_2-coated SCR catalysts exhibited promising behaviour for the mercury oxidation reaction. Although additional understanding regarding the catalytic mechanism is necessary, the influence of different flue gas components on the mercury oxidation reaction, the stability and integrity of the coated layers, etc. are required, the Au/TiO_2-coated SCR catalysts are promising candidates for the development of multi-pollutant SCR catalysts with increased mercury co-oxidation activity.

TABLE OF CONTENTS

Preface and acknowledgements……. i

Abstract…….. iii

I. Abbreviations……...……... viii

II. Notations…… x

III. List of Figures…… xi

IV. List of Tables...…… xiii

V. List of Appendices…… xv

INTRODUCTION……..... 1

PART I. LITERATURE SURVEY ……..…….... …. 5

Chap. 1. Mercury and its pollutant behaviour…….... 6

1.1. Mercury and mercury emissions……..……..... 6

1.2. Mercury emissions from coal fired power plants……..... 8

1.3. Mercury speciation in flue gases…….. 9

1.4. Impact of mercury emissions on the environment and human health…….... 11

Chap.2. Catalytic oxidation of elemental mercury in flue gases……..…… 13

2.1. Proposed mechanistic pathways for catalytic oxidation of elemental mercury……..……..…… 14

2.2. Catalysts for oxidation of elemental mercury in flue gases ……..... 16

2.2.1. Oxidation of elemental mercury by transition metal oxide catalysts... 17

2.2.2. Oxidation of elemental mercury on SCR-DeNOx catalysts…… 18

2.2.2.1. Influence of flue gas constituents on Hg^{el} adsorption/oxidation by SCR-DeNOx catalysts…… 19

2.2.2.2. Influence of catalyst composition, reaction temperature and space velocity on oxidation of elemental mercury…… 21

2.2.2.3. Loss of Hg^{el} oxidation activity……..……..... 22

2.2.2.4. Mechanism of Hg^{el} oxidation on SCR catalysts…….. 22

2.2.2.5. Enhancement of Hg^{el} oxidation activity of SCR catalysts…… 24

2.2.3. Oxidation of elemental mercury over gold and other noble metal based catalysts……..……. 24

Conclusions …….. 30
PART II. OWN CONTRIBUTIONS……..…….. 31
Chap.3. Research Objectives…….... 32
Chap.4. Experimental Protocol and apparatus……. 35
4.1. Catalysts preparation…….. 35
4.1.1. Synthesis of Au/TiO_2 catalyst powders…… 35
4.1.2. Preparation of Au/TiO_2-based suspensions…… 37
4.1.3. Coating of SCR-DeNOx monolithic catalysts with Au/TiO_2…… 40
4.2. Characterization techniques…… 42
4.3. Catalytic activity tests…….... 45
4.3.1. Mercury oxidation activity…… 47
4.3.2. DeNOx reaction…… 52
4.3.3. SO_2/SO_3 conversion…… 52
Chap.5. Preparation and characterization of Au/TiO_2-coated SCR-DeNOx catalysts..... 56
5.1. Synthesis and characterization of Au/TiO_2 catalyst powders..... 56
5.1.1. Chemistry of Au-based solution…….. 56
5.1.2. Physical-chemical characterization of Au/TiO_2 powdered catalysts…. 59
5.1.2.1. Diffuse reflectance UV-Vis (DR UV-Vis) analysis……. 59
5.1.2.2. X-ray diffraction (XRD) analysis…….. 60
5.1.2.3. Elemental composition by Energy dispersive analysis of the X-Rays (EDX)…….. 62
5.1.2.4. Field Scanning electron microscopy (FE-SEM) analysis……..... 63
5.2. Preparation and characterization of stable Au/TiO_2 suspensions……. 64
5.2.1. Stability and properties of Au/TiO_2-based suspensions……. 65
5.2.1.1. Iso-electric point (IEP) of Au/TiO_2-based suspensions…….. 65
5.2.1.2. Particle size distribution and viscosity of the Au/TiO_2 suspensions……...……... 66
5.3. SCR-DeNOx monoliths coated with thin Au/TiO_2 layers……..... 68
5.3.1. Characterization of Au/TiO_2-coated SCR-DeNOx monoliths…….. 70
5.3.1.1. Scanning Electron Microscopy (SEM) analysis……..……. 70
5.3.1.2. EDX analysis…….. 71
5.3.1.3. Surface study by Digital Microscope (DM)……... 73
5.3.1.4. Textural properties by N_2 adsorption……. 75

5.3.2. Stability of Au/TiO_2 coated layers…… 75
5.4. Conclusions…….. 76
Chap.6. Catalytic activity of Au/TiO_2-coated SCR-DeNOx catalysts..... 78
6.1. Assessment of Hg^{el} oxidation activity..... 78
6.1.1. Effect of different Au/TiO_2 coatings type on Hg^{el} oxidation activity.. 79
6.1.2. Effect of reaction temperature and HCl concentration on Hg^{el} oxidation activity…… 81
6.1.3. Effect of gold loading on Hg^{el} oxidation activity……..… 84
6.1.4. Effect of Hg^{el} initial concentration……... 84
6.1.5. Possible mechanistic pathways for mercury oxidation on Au/TiO_2-coated SCR catalysts…….. 85
6.2. DeNOx activity of Au/TiO_2-coated SCR catalysts……..…….. 87
6.2.1. Influence of NH_3/NO ratio on DeNOx activity..... 87
6.2.2. Influence of ageing process on DeNOx activity..... 89
6.3. SO_2/SO_3 conversion activity of Au/TiO_2-coated SCR catalysts..... 90
6.4. Conclusions..... 92
General Conclusions……..... 94
References…….. 98
Appendices……. 110
Curriculum Vitae……. 125
List of publications……. 127

I. Abbreviations

AC – activated carbon

AV – area velocity, (m/h)

aq. – aqueous

APH – air pre-heater

CCD – charged coupled device

DeNOx – removal of NOx compounds from flue gases

DFT – density functional theory

DLS – dynamic light scattering

DM – digital microscope

DR-UV-Vis – Diffuse reflectance in the ultaviolet-visible field

DVB - divinylbenzene

EDX (EDAX) – energy dispersive analysis of X-rays

E-Filter – electrostatic filters

ESP – electrostatic precipitator

FCC – face centered cubic crystalline configuration

FE-SEM – field emission scanning electron microscope

FF – fabric filter

ICP-MS - Inductively Coupled Plasma Mass Spectroscopy

IEP – iso-electric point

MATS - Mercury and Air Toxic Standards

MerCAP – mercury capture process implemented in United States

MFC – mass flow controller

NH_4-PA – ammonium poly-acrylate

NOx – nitrogen oxides (NO, NO_2, N_2O)

p.a – pro analysis

ppm – parts per million

ppb – parts per billion

SCR – selective catalytic reduction

SCR-DeNOx – removal of NOx from flue gases by employing SCR catalysts

SEM – scanning electron microscopy

SPR – surface plasmon resonance

ST - styrene

STP – standard temperature and pressure (temperature = 273.15 K and pressure = 0.987 atm)

TGA – thermogravimetric analysis

UNEP - United Nations Environment Program

UV – ultra-violet

VOC – volatile organic compound

WFGD – wet flue gas desulphurization

XRD – X-ray diffraction

XRF – X-ray fluorescence

3D – tri-dimensional

II. Notations

At% - atomic weight per cent

C_{SO2} – concentration of SO_2 measured after the catalyst, (ppm)

C_{SO3} – concentration of SO_3 measured after the catalyst, (ppm)

Hg^{el} – elemental mercury (Hg^0)

Hg^{ox} – oxidized mercury (Hg^{2+})

Hg^{p} – particulate mercury

Hg^{ox}_{Dowex} - concentration of oxidised mercury measured in the Dowex layer, (µg/m^3)

Hg^{el}_{AC} - concentration of elemental mercury measured in the AC layer, (µg/m^3)

k_{DeNOx} – DeNOx activity of the catalyst, (m/h)

$k_{Hg^{el}/Hg^{ox}}$ - mercury oxidation activity, (m/h)

K_{SO_2/SO_3} - conversion rate of SO_2 to SO_3 in the flue gas, (%)

$m_{coating}$ – mass of coated Au/TiO_2 on the surface of SCR substrate, (g)

$m_{uncoated_SCR}$ – mass of uncoated SCR substrate, (g)

m_{coated_SCR} – mass of coated SCR substrate, (g)

P – pressure, (atm)

S_{BET} – surface area of a material determined by N_2 absorbtion method, (m^2/g)

T – temperature, (°C)

V_{gas} – gas volume passing through reactor, (L/h)

wt.-% - weight per cent

ΔH^o – entalpy, kJ/mol

ζ – zeta potential, (mV)

η_{In} - mercury oxidation efficiency measured before the catalyst layer (by-pass values), (%)

η_{Out} - mercury oxidation efficiency measured after the catalyst layer, (%)

λ= wavelength, (nm)

III. List of Figures

Fig.1.1 *Global anthropogenic mercury emissions by sources for the year 2010*…… 8

Fig.1.2 *Schematics of a coal-fired power plant illustrating mercury transformations in flue gases*…….. 10

Fig.2.1 *Schematics of nitrogen oxides reduction and mercury oxidation over SCR catalyst*…….. 23

Fig.3.1. *Schematic representation of the research objectives covered in the PhD thesis*…….. 34

Fig. 4.1. *Schematics of deposition-precipitation synthesis method employed for preparation of nano-Au/TiO_2 catalyst powders*…….. 36

Fig.4.2. *Schematics of the* ***a)*** *Type I Au/TiO_2 suspension preparation and* ***b)*** *image of Type I Au/TiO_2 UV100-based suspension with 2 wt% solid content*…… 38

Fig.4.3. *Schematics of the* ***a)*** *Type II Au/Aerodisp suspension preparation and* ***b)*** *picture of Type II Au/Aerodisp based suspension with 2 wt% solid content*…… 39

.

Fig.4.4. *Dip-coating procedure employed for coating of SCR-DeNOx substrates with Au/TiO_2*…… 41

Fig.4.5. *Schematics of the experimental set up employed for Hg^{el} oxidation tests*…… 48

Fig.4.6. *Schematics of experimental reactor*…… 49

Fig.4.7. *Schematics of the gaseous mercury sampling arrangement*…….. 50

Fig.4.8. *SEM images of Dowex 1 × 8 resin (****A****) and iodized activated carbon pellets (****B****)*…….. 51

Fig.4.9. *Schematics of the experimental set up employed for DeNOx tests*…… 53

Fig.4.10. *Schematics of the experimental set-up employed for SO_2/SO_3 conversion tests*…… 54

Fig.4.11. *SO_2/SO_3 gas sampling train*…….. 55

Fig. 5.1. *Chloride content in the filtrate and washing liquids for 1 and 2 wt% Au/TiO_2 catalysts*…… 59

Fig. 5.2 *DR-UV-Vis spectra for TiO_2 and 2 wt.-% Au/TiO_2 catalyst powders prepared by deposition precipitation method*…… 61

Fig.5.3. *XRD patterns for 2 wt.-% Au/ TiO_2 P25 uncalcined sample (where: A – anatase; R – rutile)*…… 62

Fig.5.4. *XRD patterns for 2 wt.-% Au/ TiO_2 P25 calcined sample (where: A – anatase; R – rutile; Au – gold)*…… 63

Fig.5.5. *EDX spectra for 2 wt.-% Au/TiO_2 P25 (left) and 2 wt.-% Au/TiO_2 UV100 (right) catalyst*…… 64

Fig.5.6. *Scanning electron micrographs for:* ***A*** *and* ***B*** *– TiO_2 P25;* ***C*** *and* ***D*** *– 2 wt.-% Au/ TiO_2 P25 calcined catalyst*…… 65

Fig.5.7. *Zeta potential versus pH-value for type I and type II suspensions with 2 wt.-% solid content*…… 67

Fig.5.8. *Particle size distribution by intensity in the Type I suspensions Au/TiO_2 P25*…… 68

Fig.5.9. *Mass of Au/TiO_2 layers coated on the SCR-DeNOx monolits surface*…… 70

Fig.5.10. *Uncoated SCR-DeNOx (light cream) and 2Au/TiAerod-SCR monoliths (purple)*…… 71

Fig.5.11. *Scanning electron micrographs for:* ***A*** *– uncoated SCR;* ***B*** *– uncoated SCR with high resolution;* ***C*** *– 2Au/TiP25-SCR;* ***D*** *- 2Au/TiP25-SCR with high resolution*…… 72

Fig.5.12. *Mapping of gold element distribution on the SCR surface at 5 μm resolution:* ***A*** *– 2Au/TiAerod-SCR uncalcined and* ***B*** *- 2Au/TiAerod-SCR calcined*…… 73

Fig.5.13. *Digital microscope images and their corresponding 3D profiles for:* ***A*** *and* ***B*** *– uncoated SCR surface,* ***C*** *and* ***D*** *– 2 wt.-% Au/TiO_2-coated SCR surface and,* ***E*** *and* ***F*** *– 2 wt.-% Au/Aerodisp-coated SCR surface*…… 75

Fig.6.1.a. *Effect of Au/TiO_2 coatings type on Hg^{el} oxidation activity at 180 and 390 °C and 100 mg/m^3 HCl*…… 81

Fig.6.1.b. *Effect of Au/TiO_2 coatings type on Hg^{el} oxidation activity at 180 and 390 °C and 10 mg/m^3 HCl*…… 82

Fig.6.2.a. *Effect of reaction temperature on Hg^{el} oxidation of uncoated and Au/TiO_2-coated SCR-DeNOx monoliths at 100 mg/m^3 HCl*…… 83

Fig.6.2.b. *Effect of reaction temperature on Hg^{el} oxidation of uncoated and Au/TiO_2-coated SCR-DeNOx monoliths at 10 mg/m^3 HCl*…… 84

Fig.6.3. *Schematics of Hg^{el} oxidation mechanism at the surface of Au/TiO_2-coated SCR catalysts*…… 87

Fig.6.4.a. *DeNOx activity of Au/TiO_2-UV100-coated SCR-DeNOx catalysts at 390 °C*…… 89

Fig.6.4.b. *DeNOx activity of Au/TiO_2-P25-coated SCR-DeNOx catalysts at 390 °C*…… 89

Fig.6.4.c. *DeNOx activity of Au/TiO_2-Aerodisp-coated SCR-DeNOx catalysts at 390 °C*…… 90

Fig.6.5. *DeNOx activity of fresh and aged Au/TiO_2-coated SCR-DeNOx catalysts at 390 °C and NH_3/NO = 1.2*…… 91

Fig.6.6. *SO_2/SO_3 conversion of uncoated and gold coated SCR-DeNOx catalysts at 390 °C*…… 92

IV. List of Tables

Table 4.1 *Materials and chemicals employed for synthesis of Au/TiO_2 powdered catalysts.....* 35

Table 4.2 *Materials and chemicals employed for preparation of Au/TiO_2 stable suspensions...* 37

Table 4.3 *Bulk and surface composition of Aerodisp solid phase by XRF method..…....* 40

Table 4.4 *Materials and chemicals employed for preparation of Au/TiO_2 stable suspensions....* 40

Table 4.5 *Textural properties of the reference SCR-DeNOx catalyst determined by N_2 adsorption method.....* 41

Table 4.6 *Bulk and surface composition of the reference SCR-DeNOx catalyst by XRF method.....* 41

Table 4.7 *Characteristic parameters of the investigated catalysts……* 46

Table 4.8 *Experimental flue gas conditions for the catalytic tests.....* 47

Table 4.9 *List of gases employed for model flue gas preparation……..* 47

Table 4.10 *Geometrical dimensions of the experimental reactor.....* 49

Table 4.11 *Materials and chemicals employed for sampling of gaseous mercury .....* 50

Table 4.12 *Materials and chemicals employed for SO_2/SO_3 conversion tests.....* 55

Table 5.1 *Gold content analysis of clear liquids after filtration and washing of 2 wt.-% Au/TiO_2 P25 catalysts……..* 60

Table 5.2 *Elemental composition of 2 wt% Au/TiO_2 catalysts determined by EDX analysis….* 63

Table 5.3 *Average particles size distribution and viscosities of Au/TiO_2 suspensions……..* 69

Table 5.4 *Elemental composition of SCR uncoated and Au/TiAerod-SCR catalysts by EDX method……..* 73

Table 5.5 *Textural properties of uncoated SCR-DeNOx and of Au/Aerodisp-coated SCR-DeNOx catalyst samples……..* 76

Table 6.1 *Example of results reproducibility for Hg^{el} oxidation efficiency (%) data obtained by employing Dowex/AC sorbent traps method*…… 80

Table 6.2 *Effect of gold loadings (1 and 2 wt.-% Au) on Hg^{el} oxidation activity over Au/TiO_2-coated SCR-DeNOx monoliths at 180 °C and, 100 and 10 mg/m^3 HCl*…… 85

Table 6.3 *Effect of Hg^{el} initial concentration on mercury oxidation activity*…… 86

IV. List of Appendices

Appendix 1.1 *Physical properties of mercury element*…… 110

Appendix 1.2 *Mercury contents in various coal types from different countries*…… 110

Appendix 1.3 *Physical properties of gold element*…… 111

Appendix 4.1 *Images of Au/TiO_2 P25 based suspensions stabilized by addition of NH_4-polyacrylate and poly ethylene glycol (PEG)*…… 112

Appendix 5.1 *XRD patterns of 2 wt.-% Au/TiO_2 catalysts calcined and uncalcined*…… 113

Appendix 5.2 *FE-SEM micrographs of TiO_2 UV100 and 2 wt.-% Au/TiO_2 UV100 catalyst Powders*…… 114

Appendix 5.3 *Zeta potential versus pH for 1 wt.-% Au/TiO_2 based suspensions*…… 115

Appendix 5.4 *Example of viscosity measurements for 1 wt.-% Au/TiO_2 P25-based suspension*…… 115

Appendix 5.5 *Particle size distribution by intensity for the Au/TiO_2-based suspensions (measured by Zetamaster S system from Malvern Instruments)*…… 116

Appendix 5.6 *Specific geometric surface coverage of SCR-DeNOx substrates with Au/TiO_2 layers in µg Au/TiO_2/mm^2 SCR*…… 118

Appendix 5.7 *Elemental composition and distribution at the surface for SCR uncoated catalyst by EDX analysis*…… 119

Appendix 5.8 *Elemental composition and distribution at the surface for 1Au/TiAero-SCR catalyst by EDX analysis*…… 121

Appendix 5.9 *Elemental composition and distribution at the surface for 2Au/TiAero-SCR catalyst by EDX analysis*…… 123

Appendix 6.1 *Likely cost increase of Au-coated SCR catalysts considering only the price of gold*…… 124

Introduction

Mercury (Hg) is regarded as a hazardous atmospheric pollutant due to its persistence, long-term mobility in the atmosphere, bio-accumulation in the aquatic systems and its neurotoxic impact on human health [1 – 3]. Coal-fired power plants, waste incinerators, and cement plants are identified as the major anthropogenic sources of mercury emissions. Current estimations indicate an increase in mercury emissions from fast growing economies (especially from Asian countries) whereas releases from developed countries (Europe and the US) are expected to decline [4]. Over the past decades mercury emissions regulations have become increasingly stringent. In 2013, the US limited the emissions from coal-fired power plant units in the Mercury and Air Toxic Standards (MATS) [5] resulting in maximum emission concentration for existing power plants between 1.5 and 5.0 µg/m³ (STP, dry) at 6 vol.-% O_2 and as a 30-day average. The Chinese government passed a new emissions standard with a maximum mercury emission level of 30 µg/m³ (STP, dry) for thermal power plants [6]. In Germany, a new standard calls for a maximum mercury emissions concentration of 10 µg/m³ (STP, dry) as yearly average for power plants and waste incinerators [3, 7].

So far, it has been shown that the efficient conversion of elemental mercury (Hg^{el}) to oxidised mercury (Hg^{ox}) can be achieved by means of catalytic processes. Over the past decades, the relevant literature describes a large number of catalysts as potential oxidation catalysts for elemental mercury. Among them, however, the most commonly studied catalysts remain the commercially available V_2O_5-based SCR-DeNOx catalysts. The SCR-DeNOx catalysts were designed and commercially implemented for the reduction of nitrogen oxides (NOx) in the presence of ammonia (NH_3). Industrial SCR reactors are operated at temperatures between 160 and 430 °C and can be located upstream of the air pre-heater and

electrostatic precipitator (1), upstream of the air pre-heater and downstream of electrostatic precipitator (2), downstream of the air pre-heater and electrostatic precipitator (3) or downstream of the flue gas desulphurization system (4). The oxidation of elemental mercury and volatile organic compounds were shown to be the beneficial side reactions of the SCR catalysts, whereas the conversion of sulphur dioxide (SO_2) to sulphur trioxide (SO_3) is an undesired reaction.

As pointed out in detail in the literature, the mercury oxidation activity of SCR catalysts depends on several factors. The flue gas composition, especially the amount of hydrogen halides (HCl or HBr) directly influences the oxidation activity. Negligible oxidation occurs when HCl is absent from the flue gases and, in this case Hg^{el} is mostly adsorbed by the catalysts [8, 9]. The presence of NH_3 and NO causes a significant decrease in mercury oxidation activity [10]. Another important factor is the V_2O_5 content of the SCR catalysts. The V_2O_5 content of commercial SCR catalysts is often limited to less than 1 % in order to reduce the undesired SO_2/SO_3 conversion, hence limiting their mercury oxidation activity. The reaction temperature, catalyst age, area velocity and the presence and concentration of SO_2, SO_3, H_2O in flue gases affect, to a certain degree, the oxidation activity of the SCR catalysts.

Although the commercial SCR DeNOx catalysts co-oxidize mercury, there is a need for more active oxidation catalysts especially for flue gases with low HCl concentrations. Likely candidates include metal and metal oxides based catalysts and noble metal-based catalysts. Amongst them, gold is a very interesting candidate as mercury oxidation catalyst since is able to adsorb mercury and species like Cl_2 and HCl on its surface. Experimental investigations showed that the other flue gas components (SO_2, NO, H_2O) do not impede the mercury oxidation activity of gold-based catalysts [11, 12]. Besides, gold exhibits a certain degree of inertness to these flue gas components. However, the experimental studies described in the literature so far covered only reaction temperatures up to 225 °C.

The research activities of the PhD. thesis titled "*Developement of Au/TiO_2-coated SCR-DeNOx catalysts with increased elemental mercury co-oxidation activity under hot and cold site power plant flue gas conditions*" focused on the preparation, characterization and catalytic activity of the Au/TiO_2-coated SCR-DeNOx monolithic catalysts. The research objectives of the thesis are within the context of the actual environmental engineering problematics concerning the reduction of anthropogenic mercury emissions.

The thesis is structured in two main parts containing six chapters. Part one of the thesis is comprised of two chapters while the other four chapters are included in Part two. At

the end of the dissertation the ***General Conclusions*** of the experimental work, ***References*** and ***Appendices*** are given.

Chapter 1 summarises general knowledge from the literature about mercury emissions sources and their impact on environment and human health. ***Chapter 2*** discusses recent aspects of catalytic mercury oxidation including the potential mechanisms through which catalytic mercury oxidation might occur in the flue gases. Also, the mercury oxidation activity of several oxidation catalysts is analysed, with the focus being placed on the SCR-DeNOx and gold-based catalysts.

The research objectives of the thesis are detailed in ***Chapter 3***. The experimental research was structured and followed two main parts. First part involved the preparation and characterization of different Au/TiO_2-coated SCR-DeNOx catalysts, while the second part focused on the assessment of the catalytic activity of the prepared catalysts. The experimental protocol, apparatus and materials employed for the experimental research are presented in ***Chapter 4***. The presentation of the experimental protocol follows the same structure as the presentation of the research objectives and, it starts with a detailed description for the synthesis of Au/TiO_2 powdered catalysts followed by the preparation of different types of Au/TiO_2 stable suspensions and the coating of SCR-DeNOx monolithic catalyst with a thin Au/TiO_2 layer by employing the as-prepared suspensions. A brief description of the characterization methods employed is given as well. In the last part, the experimental protocol, experimental set-ups and materials employed for the DeNOx, SO_2/SO_3 conversion and mercury oxidation catalytic tests are given in detail.

The experimental results and their interpretation are presented in Chapter 5 and Chapter 6. **Chapter 5** starts with discussions of the preparation and characterization of Au/TiO_2 powdered catalysts. The physico-chemical properties of the powdered catalysts were investigated by employing the XRD, EDX, DR-UV-Vis and SEM methods. The next section of the chapter focused on the results obtained during the preparation of the Au/TiO_2 stable suspensions. The stability and properties of the as-prepared suspensions were investigated by employing the typical methods used for this purpose, iso-electric point, particle size distribution and rheological measurements, respectively. The last section of Chapter 5 presents the data obtained for the preparation and characterization of Au/TiO_2-coated SCR-DeNOx monolithic catalysts. A commercial SCR catalyst with 0.6 % V_2O_5 content, 2 × 2 channels and 10 cm length was employed as a substrate. Some specific characteristics of the Au/TiO_2 coated catalysts were investigated by means of SEM, DM, EDX and N_2 absorption.

Chapter 6 is assessing and discussing the mercury oxidation activity of the prepared Au/TiO_2–coated SCR-DeNOx monolithic catalysts. The mercury oxidation activities of the monolithic samples were studied in a laboratory-scale set-up under simulated flue gas conditions typical for hard coal-fired power plants. Further, the next two sections of Chapter 6 describe the DeNOx activity and SO_2/SO_3 conversions rates of the coated SCR catalysts under flue gas conditions in order to determine to which extent the presence of Au/TiO_2 layers affect these two standard properties of the SCR-DeNOx commercial catalysts.

Some of the elements of novelty and originality this research brings to the field of catalytic oxidation of elemental mercury in flue gases are briefly listed below:

- Preparation and characterization of new Au/TiO_2-coated SCR-DeNOx monolithic catalysts.
- Preparation, stabilization and characterization of Au/TiO_2 based suspensions employed for dip-coating of SCR-DeNOx monoliths.
- Assessment of mercury oxidation activity of the as-prepared Au/TiO_2-coated SCR-DeNOx catalysts. Investigations on the effect of HCl content of flue gases, reaction temperature, gold loadings and coating types are presented in this work
- Results concerning the effect of Au/TiO_2 coatings on the DeNOx activity of the coated catalysts are presented in this work.
- The influence of Au/TiO_2 coatings and gold loadings on the SO_2/SO_3 conversion of the SCR-DeNOx catalyst is investigated and discussed as well.

PART I

LITERATURE SURVEY

CHAPTER 1

Mercury and its pollutant behaviour

1.1. Mercury and mercury emissions

In the periodic table of elements, mercury is the third element of the II B group. Mercury is a constituent element of the Earth crust with an average abundance of approximately 0.05 μg/g [13, 14]. In nature, it rarely occurs as a native metal, being mostly found in different combinations in mineral ores, such as: cinnabar (HgS), livingstonite, corderoite and others [15].

Mercury is a silvery white metal which, at standard temperature and pressure, is found in the liquid state [16]. Metallic mercury (Hg^0) is highly volatile with a boiling point of 357 °C. Elemental mercury possesses a relatively high vapour pressure (2.46×10^{-1} Pa) and low water solubility (60 μg/L at 25 °C) [17]. Mercury forms two types of compounds, which are derived from its two oxidation states: Hg(I) and Hg(II). The inorganic combinations of divalent mercury (II) are more stable while the combinations of monovalent mercury (I) decompose to mercury and mercury compounds (II) under the influence of light [18]. Mercury also forms organic compounds which are characterized by covalent C – Hg bonding and high volatility at atmospheric conditions [17]. Mercury forms alloys with different metals, such as: silver, gold, tin, zinc etc. These alloys are known as amalgams. Due to its property to form amalgams, mercury has been extensively used in gold and silver mining. Nowadays, it is mainly employed for manufacturing industrial chemicals (chlorine and caustic soda) as well for electrical and electronic applications. Other uses of mercury include medicine (amalgams

for dental fillings, diuretic, topical disinfectant etc.), electrochemistry, thermometers, barometers, electron tubes, batteries, switches and others.

Because of its specific chemical and physical properties (see Appendix 1.1), mercury and its compounds exhibit high toxicity and negative effect on environment, human health and wildlife. The amount of mercury emitted into the global environment has considerably increased over the past decades [19]. According to UNEP [20], mercury pollution sources can fall under three categories:

- natural sources;
- re-emission of previously deposited mercury in landfills, water-bodies, soil, sediments;
- anthropogenic sources.

The recent estimates indicate that the current anthropogenic sources are responsible for approximately 30% of mercury emissions, while the natural geological sources account for 10% and the rest is from re-emission of previously deposited mercury [20]. Based on the UNEP (2013) report [20], mercury releases resulted from human activities amounted to 1960 tonnes for the year 2010.

Natural sources of mercury emissions into the environment include volcanoes, soil and water surfaces, geothermal activities, forest fires and rocks weathering processes. The amount of mercury emitted from these sources varies in space and time. The mercury releases into biosphere depend on a number of factors, such as: meteorological conditions, type of soil and vegetation, presence of mercury rich mineral ores and active volcanoes.

Approximately 60% of the emitted mercury into the atmosphere comes from natural sources and the **re-mobilization and re-emission process of the previously deposited mercury** from anthropogenic and natural sources [21]. Re-mobilization and re-emission occurs when the previously removed mercury from the atmospheric circulation (by wet or dry deposition) is released back into the environment [22].

Anthropogenic sources of mercury releases into the atmosphere are associated with human activities and include: fossil fuels fired power plants, cement plants, waste incinerators, chlor-alkali production, processing of mineral ores, ferrous and non-ferrous metals manufacturing processes, artisanal and small-scale gold mining and others [21]. The fossil fuel fired power plants and waste incinerators are sources of mercury emissions [20, 23], estimated to account for 70% of the total anthropogenic mercury emissions in the United States alone. The research regarding quantification of anthropogenic mercury emissions at local/regional and global scale has considerably increased over the last decades. However, the

anthropogenic mercury emission estimates at regional and global scale are still incomplete since some developing countries do not have formal mercury emissions inventories. Figure 1.1 depicts the global anthropogenic mercury emissions by source category for the year 2010.

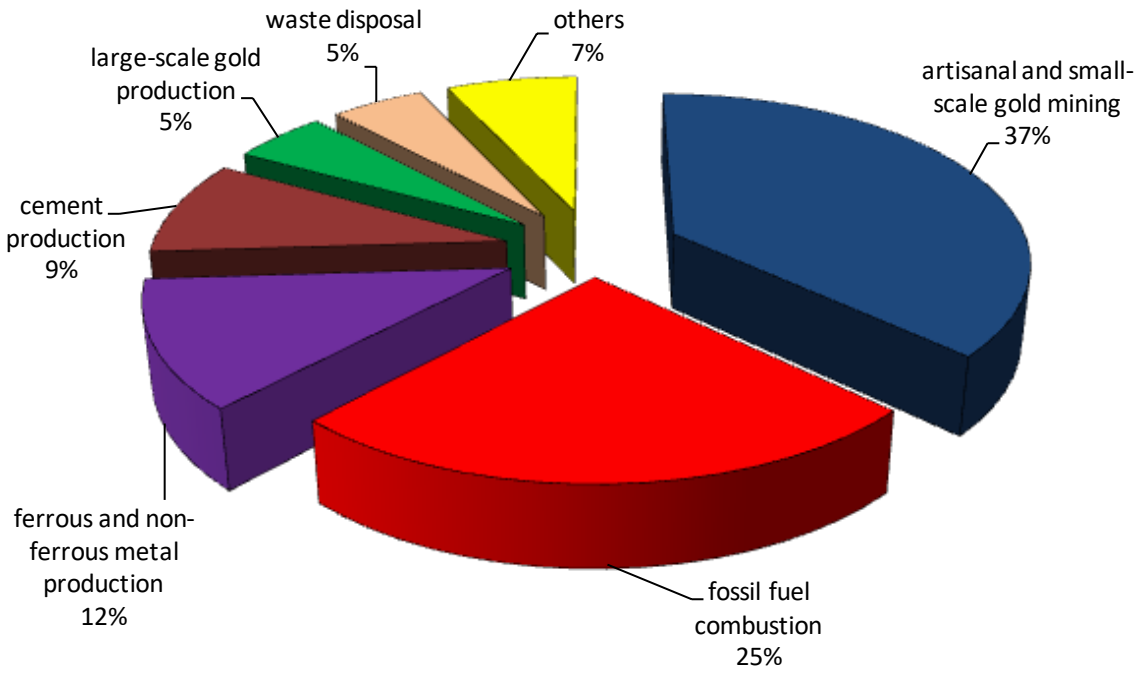

Fig.1.1 *Global anthropogenic mercury emissions by sources for the year 2010* (based on [20])

The highest contribution to the global mercury emissions are recorded in areas where combustion of coal is extensively used for electricity and heat production. Asian countries (especially China and India) are the main source of anthropogenic mercury emissions, followed by Africa, Europe and North America [21]. To date, mercury emissions models are subjected to uncertainty associated with the lack of actual measurement data for some developing countries [23].

1.2. Mercury emissions from coal fired power plants

Coal represents approximately 43 % of the total fuel used worldwide for electrical power production [21]. The flue gas emissions from coal combustion process include various pollutants, such as: carbon dioxide (CO_2), carbon oxide (CO), sulfur dioxide (SO_2), nitrogen oxides (NOx), steam (H_2O), halogenated acids (HCl, HBr), sulfur trioxide (SO_3), particulate matter (fly ash), trace elements (Hg, As, Pb, Cd, Zn and others). The concentration of these

pollutants in the flue gases after coal combustion processes is mainly influenced by the coal chemical composition. All fuels, also renewable (e.g. wood) or gaseous (e.g. natural gas), contain mercury, which is almost completely volatized during the combustion process. Generally, the mercury content of the different fuels varies between 0.01 and 2 µg/g resulting in flue gases containing 1 to 200 µg/m³ of mercury [2].

In coal, mercury commonly occurs in association with pyrite (FeS_2) and cinnabar (HgS), while some mercury may be organically bound to coal macerals [24]. The concentrations of mercury vary with coal type, coal basin and, even within the same coal basin (see Appendix 1.2). There are different types of coal: anthracite, lignite, bituminous and sub-bituminous. The anthracite coal, which is nearly pure carbon, is seldom used for electrical power generation due to its relatively high price [25]. Pyrite cleaning of coal will reduce the Hg levels. However fine grained pyrite (<70 µm) is not removed by coal cleaning. Consequently often just 1/3 of the Hg in coal is removed by the standard coal cleaning procedures [26]. Therefore, mercury from solid fuels is not completely removed by cleaning the fuel, and has to be captured from the flue gas [2].

The stable mercury species at combustion temperatures around 1000 °C is exclusively in elemental form. At temperatures below 450 °C, the equilibrium in flue gases is dominated by oxidized species like the oxide and the halogenides (X = Cl, Br and I). This low temperature equilibrium is generally not established in power plants and industrial incinerators. The halogen content of the fuel and therefore of the flue gas determines the extent to which the Hg^{el} is transformed into Hg^{ox}. The higher the halogen content the larger will be the fraction of oxidized species of the total mercury [2, 24].

The halogen content of coal-like solid fuels is dominated by chlorine species. Chlorine appears in flue gases predominantly as HCl. At low temperatures Cl_2 becomes the most stable species, however the low kinetics does not allow for Cl_2 formation in flue gases. The HCl content of flue gases from coal-combustion varies between 1 to 500 mg/m³. The bromine content in coal fuels is generally between 1 and 4 % of the chlorine content [27]. Bromine species in the flue gas are more effective in oxidizing the Hg^{el} [2, 10].

1.3. Mercury speciation in flue gases

In the high temperature regions of the coal-fired boilers, mercury is found in the elemental form (Hg^{el}). As the flue gas cools down, a series of complex reactions begin to convert the elemental mercury to oxidized (Hg^{ox}) and particle-bound mercury (Hg^{p}) [28]. Oxidized mercury is reactive and water soluble, being easily captured by activated carbon

injection and particulate collection devices or by wet flue gas desulfurization systems. Mercury speciation in flue gases is influenced by several factors, such as: coal chemistry and rank, flue gas chemistry, plant configuration, operation parameters (temperature, pressure etc), the presence or absence of pollution control devices [29]. Coal chemistry plays an important role in mercury speciation in flue gases. The pilot and full-scale tests have shown that burning "low chlorine" coal (less than 100 – 300 μg/g Cl) results in flue gas in which elemental mercury is the predominant species, while in the flue gas from burning "high chlorine" coal (>300 μg/g Cl) the oxidized form of mercury predominates [24, 28].

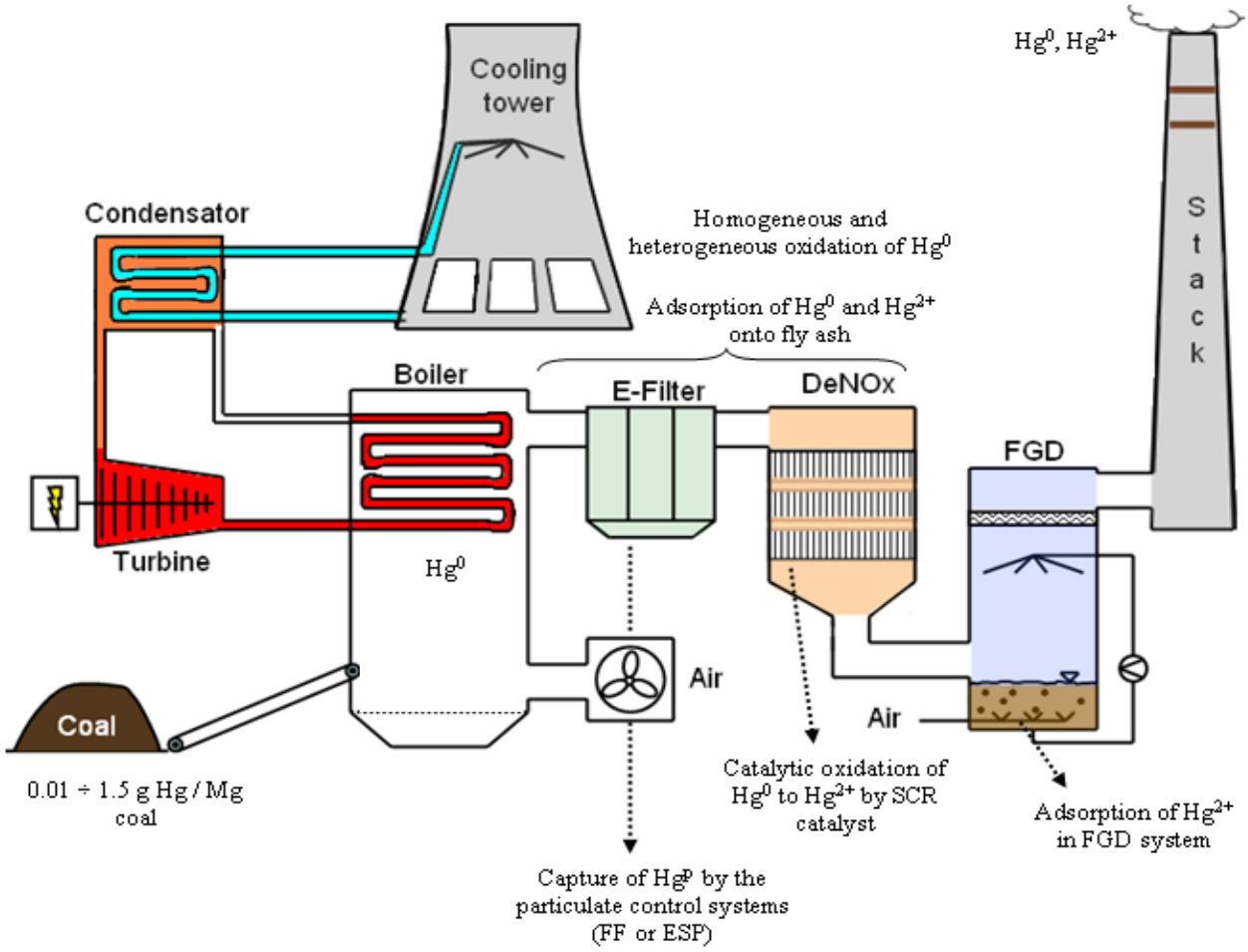

Fig.1.2 *Schematics of a coal-fired power plant illustrating mercury transformations in flue gases*

The presence of certain minerals in coal and in the fly ash resulted from coal combustion also has an influence on mercury speciation in flue gases. These minerals either enhance mercury oxidation by providing catalytically active sites or inhibit mercury oxidation after reacting with the chlorine found in flue gas. Ghorishi et al., (2005) [30] has investigated

the influence of fly ash components (Al_2O_3, SiO_2, Fe_2O_3, CuO and CaO) on mercury oxidation in flue gases. For instance, the presence of copper oxide (CuO) and iron (III) oxide (Fe_2O_3) exhibit a good catalytic activity towards mercury oxidation reaction, while calcium oxide (CaO) reduces the mercury oxidation degree by consuming the chlorine from the flue gases [30].

Because of the abundance of chlorine-containing species (HCl and Cl_2) it is believed that mercuric chloride ($HgCl_2$) is the dominant form of oxidized mercury found in the flue gases. Some authors indicate that mercuric oxide [31], nitrate [32], and sulfate [28, 33] may also be formed.

1.4. Impact of mercury emissions on environment and human health

Mercury represents a global concern due to its persistence, long-range mobility into the atmosphere, bio-accumulation in ecosystems and its long term negative impact on human health and environment. A very important factor in the impact of mercury on environment and human health is the chemical form in which it appears. Most of the mercury emitted into the atmosphere is found in gaseous elemental state. Only small amounts of mercury in oxidized (Hg^{2+}) or particle-bound ($Hg^{(p)}$) form are emitted into the atmosphere [34].

Once emitted into the atmosphere, gaseous elemental mercury has a relatively long residence time (0.5 – 2 years) [35]. Due to its physical and chemical properties (atmospheric residence time, high volatility, and chemical inertness), mercury is slowly oxidized into the atmosphere and, therefore subjected to long-range transport. Evidence of global transport of mercury consists in its presence in the Arctic ice at levels that cannot be attributed to natural or local emissions sources [22, 36]. The oxidized and particle-bound forms of mercury have a shorter residence time (hours to days), being relatively fast removed from the atmosphere by wet or dry deposition mechanisms [34].

Following the gas-phase oxidation and deposition on soil or water bodies, mercury is subjected to a large number of redox reactions. An important reaction is the methylation of inorganic mercury through microbial activity. Several microorganisms, such as: some methanogens, sulfate and iron reducers, are considered to be responsible for mercury methylation processes [37].

Mercury and its compounds represent a class of highly toxic substances for humans and wildlife. Severity of symptoms and adverse health effects following exposure differ with the multiple chemical forms or chemical species of mercury, as well as the intensity and

exposure duration (i.e. the dose) [13, 20]. All forms of mercury have the ability to accumulate, at a certain extent, in organisms and build up along the food chain [20].

Main route of human exposure to elemental mercury is by inhaling the vapors, which are absorbed by the lung tissues. Several neurological and behavioral disorders have been observed in humans after exposure to elemental mercury vapours. The specific symptoms include tremors, emotional lability, insomnia, memory loss, neuromuscular changes, and headaches [20]. Fish and shellfish consumption is the main source of metyl mercury exposure for humans. Methyl mercury has the ability to bio-accumulate and bio-magnify in the aquatic food chain [3, 20]. The amount of methyl mercury in fish depends on several factors, such as: amount of mercury deposited from the atmosphere, the naturally occurring mercury in soils, the physical, biological, and chemical properties of different water bodies and the age, size and type of food the fish eats [38]. Mercury intake of humans depends not only on the level of mercury in the fish, but also on the amount of fish consumed daily [20]. Methyl mercury exposure of pregnant women leads to impaired neurological development of the fetus brain. Vulnerability to effects of methyl mercury exposure depends on age, dose and duration of exposure [13].

CHAPTER 2

Catalytic oxidation of elemental mercury in flue gases

All types of fuel contain mercury, which is almost completely volatilized as elemental mercury (Hg^{el}) during combustion processes. However, elemental mercury has a low water solubility which makes it difficult to be removed from flue gases. Due to its relatively high water solubility, oxidized mercury (Hg^{ox}) present in flue gases is easily removed by the wet flue gas desulphurisation systems (WFGD). WFGD systems capture approximately 90 % of the Hg^{ox} from flue gases [3]. Consequently, catalytic processes that increase the amount of Hg^{ox} in flue gases are of great interest for the overall removal of mercury.

Mercury oxidation catalysts do not decrease the mercury content of flue gases as such, but rather in combination with a scrubber. For this purpose, the mercury oxidation catalyst has to be placed upstream of the flue gas scrubber. Wet scrubbing removes the acid components of flue gas, mainly SO_2, SO_3, HCl and HBr, as well as the oxidized mercury [2].

Mercury catalysts may be placed before (high dust) and after (low dust) the dust removal devices, which are often operated at temperatures between 160–430 °C. Low dust placement is less prone to clogging by large dust particles. Here, all the volatile acid constituents of the flue gas are still present, except for the nitrogen oxides NOx. In the high dust version, the most likely position to place the mercury catalyst is within the SCR-DeNOx reactor [2, 3].

A very important aspect to be considered when operating mercury oxidation catalysts in a SO_2-containing gas is its effect on the conversion reaction of SO_2 to SO_3. SO_3 is poorly captured in most scrubbers. It forms sulphuric acid mist in flue gases that leave the plant. Another unwanted side reaction to be considered is the oxidation of NO to NO_2. The oxygen

content of flue gases resulting from combustion processes varies between 2 and 8 vol.-%, which might affect the performance of mercury oxidation catalysts [2]. Also, it has to be mentioned that because of the large volumes to be treated, mercury oxidation catalysts, like any other flue gas catalysts, have to be applied in a honeycomb or plate-like structure. This arrangement is preferred in order to reduce both pressure loss and energy requirements [2].

2.1. Proposed mechanistic pathways for catalytic oxidation of elemental mercury

Schematically, the oxidation of Hg^{el} in the presence of a catalytic material can be described as follows:

$$Hg^0 + \text{oxidizing species} \xrightarrow{catalyst,\ T\,°C} Hg^{2+} + \text{reduced species} \qquad (2.1)$$

Over the years, the increasing knowledge on mercury oxidation led to the proposal of different mechanisms for the oxidation of elemental mercury in flue gases. The following paragraphs briefly discuss the potential mechanistic pathways of catalytic oxidation of elemental mercury in flue gases.

Deacon reaction

Because of the importance of the halogen species, it is proposed that the Hg^{el} oxidation in flue gases could be enhanced by chlorine atoms ($Cl^{\bullet}$) or molecules (Cl_2) produced by the Deacon reaction [39]. The Deacon reaction produces chlorine by catalytic oxidation of HCl with air or oxygen according to the overall reaction 2. The reaction is reversible and exothermic [2].

$$4\,HCl_{(g)} + O_{2(g)} \leftrightarrow 2\,Cl_{2(g)} + 2\,H_2O_{(g)} \qquad (\Delta H^o = -28.4\ kJ/mol\ HCl) \qquad (2.2)$$

The reaction takes place at about 350 to 450 °C in the presence of copper, chromium, vanadium and RuO_2 catalysts. This reaction is described by a Mars-van Krevelen type of reaction mechanism involving hydrogen abstraction from adsorbed HCl, recombination and desorption of atomic chlorine, water desorption and oxygen adsorption [40]. HBr reacts in a similar manner, whereby the bromine-Deacon reaction produces more free bromine [2, 41].

Eley-Rideal mechanism

This mechanism assumes that the elemental mercury present in the flue gas could react from the gas-phase (or as a weakly adsorbed) state with an adsorbed oxidant species, most likely HCl. According to this mechanism, HCl is dissociatively adsorbed on the V_2O_5-active sites found on the SCR catalyst surface. NH_3 and HCl species compete for the active sites. Hg^{el} reacts with the V_2O_5-chlorinated sites from the gas phase or as a weakly adsorbed species [42, 43] to form the final oxidation product, for example, as given in equations (2.3 – 2.5) [2]:

$$2\ HCl_{(g)} + 2\ V{-}O{-}V_{(s)} \leftrightarrow 2\ V{-}OH{-}V{-}Cl_{(s)} \quad (2.3)$$

$$2\ V{-}OH{-}V{-}Cl_{(s)} + Hg^{0}_{(g)} \leftrightarrow 2\ V{-}OH{-}V_{(s)} + HgCl_{2(g)} \quad (2.4)$$

$$2\ V{-}OH{-}V_{(s)} + 0.5\ O_{2(g)} \leftrightarrow 2\ V{-}O{-}V_{(s)} + H_2O_{(g)} \quad (2.5)$$

In the light of most recent experimental findings, an Eley-Rideal mechanism with adsorbed HCl reacting with gas phase or weakly adsorbed Hg^{el} does not seem plausible. Evidence of HCl adsorption on the catalyst surface was obtained by employing different surface analysis methods [44, 45]. However, it has been shown by surface analysis means that Hg^{el} adsorbs on various surfaces as well [2].

Langmuir-Hinshelwood mechanism

According to the Langmuir-Hinshelwood mechanism, the catalytic oxidation of Hg^{el} takes place between elemental mercury and the oxidant species co-adsorbed on the catalyst surface. This oxidation mechanism is likely to occur in the presence of substrates which can adsorb both HCl and Hg^{el} [2].

When investigating the catalytic oxidation of Hg^{el} in the presence of MnOx–CeO_2/TiO_2, Li *et al.* [44] proposed the Langmuir-Hinshelwood mechanism as a plausible reaction pathway. Eom *et al.* [46] formulated the rate limiting reaction of the adsorbed mercury and the absorbed chlorine species on a commercial SCR-DeNOx catalyst as described by equation (2.6):

$$SCR\text{-}cat(V^{4+}{-}O)Hg^{+}_{(ads)(s)} + 2\ SCR\text{-}cat(V^{4+}{-}Cl) \leftrightarrow SCR\text{-}cat\ (V^{4+}{-}O)\cdots HgCl_{2(ads)}\cdots(V^{4+})_{(s)} \quad (2.6)$$

Mars-Maessen mechanism

Recent research in catalytic oxidation of elemental mercury widely uses the Mars-Maessen mechanism as a most likely oxidation pathway in the presence of metal oxide-based catalysts [47, 48]. According to this mechanism, the Hg^{el} oxidation takes place between the elemental mercury adsorbed on a metal oxide (M_xO_y) surface and the lattice oxygen, forming

a binary mercury oxide. The oxidation of Hg^{el} could be described by the following equations for the CoO/TiO_2 system [2, 47]:

$$Hg_{(g)} + \text{catalysts surface} \rightarrow Hg_{(ad)(s)} \quad (2.7)$$

$$Hg_{(ad)(s)} + Co_xO_{y(s)} \rightarrow HgO{-}Co_xO_{y-1(s)} \quad (2.8)$$

$$HgO{-}Co_xO_{y-1(s)} + \tfrac{1}{2}\, O_{2(g)} \rightarrow HgO_{(ad)(s)} + Co_xO_{y(s)} \quad (2.9)$$

$$HgO_{(ad)(s)} + 2\, HCl_{(g)} \rightarrow HgCl_{2(g)} + H_2O \quad (2.10)$$

Firstly, the gaseous Hg^{el} is physically adsorbed on the catalyst surface to form $Hg^{el}_{(ad)}$. Then the $Hg^{el}_{(ad)}$ reacts with the lattice oxygen from the catalyst to form a weakly adsorbed mercuric oxide. The physical adsorption of Hg^{el} on the catalyst surface takes place even at low reaction temperatures, although $Hg^{el}_{(ad)}$ conversion to $HgO_{(ad)}$ is accelerated by increasing the temperature [39]. A further step of the Mars-Maessen mechanism involves the re-oxidation of catalytic metal oxide by gaseous oxygen. In the last step of this mechanism, the $HgO_{(ad)}$ reacts with HCl or HBr to form the volatile mercury halogenides which are released from the catalyst surface [2].

2.2. Catalysts for oxidation of elemental mercury in flue gases

Over the past decades a significant amount of research has been devoted to developing and implementing new catalysts for elemental mercury oxidation in flue gases. Academia and industry have directed their efforts towards this purpose. Research has been carried out at laboratory, pilot and full scale [2]. These catalysts fall into one of the following categories:

- supported-transition metals and metal oxides;
- selective catalytic reduction (SCR) catalysts;
- supported-noble metals.

It is now known that the activity of almost all mercury oxidation catalysts studied so far depends on the halides concentration (HCl and/or HBr) in the flue gases to be treated [2]. In the following sections, the main types of catalysts employed for oxidation of elemental mercury and the effect of different flue gas components and reaction temperature on catalytic oxidation of elemental mercury are discussed.

2.2.1. Oxidation of elemental mercury by transition metal oxide catalysts

The Hg^{el} oxidation activity of this class of catalysts was mainly investigated under laboratory conditions where parameters as temperature, flue gas composition and metal oxide loadings were varied. The catalytic active metal oxides are deposited most commonly on alumina (Al_2O_3) and titania (TiO_2). The role of the support is not only to stabilize and ensure a high metal dispersion degree but also, in certain cases, to participate in the Hg^{el} oxidation reaction [2].

Copper oxide particles, titania-supported-CuO, γ-alumina and titania-supported $CuCl_2$ are potential Hg^{el} oxidation catalysts in the presence of HCl at low temperature [49 - 52]. Kamata *et al.* [49] observed an increase in oxidation of gaseous Hg^{el} at 150 °C in the presence of higher HCl concentration. Yamaguchi *et al.* [50] investigated further details of the Hg^{el} oxidation activity of CuO nano-particles and noted a decrease in catalytic activity when CuO nano-particle size increased from 50 nm to 620 nm. Another study [52] discussed the performance of $CuCl_2/\gamma\text{-}Al_2O_3$ catalyst with different $CuCl_2$ loads and found an increase in oxidation activity with increasing the $CuCl_2$ content up to 10 wt.%. $CuCl_2$ acts as a redox catalyst oxidizing Hg^{el} by being reduced to CuCl, following a re-chlorination back to $CuCl_2$ in the presence of O_2 and HCl [2, 52].

The Hg^{el} oxidation activity of cobalt oxide-based catalysts was shown to be affected by the Co loading and the oxidation temperature. Hg^{el} oxidation efficiencies higher than 80% were achieved when the Co content was in the 2.5 and 7.5 wt.-% range and at temperatures between 120–330 °C. Liu *et al.* [47] attributed the good catalytic performance of Co-based catalysts to well-dispersed Co_3O_4 species in the catalysts [2]. A more recent experimental study investigated the Hg^{el} oxidation activity of Co_xMn_yTi catalysts in the absence of HCl [53]. Oxidation efficiency of 98 % was obtained in the presence of O_2 at reaction temperature of 150 °C and Co loads of 6 %.

Another interesting class of Hg^{el} oxidation catalysts includes the Mn and MnO_x-based catalysts. Several studies suggested that manganese oxide-based catalysts may display good Hg^{el} oxidation efficiency under simulated flue gas conditions [54-56]. It was found that in the absence of HCl from the flue gas, the MnO_x effectively adsorbed gaseous Hg^{el} with an optimum at 230 °C, whereas the Hg^{el} adsorption was suppressed and high mercury oxidation efficiencies achieved in HCl or Cl_2-containing flue gases [54]. A subsequent paper [55] investigated the Hg^{el} adsorption and oxidation in the presence of Mn oxide (1 wt.-% Mn), supported on $\alpha\text{-}Al_2O_3$ within the 100–250 °C temperature range. The experimental results indicate that the oxidation activity of this type of catalyst decreases at temperatures below 250

°C. Xu *et al.* [56] studied the adsorption and oxidation abilities of Mn/MgO catalysts at low reaction temperatures. They found that when the Mn loadings were 10 wt.%, removal efficiencies of 82 % were reached at 120 °C. Based on the surface analysis results it was concluded that Hg^{el} was adsorbed and oxidized on the surface of the catalysts. Doping the Mn–oxide/α-Al_2O_3 catalysts with molybdenum (Mo) resulted in high Hg^{el} oxidation in gases with 5 ppm HCl, even in the presence of SO_2. Most likely the Mo doping improved the MnO_x particles dispersion, thereby increasing the Hg^{el} oxidative potential at low temperatures [2, 55]. In another study [57] the MnO_x-CeO_2/TiO_2 catalyst was highly active for Hg^{el} oxidation at 200 °C. The flue gas components NO and SO_2 inhibited to a certain degree the Hg^{el} oxidation while in the presence of 10 ppm HCl plus 4 % O_2, 100 % oxidation efficiency were achieved.

Hg-oxidation activity of cerium oxide-based catalysts has also been reported in the literature [48, 58-60]. Li et al. [58] investigated the catalytic properties of the CeO_2/TiO_2 system in HCl, NO, and SO_2 containing simulated flue gases. A fairly high CeO_2/TiO_2 mass ratio of 1.5 considerably improved oxidation efficiency. Oxidation activity increased with rising temperatures up to 250 °C, and dramatically decreased at temperatures up to 400 °C. HCl in the gas phase considerably increased the activity in the presence of oxygen [58]. It was found that in the absence of SO_2 the CeO_2/TiO_2 catalyst exhibited good oxidation activity in the presence of HCl [59]. On the other hand, under different reaction conditions SO_2 exhibited different effects. For instance, in pure N_2 atmosphere SO_2 inhibited the Hg^{el} oxidation, while in N_2 + O_2 atmosphere low concentrations of SO_2 promoted Hg^{el} oxidation, whereas higher SO_2 concentrations decreased the oxidation activity of the catalyst [60].

Kong *et al.* [61] studied Hg^{el} oxidation activity of rod-shaped nano-Fe_2O_3 in a fixed bed reactor arrangement. The Hg^{el} oxidation activity increased considerably with decreasing particle size. Hg^{el} oxidation increased significantly at temperatures between 75 and 300 °C, and decreased at higher temperatures. The decrease of Hg^{el}-oxidation activity at 400 °C was attributed to the sintering of the Fe_2O_3 nano-particles [2].

2.2.2. Oxidation of elemental mercury on SCR-DeNOx catalysts

V_2O_5-based SCR-DeNOx catalysts have been commercially available since the 1980s, and are the most commonly implemented technology for the reduction of nitrogen oxides (NOx) with ammonia (NH_3) [3]. The catalyst consists of a porous titanium dioxide monolithic substrate in which vanadium pentoxide (V_2O_5), and tungsten trioxide (WO_3) or molybdenum

trioxide (MoO_3) are dispersed [2, 62]. In power plants, SCR-DeNOx reactors are installed in different arrangements, as follows [3]:

- Upstream of the air pre-heater (APH) and electrostatic precipitator (ESP) referred to as **hot site, high dust** (T = 340 to 430 °C).
- Upstream of the APH and downstream of the ESP referred to as **hot site, low dust.**
- Downstream of the APH and the ESP referred to as **cold site and low dust** (T = 160 to 240 °C).
- Downstream of flue gas desulfurisation (FGD) referred to as **tail-end** (T = 160 to 240 °C, in this configuration no co-removal of the oxidized mercury can be achieved).

Besides reducing the NOx in the presence of NH_3, SCR catalysts oxidise volatile organic compounds [63, 64] and convert gaseous Hg^{el} to Hg^{ox}, particularly in the presence of HCl [8, 10, 42, 65, 66]. In another side reaction, SCR catalysts are known to convert sulphur dioxide (SO_2) to sulphur trioxide (SO_3) [3, 66]. Currently, SCR catalysts are being developed as multi-pollutant control devices [2]. The overall Hg^{el} oxidation reaction can be summarised as in equation (2.11):

$$Hg + 2\ HCl + 0.5\ O_2 \rightarrow HgCl_2 + H_2O \qquad (2.11)$$

This section covers a number of aspects regarding Hg^{el} oxidation on SCR-DeNOx catalysts. It starts by discussing the influence of flue gas components (halogens/hydrogen halides, NH_3, SO_2/SO_3, NOx), composition of the SCR catalysts and temperature on the Hg^{el} oxidation reaction. In addition, the role of flue gas species on mercury oxidation reaction and the deactivation of SCR catalysts are briefly covered. A short discussion on mechanistic pathways and modelling of Hg^{el} oxidation over SCR catalysts follow [2].

2.2.2.1. Influence of flue gas constituents on Hg^{el} adsorption/oxidation by SCR-DeNOx catalysts

Hg^{el} adsorption on the SCR catalyst surface was observed to occur in the absence of hydrogen halides from flue gases [8-10]. Addition of halides (HCl or HBr) and/or NH_3 to the simulated flue gas leads to rapid mercury desorption [9, 10, 77]. The experimental results of Stolle et al. [10] show that even at 390 °C, low concentrations of hydrogen halides (5 mg/m^3 HCl or 0.5 mg/m^3 HBr) suppressed the Hg adsorption on SCR catalysts below the detection limit. Strong Hg adsorption in the presence of H_2SO_4 was reported by Eswaran and Stenger

[9]. Hg^{el} adsorption slightly increased when SO_2 was present [8]. Straube *et al.* [8] suggested that mercury adsorption involved chemisorption and the formation of Hg–O bonding on the SCR catalyst surface. Another interesting finding was the observed link between the V_2O_5 content and the Hg adsorption extent on the SCR catalysts [2, 8, 10].

Laboratory-scale experimental studies proved that the activity of SCR catalysts for Hg^{el} oxidation under simulated flue gas conditions is strongly linked to the halide species and their concentrations [2, 10, 42, 51, 66-68]. He *et al.* [42] reported Hg^{el} adsorption and oxidation over an HCl pretreated SCR catalyst. Adsorption and a certain degree of oxidation were recorded when employing the HCl pretreated catalyst, suggesting that adsorbed HCl reacted with adsorbed Hg^{el} to form Hg^{ox} [2].

Several experimental studies [3, 10, 66, 69] mention an increase in Hg oxidation with increasing HCl concentrations. In order to assess the effect of HCl on Hg^{el} oxidation, its concentration was varied between 0 and 500 ppm [2]. Schwämmle *et al.* [66] investigated the effects of catalysts wall thickness and pitch at different HCl concentrations. It was found that there was an increase in Hg^{el} oxidation with wall thickness and pitch for all HCl concentrations studied, prompting the authors to suggest that Hg^{el} oxidation is not only a surface reaction. In another study, Eswaran and Stenger [70] employed honeycomb and plate-like SCR catalysts to investigate the effect of HCl, HBr and HI on Hg^{el} oxidation in a lab-scale reactor. Compared to HCl, the HBr and HI added in small amounts (2 ppm) had a stronger effect on Hg oxidation. The results of Stolle *et al.* [10] showed that at an equal mass concentration, HBr is more effective than HCl by a factor of 10. Pilot-scale results obtained by Cao et al. [71] revealed that, in the presence of different commercial SCR catalysts, Hg^{el} oxidation was enhanced by the addition of hydrogen halides in the following order: ***HBr, HI, and HCl or HF***. However, it must be considered that the measurement of Hg^{el} and Hg^{ox} by the authors might have been hampered by the presence of HBr and HI in the flue gas [2].

A large number of studies mentioned the negative effect of NH_3 addition on Hg^{el} oxidation by SCR catalysts in the presence of HCl and NOx [10, 68, 69, 72]. Hong *et al.* [68] observed that increasing the NH_3/NO ratio led to a decrease in Hg^{el} oxidation activity of SCR catalysts at 350 °C. Eswaran and Stenger [9] explained the decrease in Hg^{el} oxidation by the fact that NH_3 caused Hg^{el} to desorb from the SCR catalyst surface. Eom *et al.* [46] suggests that the decrease in Hg^{el} oxidation in the presence of NH_3 is caused by the adsorption of both HCl/Hg^{el} and NH_3 on the same active sites, and the reaction rate of NH_3 is much faster than the reaction rate of Hg^{el} [2]. A recent study [10] points out that the NH_3 present in flue gases not only inhibits mercury oxidation but also causes, to some extent, the reduction of Hg^{ox}

back to Hg^{el}. The effect of NH_3 on the reduction of Hg^{ox} back to Hg^{el} is stronger in the presence of NO. The experimental results obtained by Madsen et al. [73] suggested that at temperatures higher than 325 °C a part of the Hg^{ox} was reduced back to Hg^{el} by NH_3. Also, it was observed that VOC removal on SCR catalysts induced some Hg^{ox} reduction [10] according to equation (2.12).

$$HgCl_2 + NH_3 + 0.25\ O_2 \rightarrow Hg^{el} + 2\ HCl + 0.5\ N_2 + 0.5\ H_2O \quad (2.12)$$

SO_2 and SO_3 present in the flue gases are known to affect the Hg^{el} oxidation activity of commercial SCR catalysts [9, 10, 65, 74, 75]. The results obtained by Zhuang *et al.* [65] indicated that SO_2 and SO_3 had a mitigating effect on Hg^{el} oxidation by SCR catalysts in the presence of HCl. This behavior was attributed to the competitive adsorption of SO_2, SO_3 and HCl on the SCR catalyst surface active sites [65]. It was observed that at 380 °C, increasing the SO_2 concentration from 1200 mg/m^3 to 7000 mg/m^3 caused a small increase in Hg^{el} oxidation activity of a SCR catalyst [74]. On the other hand, Stolle *et al.* [10] noted that the addition of 2000 mg/m^3 SO_2 significantly reduced the oxidation activity. However, in HBr-containing gases the effect of SO_2 on Hg^{el} oxidation was smaller. Also, Cao *et al.* [75] observed that Hg^{el} oxidation increased with increasing the SO_3 content to a maximum of 50 ppm. The addition of H_2SO_4 to a simulated flue gas increased the Hg oxidation activity of a commercial SCR catalyst, especially in the presence of HCl [9]. NO and NO_2 impact the Hg^{el} oxidation activity of SCR-DeNOx catalysts [10] with NO_2 having a stronger effect than NO. This behavior was confirmed by the results of [76] where NO present in flue gases had a promotional effect on mercury oxidation over a CeO_2-modified SCR catalyst.

2.2.2.2. Influence of catalyst composition, reaction temperature and space velocity on oxidation of elemental mercury

Vanadium content of SCR catalysts affects their Hg^{el} oxidation capacity as well. Higher vanadium content leads to a higher oxidation activity [10, 43, 67]. One study reported Hg^{el} oxidation of 90% when vanadium content was 1.1–1.2 wt.-% and less than 40% when the content was 0.5 wt.-% [43]. This was also confirmed by the experimental results of [10]. Kamata et al. [67] observed an increase in Hg^{el} oxidation almost linearly with VOx loadings up to 10 wt.-% [2].

It was observed that high temperatures could limit the extent of Hg^{el} oxidation over SCR-DeNOx catalysts [3, 8, 74, 77], most likely due to desorption of mercury from the

catalyst surface [78]. When using a plate SCR catalyst, Rallo *et al.* [74] observed a dramatic decrease of mercury oxidation once the reaction temperature was higher than 300 °C. Similar results were obtained for a honeycomb catalyst, only that the decrease in Hg^{el} oxidation activity was influenced by reaction temperature and low HCl content (10 mg/m^3) [3]. Other studies described a similar loss of Hg^{el} oxidation activity with increasing flue gas temperature and space velocity [77, 79, 80]. A bench scale study by Lee *et al.* [79] on a honeycomb catalyst under simulated coal combustion flue gas reported significant Hg^{el} oxidation activity loss (from 83 to 30%) at 400 °C and 4000 h^{-1} space velocity compared to 88% Hg oxidation at 350 °C and 2000 h^{-1} space velocity. The lab-scale study conducted by Gao *et al.* [77] showed that increasing the space velocity from 115 h^{-1} to 230 h^{-1} resulted in an approximately 15 % decrease of Hg^{el} oxidation efficiency. On the other hand, in the presence of 10 ppm H_2SO_4, 15 ppm HCl and 1000 ppm SO_2 a higher Hg^{el} oxidation was observed once the temperature increased from 340 to 370 °C [2, 9].

2.2.2.3. Loss of Hg^{el} oxidation activity

Among other factors, long term Hg^{el} oxidation activity of SCR catalysts is dependent on the catalyst age. Kamata *et al.* [69] conducted a series of experiments, aiming to clarify the aging process of SCR catalysts. Samples of catalysts which had been in service for different time periods and fresh catalysts were employed. They observed a loss of Hg^{el} oxidation activity as the operation time increased. This behavior was more pronounced as NH_3 concentration increased [2].

The most common catalyst poisons include arsenic (As), selenium (Se), potassium (K), sodium (Na), calcium (Ca), phosphorus (P) and sulfur trioxide (SO_3) [2]. Crocker *et al.* [81] studied the influence of fly ash components (Ca, Na) and gas phase species (NH_3, SO_2 and P) on SCR catalyst deactivation by the formation of sulfates and phosphates. Thermogravimetric analysis (TGA) results showed that higher temperatures led to higher sulfation rates. NH_3 and P from flue gas enhanced sulfate and phosphate formation on SCR catalysts. DeNOx activity of SCR catalyst decays as gas phase arsenic oxide As_2O_3 reacts with V_2O_5 active sites [2, 82, 83].

2.2.2.4. Mechanism of Hg^{el} oxidation on SCR catalysts

One of the aims of recent studies is to elucidate the mechanism through which Hg^{el} is oxidized on the SCR catalyst surface. The mercury oxidation mechanism has to consider the critical promotional impact of HCl and the inhibitory effect of ammonia (or the DeNOx

reaction). Because of the impact of ammonia, mercury oxidation takes place mostly at the outlet of the SCR reactor after NH_3 is consumed (see Figure 2.1) [2].

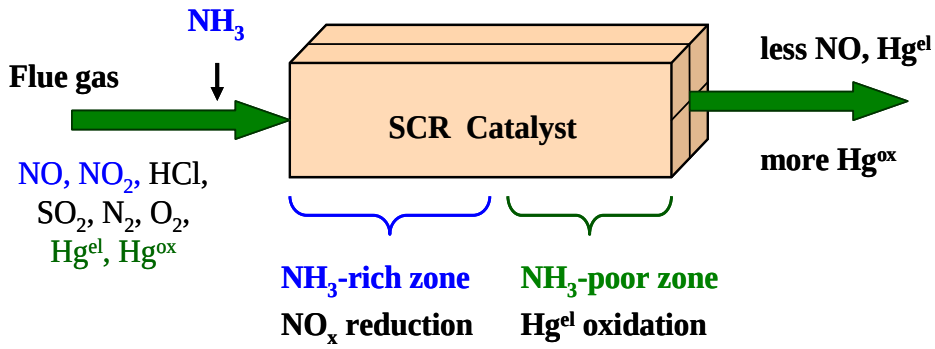

Fig.2.1. *Schematics of nitrogen oxides reduction and mercury oxidation over SCR catalyst* [2].

So far, several mechanisms were proposed for oxidation of elemental mercury on SCR catalysts. An early paper by Niksa and Fujiwara [41] proposed a model that was based on an Hg-oxidation mechanism in which NH_3 and HCl species compete for the V_2O_5-active sites from the catalyst surface. The gaseous Hg^{el} reacts with adsorbed HCl, either from the gas-phase or as a weakly adsorbed species in an Eley-Rideal type of mechanism. Senior [84] proposed a model based on an Eley-Rideal mechanism in which the adsorbed Hg^{el} reacts with gaseous HCl. According to the Senior model, Hg^{el} competes with NH_3 for V_2O_5 active sites [2]. Gao et al. [77] proposed that Hg oxidation occurs via an Eley-Rideal mechanism with HCl being firstly adsorbed on the catalyst surface to form surface active species.

The more recently proposed Hg-oxidation mechanisms are based on the surface analysis conducted on SCR catalysts. Evidence of HCl and Hg^{el} adsorption onto the SCR catalyst surface active sites were recently given [8, 42, 43, 65]. He *et al.* [42] proposed that Hg^{el} oxidation over SCR catalysts occurs via a Langmuir-Hinshelwood mechanism. A similar mercury oxidation mechanism was proposed by Eom *et al.* [46]. According to the Langmuir-Hinshelwood mechanism, both HCl and Hg^{el} species are adsorbed onto the SCR catalysts active sites, followed by the formation of $HgCl_2$ and its desorption from the catalyst surface [2]. Eom *et al.* [46] considered that Hg^{el} oxidation proceeds with the reaction of gaseous Hg^{el} with vanadium oxychloride complexes from the catalyst surface, therefore a first layer of $Hg_{(ads)}$ is formed. Once the first layer is formed, the rest of the Hg from flue gas is adsorbed and reacts with chloride complexes from the catalyst surface to form multi-layers of $HgCl_2$ [2]. A recent study [76], proposed that mercury oxidation occurs via a Mars-Maessen mechanism, where lattice oxygen of V_2O_5 reacts with adsorbed elemental mercury.

2.2.2.5. Enhancement of Hg^{el} oxidation activity of SCR catalysts

Even though the commercially available SCR catalysts exhibit a certain degree of mercury oxidation activity, there is a need for more active oxidation catalysts [3]. Therefore, a number of recent papers focused on enhancing the mercury oxidation activity of SCR-DeNOx catalysts. One of the ways to enhance Hg-oxidation activity is by applying/impregnating small quantities of metal oxides onto the SCR-DeNOx catalyst surface [2]. Published studies reported results regarding the Hg-oxidation activity of RuO_2/SCR [85], CuO/SCR, NiO/SCR, ZnO/SCR [86], CeO_2 [76, 87], MnO_x, CuO_x and VO_x impregnated SCR catalysts [88], Au/TiO_2-coated SCR [3].

It appears that the RuO_2-modified SCR catalysts exhibit good Hg-oxidation activity even in the presence of NH_3 at 350 °C. Hg-oxidation activity increased up to 90% with increasing Ru loading up to 2 wt.-%, and at 12 ppm HCl content of the simulated flue gas [85]. The experimental results of [86] showed that the CuO impregnated SCR catalyst exhibit the highest Hg-oxidation activity. However, the investigation also showed that the activity improvement by metal oxides might not be stable in SO_2-containing flue gases [2]. Chiu et al. [88] investigated the mercury oxidation activity of SCR catalysts impregnated with different transition metals and found Cu-impregnated catalysts to be the most effective under flue gas conditions with average oxidation > 95 %. Two recent studies [76, 87] investigated Hg^{el} oxidation activity of CeO_2 doped SCR catalysts under flue gas conditions. The CeO_2 impregnated catalysts showed the best performance for Hg^{el} oxidation at 250 °C reaction temperature [76].

2.2.3. Oxidation of elemental mercury over gold and other noble metal based catalysts

Noble metal catalysts are promising for mercury oxidation applications due to their ability to adsorb Hg^{el} on their surfaces and to form solid solutions in a process known as amalgamation. This property is well known for the case of gold and has been exploited for decades in gold mining and analytical chemistry. The amalgamation type of adsorption can serve as a first step followed by oxidation and desorption of mercury as a volatile halide [2].

In the absence of halogen species and oxygen, noble metals adsorb elemental mercury even at temperatures as high as 400 °C. This was confirmed in a recent lab scale study conducted by Poulston et al. [89] in fuel gasification gases containing Hg^{el}. Mercury adsorption capacity of platinum Pt and palladium Pd supported on Al_2O_3 were experimentally

measured at temperatures between 204 and 388 °C in simulated fuel gases. Up to 14 wt.-% Hg was detected in the Pd-based material [2, 89].

Platinum Pt [90, 91], palladium Pd [12,91], ruthenium oxide RuO_2 [85], and iridium Ir [38] have been tested in laboratory and pilot scale in order to determine their potential as mercury oxidation catalysts. The tests involved the use of noble metal catalysts as powders, foil and coated on different supports, such as: alumina beads [91], alumina beads imbedded in fabric filters [12] and titania [85].

Presto and Granite [91] investigated the mercury oxidation at 149 °C under simulated flue gas conditions in the presence of Pd and Pt (1 wt.-%) supported on alumina beads. The HCl and O_2 contents were varied. The Pd and Pt based catalysts gradually lose their catalytic activity over time. This deactivation behavior was explained by the formation of Pt and Pd oxides during exposure to O_2 [91]. Schofield [90] explained the oxidation of Hg^{el} on Pt as a two-step process. In the first step, the non-volatile HgO was formed. When HCl was present, the HgO was converted into the volatile $HgCl_2$ and desorbed, thereby the reaction could proceed. It should be noted that the mercury oxidation on Pd and Pt increased with temperature. Pt catalysts for diesel exhaust application are known to effectively oxidize SO_2 to SO_3 [92]. Results on this undesirable side effect reaction have not been reported so far for the Hg^{el} oxidation catalysts. It is speculated that at the fairly low reaction temperature of 150 °C employed by Presto and Granite [91], this reaction might have not been fast enough [2]. Hrdlicka et al. [12] found that at 150 °C and in the presence of HCl/Cl_2 and oxygen the mercury oxidation rate was within the range of 50–80% on 1 wt.-% Pd/Al_2O_3 coated fabric filters [2].

The RuO_2/TiO_2 catalysts might be promising for mercury oxidation in coal-fired flue gases as well [85]. The lab scale investigation was conducted between 150 and 350 °C with most of the flue gas components present. The poisoning effect of SO_2 was low. The conversion of SO_2 to SO_3 by the catalyst was imperceptible. The authors observed that the oxidation activity increased with the HCl content up to 5 ppm and leveled off thereafter. The catalyst was shown to generate some Cl_2 from HCl according to the Deacon reaction [2, 85].

Oxidation of Hg^{el} by gold based catalysts

The experimental studies regarding oxidation of Hg^{el} by gold-based catalysts have concentrated on the temperature range between 140 and 225 °C. Due to the ability to adsorb Hg on its surface and to form an amalgam with it, gold is considered a very promising candidate for mercury oxidation. An interesting application of this Au-Hg amalgamation

property is the MerCAP process [93], which involves Hg^{el} adsorption from flue gas on fixed Au-coated structures followed by thermal regeneration of the gold sorbent and Hg recovery [2].

For the adsorbed mercury to be oxidized, a reactant is necessary. Gold also has the ability to adsorb species like Cl_2 and HCl on its surface. Adsorbed Cl_2 molecules are dissociated to chlorine atoms [11] which further react with the adsorbed mercury. The dissociative adsorption of HCl on Au is presumably weaker, since the dissociation energy of Cl_2 is smaller and the bond length is higher by comparison to HCl [2, 94]. The critical importance of the adsorption of HCl on gold was supported by the observation of [91] that when HCl was removed from gas stream, Hg^{el} oxidation continued but with a considerable decrease. Presto and Granite [91] showed that increasing the HCl concentration above 50 ppm had no further impact on the reaction rate with Hg^{el}. Zhao et al. [11] observed, for the elemental mercury oxidation across gold on Teflon-coated quartz filters, that in the presence of chlorine Cl_2 (10 ppm) the oxidation of Hg^{el} proceeded much faster than with HCl. Apparently HCl decreased the effect of Cl_2 [2].

Gold exhibits a certain degree of inertness to other flue gas components (SO_2, H_2O, NO, organic compounds). Experimental investigations showed that these species did not limit Hg^{el} oxidation [3, 11, 12]. The addition of these flue gas constituents did not seem to influence the elemental mercury oxidation in the presence of Cl_2. Compared to the chlorine species, NO, SO_2 and H_2O seemed to interact to a far lesser degree with Au surfaces [11, 12]. The Au/TiO_2 coated fabric filters showed an increased mercury oxidation in the presence of HCl and NO, suggesting that there might be a synergistic effect between HCl and NO in the presence of gold [12]. Removing the oxygen from an HCl containing simulated flue gas caused the Hg^{el} oxidation on Au catalyst to decrease [2, 91].

Pilot [95, 96] and full scale [97,98] investigations were conducted with the main objective to demonstrate the effectiveness and deactivation properties of a commercial gold catalyst wash coated on γ-alumina honeycomb substrate in promoting Hg^{el} oxidation in flue gases from coal combustion. The catalyst modules were located downstream of a particulate control device [98] and in the flue gas scrubber inlet duct [97]. The flue gas contained only about 2 ppm HCl and 500 pm SO_2 [2]. The in-plant demonstration at a temperature of 180 °C ended after 17 months of operation because of the increased drop in pressure caused by the deposit of fly ash in the small flow channels of the honey-comb type catalyst used. The decrease in mercury oxidation activity of the catalyst as such was moderate [3].

Boreskov et al. [50] measured a low SO_2 oxidation rate for Au catalysts in comparison to Pt. Therefore the assumption is that this side reaction might be small. The effect of bromine species like HBr has not been reported yet in the literature [2]. All of the available studies on the mercury oxidation activity of gold-based catalysts have been conducted under cold-site conditions at temperatures up to 225 °C. To date, there is a lack of knowledge about the hot site mercury oxidation activity of Au-based catalysts [3].

Synthesis methods for gold-based catalysts

Generally, the laboratory scale experimental studies reported so far employ the Au-based catalysts as powders or coated on different type of supports. Therefore, a large number of synthesis methods for gold-based catalysts are presented in detail in the literature. The following paragraphs briefly describe some of these preparation methods.

Impregnation – consists of suspending the porous support in a large volume of solution made of a gold salt, from which the solvent is further evaporated. This procedure is followed by drying and reducing of the obtained product. A number of gold salts are used as precursors, such as: hydrogen tetrachloroaurate [99], gold chloride [100].

Deposition–precipitation - due to its effectiveness in depositing highly dispersed gold nano-particles on different supports deposition-precipitation is the most widely used method for preparation of gold based catalysts. The method consists in precipitating the gold precursor in a solution by raising the pH followed by further deposition of gold species from the solution on a support surface. The pH of the hydrogen tetrachloroaurate (HAuCl4) solution is adjusted to a fixed point in the range 6 to 10. The pH value is chosen based on the isoelectric points of the metal oxides used as supports [101]. The pH adjustment is done by the addition of different precipitating agents, such as sodium hydroxide [102, 103], potassium hydroxide [104], urea [105], ammonium hydroxide [106], sodium carbonate [107]. The gold nano-particles size is directly influenced by the preparation parameters: initial solution concentration (~ 10^{-3} M), pH (6 ÷ 10), temperature (50 ÷ 90 °C), type of support, the order of supplying the components, ageing and washing procedure, calcinations conditions.

Co-precipitation method consists in simultaneous precipitation of the active phase (gold) and the support (generally a transitional metal oxide) in a solution. Generally, the nitrates of transitional metals are employed as support precursors while the hydrogen tetrachloroaurate (HAuCl4) solution is used as gold source. Iron oxide [108, 109, 110], cobalt oxide [108], zinc oxide [109], nickel oxide [109], lanthanum oxide [109], cerium oxide [111]

are some of the oxides used as supports for the gold catalysts prepared by co-precipitation method.

Photo-deposition of gold nano-particles on a substrate surface consists in irradiating with a UV lamp the gold – support suspension after adjusting its pH by addition of a base [106, 112]. The photo-deposition method presents few advantages over deposition-precipitation method: the extent of gold deposition is higher; the heat treatment is unnecessary since gold is reduced by UV radiation and the Au nano-particle produced by photo-deposition could be smaller.

Chemical vapor deposition implies the reaction of an organo-gold compound with the surface of a support, followed by the decomposition of the gold precursor to metallic gold particles. The organo-gold compounds used as precursors are dimethylgold (III) acetylacetonate [113], dimethylgold (III) benzoylacetonato [114] etc.

Ion exchange method is mostly employed for preparation of gold on zeolites supports [115]. The term ion-exchange implies that the protons, cations or anions on the support surface are replaced by the gold ion complexes found in the solution. The gold ethylene diamine complex $[Au(en)_2]^{3+}$ [116] has been employed for cationic exchange while hydrogen tetrachloroaurate ($HAuCl_4$) was used for anionic exchange [117].

Sol-gel method is mainly used to prepare gold particles incorporated in an oxide matrix. The literature data classifies the synthesis of metal oxide supported gold particles via sol-gel method in two categories. The first route consists in incorporating mono-dispersed gold nano-particles into metal alkoxide solutions to be gelled [118]. The second route involves the addition of a soluble gold containing compound to a porous oxide gel followed by the UV or thermal reduction of gold [118, 119]. The sol-gel method was developed for the preparation of gold-containing oxides thin films.

Sonochemical method is an alternative technique that can be employed for the deposition of gold particles on different supports. The method consists of ultrasonicating the gold precursor in the presence of an inorganic support [120]. Applying ultrasounds to a gold precursor-inorganic oxide mixture induces chemical changes due to cavitation phenomena caused by the formation, growth and implosive collapse of bubbles in the suspension [119], which enhances the deposition of gold nano-particles on the support surface [121].

Spray technique developed by Uematsu *et al.* [122], involves the preparation of gold supported catalysts by using a mixture of aqueous solution of gold hydrogen tetrachloroaurate and titanium tetrachloride precursor which was atomized by an ultrasonic device. The formed catalyst particles were collected on a glass filter at the reactor exit [122]. The above

mentioned method was later modified by Fan *et al.* [123]. They employed a suspension of hydrogen tetrachloroaurate and powdered titanium dioxide, suspension which was atomized to produce a mist without the separation of the components followed by calcination of the obtained gold-supported catalyst [123].

Deposition of colloidal gold onto supports – this method involves the preparation of a gold colloidal suspension by reducing the hydrogen tetrachloroaurate with sodium borohydride ($NaBH_4$) [124, 125] in the presence of polyvinyl alcohol [125], polyvinylpirolidone [126], sodium citrate - tannic acid mixture [125], which are used as stabilizers. By dipping the support into the colloidal suspension, gold is adsorbed on the support surface.

Other less conventional methods for preparation of gold-based catalysts, which are not discussed in detail here, include ion beam deposition [127], in situ reduction [128], magnetron sputtering [129, 130], and thermal relaxation [131].

Generally, the size of the gold particles prepared by the different methods reported in the literature varies between 2 and 50 nm. The gold particles size and the dispersion degree are influenced by a number of factors, such as: synthesis method, synthesis parameters, gold loading, type of support, and activation treatment. For catalytic purposes, it is desired to achieve a high dispersion of gold particles on the support, increasing in this way the proportion of the active sites exposed to the reactants [132]

Conclusions

Over the past decades, the academia as well the industry, devoted significant resources for developing and implementing new catalysts for the oxidation of elemental mercury. To this end, the research was carried out at laboratory, pilot and full scale. The experimental results presented in the literature describe the role of flue gas components, reaction temperature and active catalytic compounds on the mercury oxidation activity. It has been established that the mercury oxidation activity of most of the catalysts studied depends on the presence and concentration of hydrogen halides (HCl, HBr) in the flue gases to be treated. Reaction temperature plays an important role as well. The experimental research showed great variations in mercury oxidation activity with temperature, mostly due to the different active compounds present in the catalysts as well their loads.

Several type of catalysts were intensively studied so far, including SCR-DeNOx catalysts, metal and metal-oxide based catalysts and, noble metal based catalysts. Commercially available SCR-DeNOx catalysts were most studied due to their co-oxidation potential for elemental mercury in flue gases. Most recent research focused on improving the co-oxidation activity of this type of catalysts by coating/impregnating the SCR monoliths with different metals and metal oxides. The experimental results showed that the improvement in mercury oxidation activity was dependent on the type of metal coated on the surface of the SCR catalysts.

Noble metal based catalysts are an interesting class of catalysts studied as mercury oxidation catalysts at laboratory and pilot scale. Due to their ability to absorb mercury on their surface, noble metal based catalysts showed good oxidation activity even at low temperatures and loadings. Amongst these catalysts, gold based catalysts seem to be promising candidates for oxidation of elemental mercury. Experimental studies conducted so far investigated the catalytic activity for mercury oxidation at temperatures up to 225 °C. To date, there is a lack of knowledge about the high temperature oxidation activity of gold based catalysts. Also, little is known about their SO_2/SO_3 conversion activity

PART II

Own Contributions

CHAPTER 3

Research Objectives

Nowdays, mercury oxidation is regarded as a very important part of environmental engineering. Many experimental investigations presented in the literature over the past decades focused on developing and implementing new catalyst for oxidation of elemental mercury in flue gases. Amongst these catalysts, metal and metal oxides (CuO, Co,CeO_2, MnOx etc.), noble metal (Pd, Pt, Au, Ir) and the commercial V_2O_5-WO_3-(MoO_3)/TiO_2 catalyst (known as SCR-DeNOx) have shown great potential as mercury oxidation catalysts.

The SCR-DeNOx catalysts received increasing attention due to their mercury oxidation activity, which is an important co-benefit of the SCR systems already installed in coal fired power plants. Several studies reported increased co-oxidation activity of elemental mercury for the SCR-DeNOx catalysts coated/impregnated with different metals or metal oxides. Therefore, the main objective of this PhD work is the ***improvement of mercury co-oxidation activity of a commercial SCR-DeNOx monolithic catalyst by applying a thin Au/TiO_2 layer on its surface***. The fact that the mercury oxidation is a fast reaction, occurring near to the surface of the catalyst, the limited number of studies on gold-based catalysts for mercury oxidation and, the cost of gold were three main factors motivating this research avenue. A schematic representation of the research objectives is given in ***Fig. 3.1***.

The first research objective was to ***identify and implement the most economically suitable method for coating the surface of SCR-DeNOx monoliths with a thin Au/TiO_2 layer***. To this end, a commercial reference SCR-DeNOx catalyst was coated with a nano-structured TiO_2 layer containing finely dispersed gold nano-particles by employing the dip-coating method. Considering that the dip-coating method consists of immersing a substrate in

a suspension containing the active compound (in this case the Au/TiO_2 particles), the necessity of preparing relatively long-term stable Au/TiO_2-based suspensions arises. Different types of Au/TiO_2 suspensions were prepared and stabilized by addition of dispersing agents and their characteristic properties were investigated (particles size distribution in the suspension, iso-electric point and rheological properties).

The physico-chemical properties of catalysts are known to affect their catalytic activity towards certain reactions. Therefore, a second objective of this research was ***the physico-chemical characterization of uncoated and Au/TiO_2-coated SCR-DeNOx monolithic catalysts***. The surface of uncoated and coated SCR-DeNOx monoliths were investigated by means of SEM, EDX and digital microscope means. The BET surface area, pore volume and size were determined by N_2 adsorption means.

As mentioned above, the prepared Au/TiO_2-coated SCR catalysts were designed with the aim of increasing the mercury co-oxidation activity of a commercial SCR-DeNOx catalyst employed as a substrate. Therefore, the next research objective focused on ***investigating the mercury oxidation activity of the uncoated and Au/TiO_2-coated SCR catalysts***. The mercury oxidation activities were studied in a laboratory-scale reactor under simulated flue gases typical for coal-fired power plants. All the catalytic tests employed honeycomb shaped monolith samples with 2 × 2 channels. The catalysts length and gas flows were adjusted to simulate flow conditions and residence times characteristics to one layer of catalyst in an industrial SCR-DeNOx reactor. The oxidation activities were investigated in the absence of NH_3 and at the 180-390 °C temperature range (the so-called cold and hot sites of flue gases in coal-fired power plants). The effect of gold loads, coating types, HCl concentrations in the flue gas and reaction temperature were of interests in this study.

The SCR-DeNOx catalysts are the most commonly implemented technology for reduction of NO_x in the presence of NH_3. Hence, the fourth objective of the experimental research was to ***study the effect of Au/TiO_2 coatings on the $DeNO_x$ activity of the SCR catalyst employed as a substrate***. The NOx reduction experimental tests were conducted in a laboratory-scale set-up at 390 °C and in the presence of NH_3/NO ratios of 1 and 1.2.

Besides reducing NOx and oxidizing elemental mercury, SCR catalysts convert SO_2 to SO_3 in the presence of oxygen. ***The study of the effect of different Au/TiO_2 coating types and gold loadings on SO_3/SO_3 conversion*** was another research objective. The SO_2/SO_3 conversion tests were performed at 390 °C and in the absence of NH_3, HCl and Hg^{el} in the simulated flue gases.

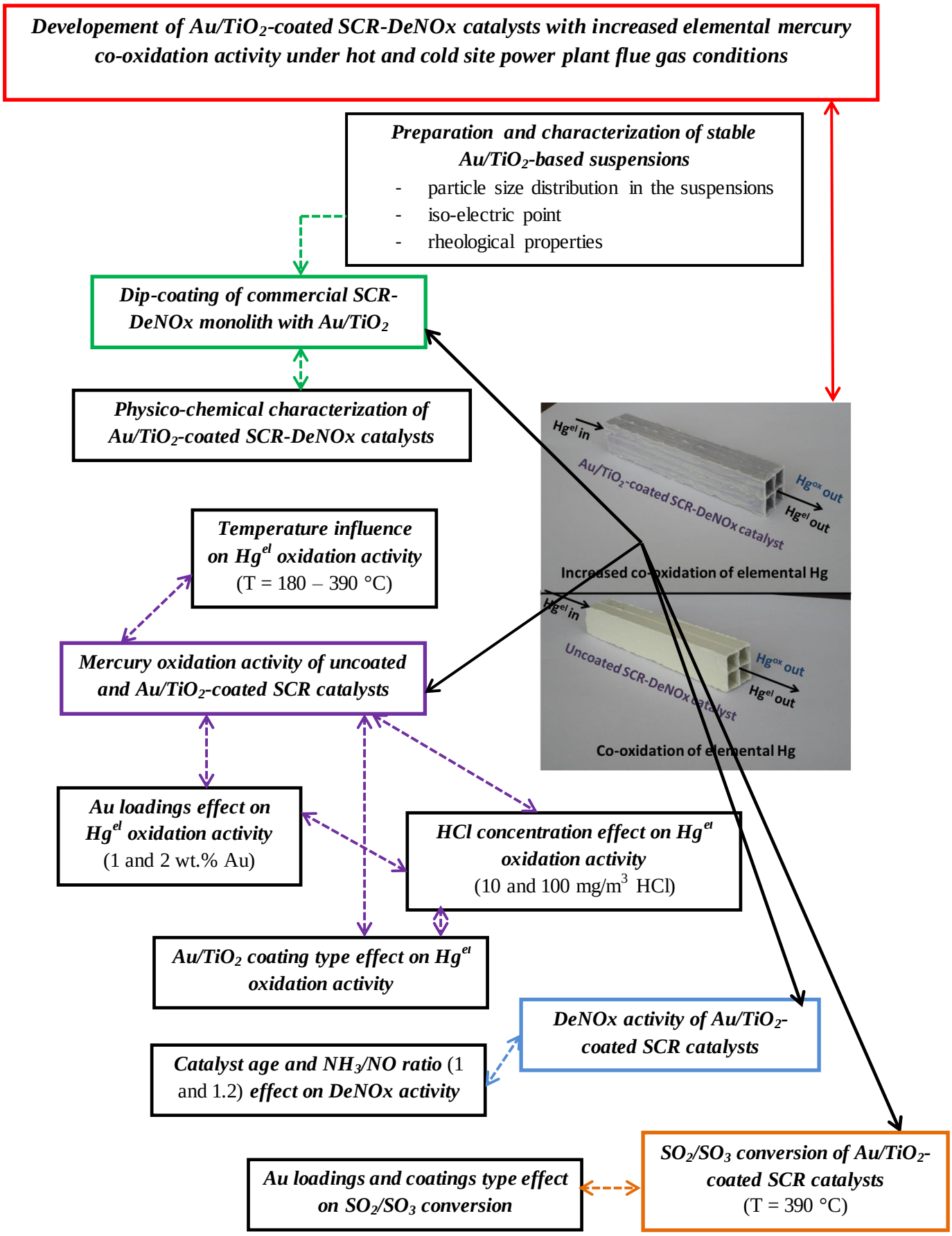

Fig.3.1. *Schematic representation of the research objectives covered in the PhD thesis*

CHAPTER 4

Experimental protocol and apparatus

4.1. Catalysts preparation

A number of different Au/TiO_2-coated SCR-DeNOx catalysts were synthesized for this study. The preparation of Au/TiO_2-coated SCR catalysts consists of three stages. Firstly, different Au/TiO_2 catalysts powders with 1 and 2 wt.-% Au were synthesized by deposition-precipitation method. Secondly, the obtained Au/TiO_2 catalyst powders were then employed for the preparation of stable suspensions. In the last stage, a commercially available SCR-DeNOx catalyst was coated with a thin Au/TiO_2 layer by dip-coating the SCR monoliths in the as-prepared suspensions. The synthesis details are listed below.

4.1.1. Synthesis of Au/TiO_2 catalyst powders

The materials and chemicals employed for the synthesis of Au/TiO_2 powdered catalysts are listed in ***Table 4.1***.

Table 4.1 *Materials and chemicals employed for synthesis of Au/TiO_2 powdered catalysts*

Chemicals/Materials	Producer	Purity	Observations/Properties
$HAuCl_4 \cdot 3H_2O$	Alfa Aesar	99.99	42.92 % Au
TiO_2 P25	Evonik	85 % anatase, 15 % rutile	S_{BET} = 50 ±15 m^2/g, crystallite size 21 nm
TiO_2 Hombikat UV100	Sachtleben	100 % anatase	S_{BET} = 10 ÷ 300 m^2/g crystallite size 1 ÷ 200 nm
NH_4OH		0.1 M	pH adjustment
Deionized water	Own production		≤ 5 µS/cm
Cellulose nitrate filters	Sartorius		pore size 0.45 µm

The nano-Au/TiO_2 catalyst powders were prepared by employing the deposition-precipitation method [101, 102]. ***Fig.4.1*** depicts the schematics of the deposition-precipitation synthesis method. The calculated amount of $HAuCl_4 \cdot 3H_2O$ to obtain 1 and 2 wt% Au in the final catalysts was dissolved in deionized water. The solutions pH was carefully measured and adjusted to 7 - 8 by addition of NH_4OH 0.1 M. Then, the solution was heated to 70 $^{\circ}C$ and the TiO_2 support was added stepwise. The obtained suspension was maturated at 70 °C by continuously stirring for one hour. In order to separate the solid from solution, the suspension was vacuum filtered (by employing cellulose filters with 0.45 μm pore size). The obtained solid samples were washed several times with deionized water (until the disappearance of Cl^- ions) and dried overnight in a drying cabinet at 100 °C. After drying, the catalysts were calcined at 400 °C (temperature was increased with a 2 °C/min temperature ramp) in airflow for 4 hours. Following calcination, the non-crystalline Au^{3+} found on TiO_2 surface was reduced to metallic Au^0. The calcined catalyst powders were further employed for the preparation of Au/TiO_2 stable suspensions.

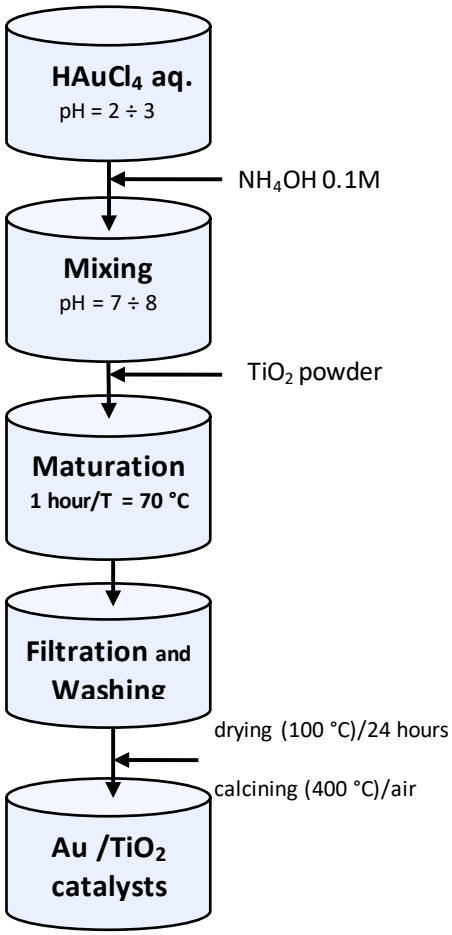

Fig. 4.1. *Schematics of deposition-precipitation synthesis method employed for preparation of nano-Au/TiO_2 catalyst powders*

4.1.2. Preparation of Au/TiO_2-based suspensions

The chemicals and materials employed for preparation of Au/TiO_2 suspensions are given in ***Table 4.2***.

Two types of Au/TiO_2-based suspensions were prepared as follows:

Type I: This type of suspension was prepared by using Au/TiO_2 catalysts prepared by deposition-precipitation method from TiO_2 powders. A calculated amount of Au/TiO_2 catalyst powder (equivalent to 2 wt.-% solid content in the final suspension) was added to the dispersing medium (NH_4Cl 5 mM with pH 7-8) and, magnetically stirred for approximately 10 minutes. Meanwhile, the suspension's pH was readjusted to ~ 7 by addition of NH_4OH 0.1 M solution. Then, the suspensions were probe sonicated for 5 minutes by employing the Bandelin HD70 system in the puls mode. Afterwards, a calculated amount (equivalent to 0.35 wt-%) of NH_4-polyacrylate Dolapix PC 21 was added, and the suspension was stirred for 15 minutes. Schematics of the suspension preparation and an image of the final suspension are given in ***Fig. 4.2***.

Table 4.2 *Materials and chemicals employed for preparation of Au/TiO_2 stable suspensions*

Chemicals/Materials	Producer	Purity	Observations/Properties
$HAuCl_4 \cdot 3H_2O$	Alfa Aesar	99.99	49.92 % Au
Au/TiO_2 P25	Own production	1 and 2 wt.-% Au	calcined powders
Au/TiO_2 UV100	Own production	1 and 2 wt.-% Au	calcined powders
TiO_2 P25 and UV100			details in **Table 4.1**
NH_4Cl	Carl Roth	≥ 99.5 %	
NH_4OH		0.1 M	for pH adjustment
HCl		0.1 M	for pH adjustment
NH_4-PA Dolapix PC21	Zschimmer & Schwarz		dispersing agent
Deionized water	Own production		≤ 5 µS/cm
Aerodisp W740X	Evonik	40 wt.-% TiO_2	commercial suspension

Type II: The calculated amount of $HAuCl_4 \cdot 3H_2O$ to obtain 1 and 2 wt% Au in the final catalysts was dissolved in deionized water. The solution pH was carefully adjusted to 7-8 by addition of NH_4OH 0.1 M. The solution was heated to 70 °C and the pH value controlled and kept to 7-8. Afterwards, a calculated amount (equivalent to 2 wt.-% solid content) of TiO_2 support in the form of Aerodisp W 740 X stable suspension with 40 wt.-% solid content was

added step-wise and, kept under continuous stirring for 1 h at 70 °C. The obtained suspension was left to cool down and, the final pH was recorded. Schematics of suspension's preparation and an image of the final suspension are given in ***Fig. 4.3***. The preparation of ***Type II*** Au/TiO_2-based suspensions was motivated by the need to eliminate some of the stages necessary for preparing ***Type I*** suspensions, i.e. synthesis, drying and calcining of Au/TiO_2 catalyst powders, suspension stabilization by electro-steric means and agglomerates breakage by ultrasonication.

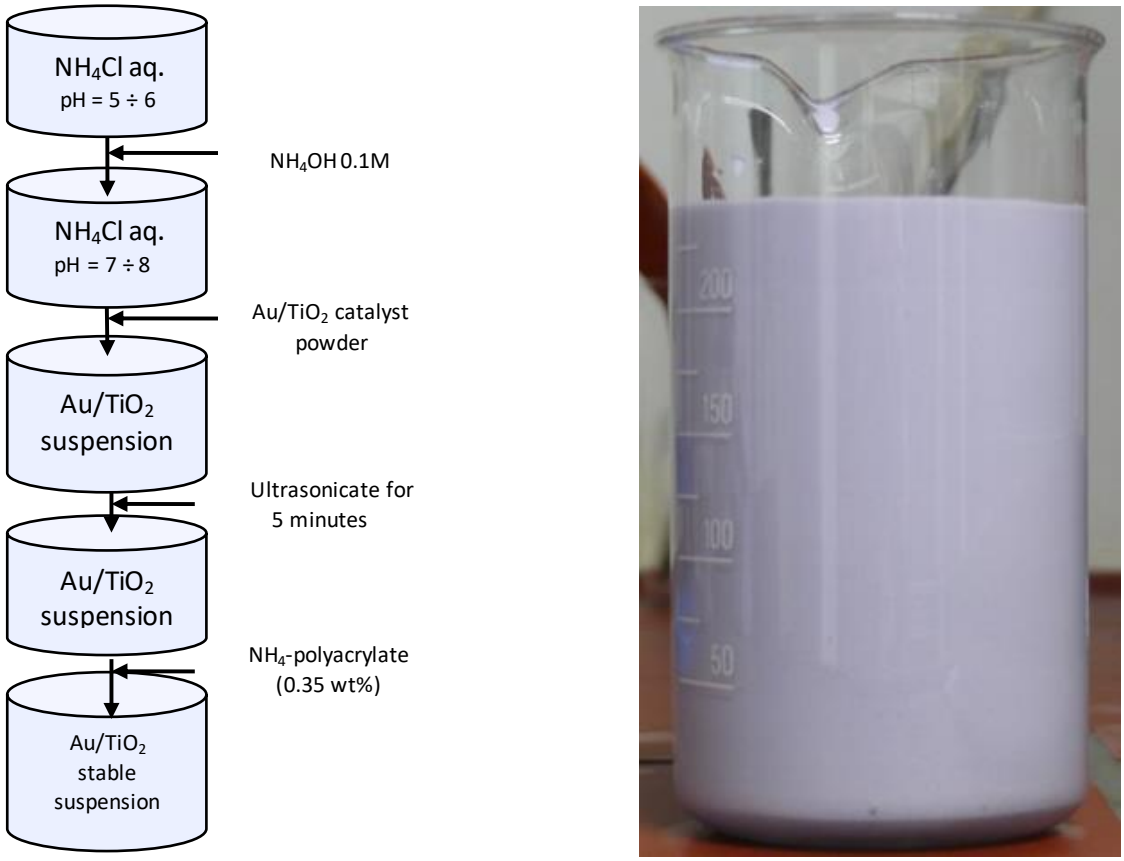

a) **b)**

Fig.4.2. *Schematics of the **a)** procedure for preparation of Type I Au/TiO_2 suspension and **b)** image of Type I Au/TiO_2 UV100-based suspension with 2 wt% solid content*

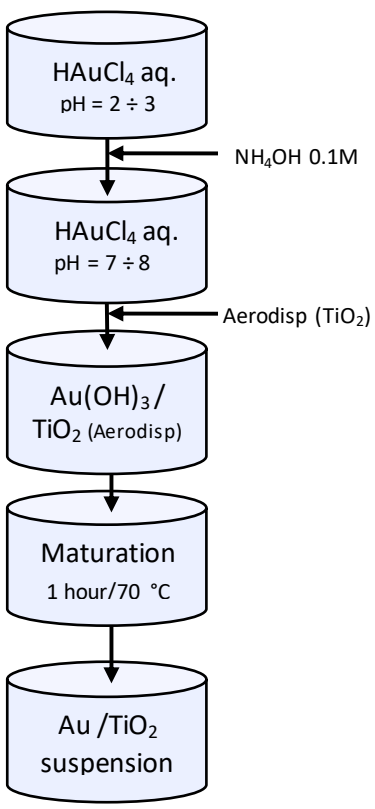

a) **b)**

Fig.4.3*. Schematics of the* ***a)*** *procedure for preparation of Type II Au/Aerodisp suspension and* ***b)*** *picture of Type II Au/Aerodisp based suspension with 2 wt% solid content*

The commercially available Aerodisp W 740 X aqueous suspension consists of hydrophilic fumed TiO_2 suspended particles with typical mean aggregate size ≤ 100 nm. The producer does not offer detailed information concerning the chemical composition of the suspension. The chemical composition of Aerodisp suspension is of interest for the catalytic activity of the prepared Au/Aerodisp-coated SCR-DeNOx catalysts. To this end, a quantitative analysis of the chemical composition of the Aerodisp solid phase was performed by means of XRF. The XRF analysis results are given in ***Table 4.3***.

Table 4.3 *Bulk and surface composition of Aerodisp solid phase by XRF method*

	TiO_2 (%)	**SiO_2** (%)	**Al_2O_3** (%)	**V_2O_5** (%)	**Na_2O** (%)	**P_2O_5** (%)	**MgO** (%)	**WO_3** (%)
Surface	65.63	0.13	33.63	0.03	0.23	0.34	-	-
Bulk	70.88	0.05	28.23	0.03	0.30	0.35	0.09	0.05

4.1.3. Coating of SCR-DeNOx monolithic catalysts with Au/TiO_2

The second step in preparing the Au/TiO_2 coated SCR catalysts consisted of dip-coating monolithic commercial SCR-DeNOx catalysts samples (Ceram Porzellanfabrik Frauental, Austria) in the as-prepared suspensions type I or II. The chemicals and materials employed for this procedure are listed in ***Table 4.4***. A schematics of dip-coating procedure is depicted in ***Fig.4.4***.

Table 4.4 *Materials and chemicals employed for preparation of Au/TiO_2 stable suspensions*

Chemicals/Materials	Producer	Observations
SCR-DeNOx catalyst	Ceram Porzellanfabrik Frauental	honeycomb shaped, see ***Table 4.5, 4.6 and 4.7***
Au/TiO_2 based suspensions	own production	2 wt.-% solid content
TiO_2 based suspensions	own production	2 wt.-% solid content
TiO_2 Aerodisp suspension	Evonik	40 wt.-% solid content

Textural properties of the commercial SCR-DeNOx catalyst employed as substrate were investigated by nitrogen adsorption-desorption method and, the results given in ***Table 4.5***. The SCR-DeNOx catalysts composition (bulk and at surface) was studied by X-ray florescence means and the results are presented in ***Table 4.6***.

Table 4.5 *Textural properties of the reference SCR-DeNOx catalyst determined by N_2 adsorption method*

BET surface (m^2/g)	Pore volume (cm^3/g)	Pore diameter (nm)
61.5 ± 0.53	0.22	20.86

Table 4.6 *Bulk and surface composition of the reference SCR-DeNOx catalyst by XRF method*

	TiO_2 (%)	SiO_2 (%)	Al_2O_3 (%)	V_2O_5 (%)	WO_3 (%)	CaO (%)	MgO (%)	Fe_2O_3 (%)	SO_3 (%)	Others* (%)
Surface	78.2	8.71	2.17	0.61	5.99	1.7	0.23	0.36	1.69	0.34
Bulk	77.7	8.04	2.59	0.61	5.76	2.4	0.46	0.38	1.83	0.23

*Na_2O; K_2O; P_2O_5; As

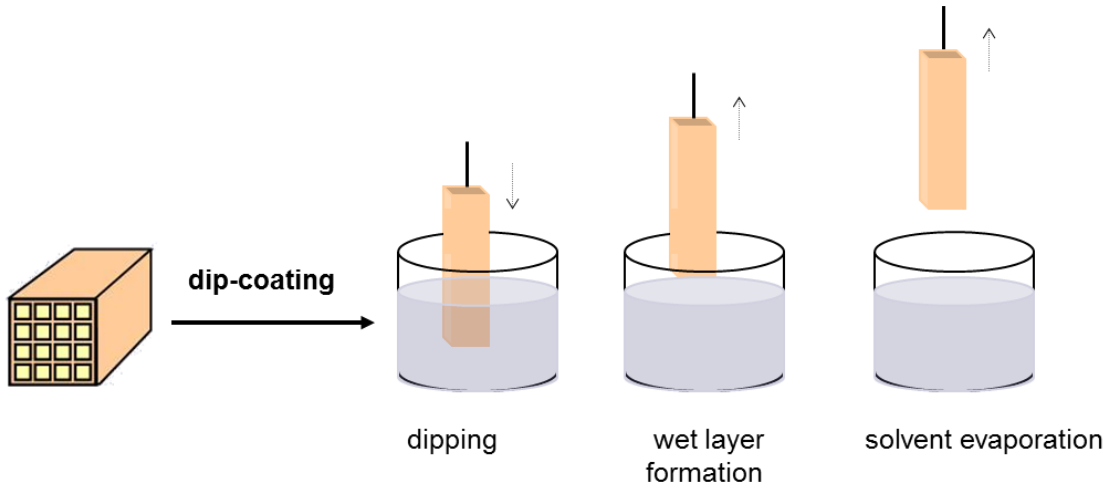

Fig.4.4. *Dip-coating procedure employed for coating of SCR-DeNOx substrates with Au/TiO_2*

Prior to the dip-coating procedure, approximately 10 cm long SCR honeycombs (cut from the main catalyst block) with 2 × 2 channels, 7.1 mm pitch and 0.87 mm wall thickness (with average mass of ~ 11 g and, average geometrical surface area of ~ 0.0161 m^2) were washed with deionised water in an ultrasonic bath for 15 minutes in order to remove the impurities from the surface. The SCR honeycombs were dried overnight in a drying cabinet at 120 °C. After cooling down for at least one day, the honeycomb monoliths were weighed and, further employed for dip-coating procedure. The dipping operations were conducted at ambient temperature and pressure. A number of dip coating parameters, such as: surrounding humidity, dipping speed and the angle at which the substrate is removed from suspension were not controlled.

The clean SCR substrates were vertically immersed into the Au/TiO_2 based suspension for one minute so that the suspension could get into the pores of the SCR substrate and, then pulled out. The excess of suspension was removed from the substrates surface by holding the sample in a vertical position. Afterwards, the coated samples were dried overnight in a drying cabinet at 120 °C. After drying, the samples were stored in a desiccator for a few days to cool down. The cooled uncoated and coated substrates were weighed with a high precision analytical scale (resolution 0.1 mg) and, the mass of coated layers was determined as follows: $m_{coating} = m_{coated_SCR} - m_{uncoated_SCR}$.

Knowing the mass of Au/TiO_2 coating and the geometrical surface of the SCR samples it was possible to calculate the specific geometrical surface coverage (in µg Au/TiO_2/mm^2 of SCR surface). Calcination of Au/TiO_2 coated monolithic substrates at 400 °C/4 hours in air was performed with the aim to stabilize the coated layers and to remove any

organic / volatile compounds initially found in the Au/TiO_2- suspensions employed for dip-coating.

4.2. Characterization techniques

A number of methods were employed for the characterization of powdered Au/TiO_2 and Au/TiO_2-coated SCR-DeNOx monolithic catalysts. The characterization methods are listed and briefly discussed in the following paragraphs.

Inductively Coupled Plasma Mass Spectroscopy (ICP-MS)

Gold contents of clear liquids resulted after Au/TiO_2 catalysts filtration and washing procedures were determined according to DIN EN ISO 11885 protocol on an Elan DRC II system (Perkin Elmer) with detection limit of 0.01 mg/L. Gold contents of the clear liquid from a 2 wt.-% Au/Aerodisp suspension were measured by employing the same system. Gold content analysis was conducted at an external laboratory (InfraLeuna Laboratory, Merseburg, Germany).

X-ray diffraction (XRD)

Powder diffraction data was collected on a PANanalytical (Netherlands) system using Cu-Kα radiation (λ=0.154 nm). Data were collected in the 10 – 120 ° in 2θ mode. Samples investigated by XRD method were as follows: calcined and uncalcined 1 wt.-% Au/TiO_2 powdered catalysts and, calcined and uncalcined 2 wt.-% Au/TiO_2 powdered samples. By employing this characterization technique, it was possible to identify the crystalline phases (gold, TiO_2 anatase and rutile) and, to determine the influence of calcination procedure on the gold particles (reduction of Au^{3+} to Au^0) and on the TiO_2 substrate (any possible anatase to rutile phases transformation occurring during the high temperature calcination process). The XRD analysis was conducted at an external laboratory at Martin Luther University (Halle, Germany).

Diffuse reflectance UV-Vis (DR UV-Vis)

DR UV-Vis spectra for the 2 wt.-% Au/TiO_2 P25 and 2 wt.-% Au/TiO_2 Hombikat UV100 catalyst powders as well the TiO_2 P25 and TiO_2 Hombikat UV100 substrates were collected on a Shimadzu UV-2450 spectrophotometer (Japan) equipped with an integrating sphere unit (ISR-2200). DR-UV-Vis spectra were collected in absorbance mode over the 800 to 190 nm wavelength range with a 0.2 nm step and 2 nm slit width. $BaSO_4$ powder was

employed for background correction. The DR UV-Vis data were obtained at an external laboratory at Gheorghe Asachi Technical University (Iasi, Romania)

Energy dispersive analysis of the X-Rays (EDX)

Elemental composition at the surface for 2 wt.-% Au/TiO_2 (P25 and UV100) catalyst powders and Au/TiO_2-coated SCR-DeNOx catalysts was determined by employing the QUANTA 200 3D electronic microscope equipped with an energy dispersive analysis of X-Ray (EDAX) system (FEI Netherlands). The specimens to be investigated were prepared by dry dispering the catalyst powder or monolithic sample on a carbon tape and further inserting it in the analysis chamber. The EDX data were obtained at Gheorghe Asachi Technical University (Iasi, Romania).

Scanning electron microscopy (SEM)

The surface morphology of the powdered Au/TiO_2 catalysts and Au/TiO_2-coated SCR-DeNOx monolithic catalysts was investigated on a field emission scanning electron microscope (FE-SEM) Mira Tescan (Czech Republic) and by SEM using the Hitachi S-4800 system (Japan), respectively. SEM images were typically obtained with acceleration voltages of 15 kV, while FE-SEM images were obtained in high vacuum mode with acceleration voltages of 20 kV. The specimens to be investigated were prepared by dry dispersing the sample on a carbon tape and, subsequently coating the sample with carbon or gold to avoid charging. The FE-SEM images were obtained at Gheorghe Asachi Technical University (Iasi, Romania), while the SEM micrographs were obtained at Otto von Guericke University (Magdeburg, Germany).

Digital microscope (DM)

The surface of uncoated SCR-DeNOx and that of Au/TiO_2-coated SCR-DeNOx monolithic catalysts were investigated by a digital microscope VHX-2000 from Keyence (Japan). The DM VHX-2000 consists of a high resolution CCD camera with a high intensity lamp and high processing capabilities. The surface topography of the samples was investigated by employing the 3D option of the microscope. The DM images were obtained at the Centrum for Engineering Sciences (ZIW) of Martin Luther University (Merseburg, Germany).

Nitrogen physisorption

Surface area (S_{BET}) and porous properties of the coated samples were determined by nitrogen adsorption at – 196 °C on a TriStar system (Micromeritics Instruments, USA). For this purpose the coated monoliths were crushed using a mortar and a pestle. Prior to the sorption (adsorption-desorption) measurements, the samples were out-gassed overnight at 150 °C. The specific surface area was calculated using the standard BET method. The total pore volume was estimated from the amount of nitrogen adsorbed at a relative pressure p/p_0 of 0.99, assuming complete surface saturation with N_2 and, where p and p_0 denote the equilibrium pressure and saturation vapour pressure, respectively. The nitrogen physisorption experiments were conducted at an external laboratory of Strasbourg University, (Strasbourg, France).

X-ray fluorescence (XRF)

Quantitative determination of the chemical composition, at the surface and bulk, of SCR-DeNOx monolithic catalyst was performed on a XRF system Axios 1 kW (PANalytical, USA). The XRF spectrometer is equipped with a Super Sharp Window Tube with Rh anode. For surface analysis, the specimens were cut from the monolithic SCR catalysts and analyzed. For bulk analysis, the SCR monolith was crushed to a fine powder and then analyzed. The chemical composition of SCR catalyst by XRF method was performed at the external STEAG Energy Services LLC laboratory (USA).

Isoelectric point (IEP)

The isoelectric points of the Au/TiO_2–based suspensions were determined by measuring their zeta potential (ζ) as a function of pH. The zeta potential was measured on a Zetamaster S system from Malvern Instruments (Germany). The zeta potential measurements were conducted in NH_4Cl 5 mM electrolyte solution. The experiments were carried out using diluted suspensions (from 20 mg/mL initial concentration down to 2 mg/mL solid content). The pH adjustment was done by addition of NH_4OH 0.1 M and HCl 0.1 M solutions. The experimental measurements of zeta potential were conducted at the laboratory of Pharmacy Faculty, Martin Luther University (Halle, Germany).

Particle size distribution

The particle size distribution in the suspensions was determined by employing the Zetamaster S system from Malvern Instruments (Germany) and a dynamic light scattering system (DLS) HPPS-ET, Malvern Instruments (Germany). A small amount of suspension was diluted in distilled water and placed in a cuvette, the cuvette inserted in the analysis system and the particle size measurements were conducted. The particle size distribution measurements were conducted at the laboratory of Pharmacy Faculty, Martin Luther University (Halle, Germany).

Viscosity measurements

The viscosity of the as prepared suspensions was determined by employing the AR 2000 system from TA Instruments (USA). The measurements were conducted at 30 °C and 100 s^{-1} shear rate for a ten minute period. The rheological properties of the as-prepared suspensions were determined at the laboratory of Martin Luther University, (Merseburg, Germany).

4.3. Catalytic activity tests

The catalytic activity of uncoated SCR-DeNOx and Au/TiO_2-coated SCR-DeNOx monolithic catalysts was investigated for three different reactions, elemental mercury (Hg^{el}) oxidation reaction, NO_x reduction by NH_3 (DeNOx) reaction and, SO_2/SO_3 conversion. The following paragraphs describe in detail the experimental set-ups employed, as well as the experimental protocols involved. A list of the catalysts investigated and their characteristics is given in ***Table 4.7***.

Before the activity testing experiments, all catalyst the samples were aged for one week (see ***Table 4.8***). Catalytic investigations were conducted under the standard conditions summarized in ***Table 4.8***. Prior to the catalytic tests, the samples were conditioned under simulated flue gas conditions characteristic to each type of reaction, as follows: 24 hours for Hg oxidation and DeNOx catalytic reactions and, 48 – 72 hours for SO_2/SO_3 conversion tests. Catalysts length and gas flow were adjusted to simulate flow conditions and residence time characteristic to one layer of catalyst in a SCR-DeNOx industrial reactor. For this purpose, area velocity (AV = ratio of flue gas volume under standard conditions per geometric surface area of catalysts exposed to simulated flue gas) was of approximately 21m/h.

Table 4.7 *Characteristic parameters of the investigated catalysts*

Catalyst name	Coating type	Pitch (mm)	Wall thickness (mm)	Channel (mm)
SCR-uncoated	-	7.1	0.87	6.23
2Au/TiP25-SCR	2 wt.-% Au/TiO_2 P25	7.1	0.87	6.23
1Au/TiP25-SCR	1 wt.% Au/TiO_2 P25	7.1	0.87	6.23
TiP25-SCR	TiO_2 P25	7.1	0.87	6.23
2Au/TiUV100-SCR	2 wt.% Au/TiO_2 UV100	7.1	0.87	6.23
1Au/TiUV100-SCR	1 wt.% Au/TiO_2 UV100	7.1	0.87	6.23
TiUV100-SCR	TiO_2 UV100	7.1	0.87	6.23
2Au/TiAerod-SCR	2 wt.% Au/TiO_2 Aerodisp	7.1	0.87	6.23
1Au/TiAerod-SCR	1 wt.% Au/TiO_2 Aerodisp	7.1	0.87	6.23
TiAerod-SCR	TiO_2 Aerodisp	7.1	0.87	6.23

When changing experimental parameters (temperature and/or HCl concentration), catalyst samples were left for more than 2 hours under the new conditions prior to mercury measurements in order to make sure that the stationary conditions for mercury concentration downstream of the catalyst were achieved.

Table 4.8 *Experimental flue gas conditions for the catalytic tests*

Reaction / Parameter	T °C	O_2 vol.-%	H_2O vol.-%	Hg^{el} µg/m^3	SO_2 ppm	NO Ppm	NH_3 ppm	HCl mg/m^3
Hg oxidation	180 ÷ 390	4	7	60 ÷ 130	700	400	-	10 ÷ 100
DeNOx	390			-	700		400 ÷ 480	-
aging and SO_2/SO_3 conversion					600		-	

Table 4.9 provides a list of gases employed for preparation of model flue gases. Nitrogen and/or dried compressed air, purified by active carbon, was used as carrier gas.

Table 4.9 *List of gases employed for model flue gas preparation*

Gases	Producer	Purity	Observations
N_2	Air Liquide	5.0	
NO	Air Liquide	2.5	
NH_3	Air Liquide	3.8	compressed liquefied gas
SO_2	Air Liquide	3.8	compressed liquefied gas
compressed air	own production		purified by freeze drying and active carbon

For calibration purposes, reference compressed SO_2 (850 ppm ± 17 ppm) and NO (300 ppm ± 5.9 ppm) gases in nitrogen were employed. The calibration gases were purchased from Air Liquide (Germany).

4.3.1. Mercury oxidation activity

The Hg^{el} oxidation activity of uncoated SCR and Au/TiO_2-coated SCR catalysts was investigated at laboratory scale by employing the experimental set-up given in ***Fig.4.5***. The experimental set-up consists of three units: model gas generation, reactor and gas analysis systems. The model flue gas of 215 L/h (wet, STP) was generated by mixing three different gas streams. As carrier gas, generally air and/or nitrogen metered by mass-flow controllers (MFC) were used. SO_2 and NO were added to the carrier gas by means of MFCs with a flow rate that the final gas contained the required pollutant concentration. With the second gas stream generated by a MFC controlled air flow, the elemental mercury concentration was introduced by means of a temperature controlled permeation tube (permeator from Breitfuss Messtechnik, Germany). The third gas stream introduced the water vapors in the model flue gas by employing the digital Hovacal system from IAS Schmaeh (Germany). The calculated water mass flow (0.2 g/min) was metered by MFC means and evaporated at 190 °C into a controlled air stream by the Hovacal evaporator. The HCl containing gases were generated by evaporating appropriate solutions of hydrochloric acid.

The honeycomb shaped catalyst samples with 2 × 2 channels and length of approximately 10 cm were placed in a glass reactor consisting of two concentric tubes as depicted in ***Fig 4.6***. Prior to inserting the catalyst test element in the reactor, its outer part was isolated with glass wool, ensuring this way that the simulated gas would flow only through the inner channels

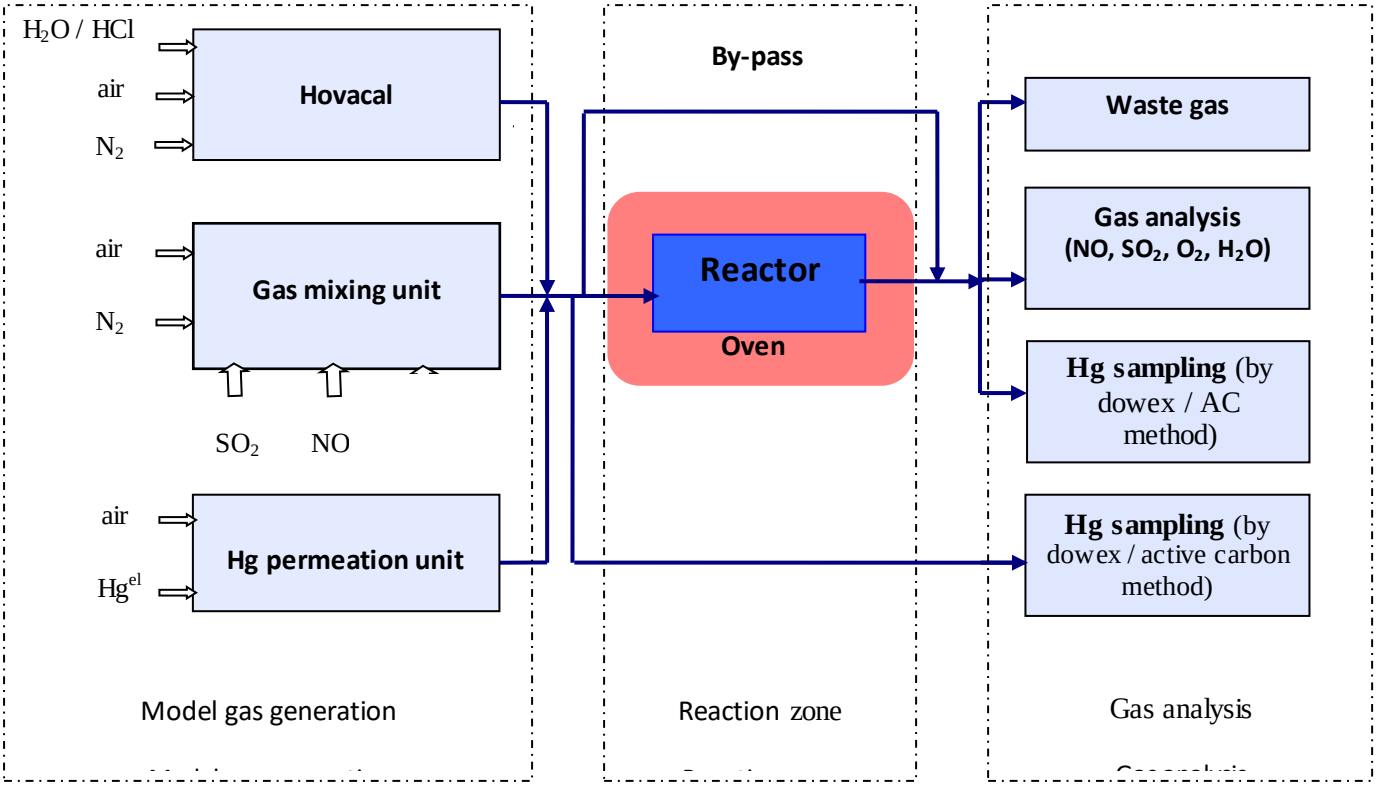

Fig.4.5. *Schematics of the experimental set up employed for Hg^{el} oxidation tests*

The inner tube of the glass reactor has 8 slits through which the model flue gas can pass. Simulated flue gas enters to the outer tube where it is heated to the required experimental temperature. Afterwards, the gas flow is passed through the inner reactor slits and then through the catalyst. The dimensions of experimental glass reactor are summarized in ***Table 4.10***.

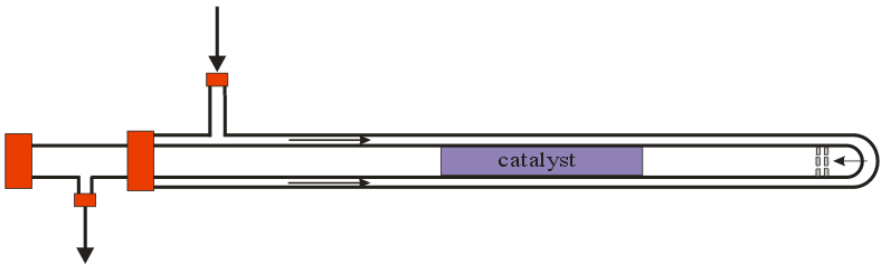

Fig.4.6*. Schematics of experimental reactor*

Table 4.10 *Geometrical dimensions of the experimental reactor*

	Length (mm)	Diameter (mm)	Total length (mm)	Hose connections (mm)
Outer tube	680	40 × 1.5	780	12 × 1.5
Inner tube	740	32 × 1.5		12 × 1.5

Gaseous mercury analysis

In order to determine the mercury oxidation activity of the catalysts, the dry mercury sorbent-trap method was employed [133, 134]. For this purpose, the gaseous mercury was sampled before the inlet of the reactor and at the outlet of the reactor. The mercury gas sampling trains consist of two Dowex /active carbon (AC) traps placed in parallel and heated at 85 °C followed by fritted wash bottle (for trapping the condensed water), pumps, gas counters and O_2 measurement system. The sorbent traps are connected to the experimental set-up by heating tubes kept at 180 °C to avoid deposition of oxidized mercury. In the sorbent traps, a layer of Dowex^{TM} 1 × 8 anionic fine mesh resins (mesh size 100 µm) was followed by a layer of iodized activated carbon pellets. The oxidised Hg was selectively adsorbed by the Dowex layer while the elemental Hg was retained in the activated carbon layer. For each reaction parameter, three gaseous mercury samplings were taken with sampling time of 40 minutes. For each sampling, two Dowex/AC sorbent traps were placed in parallel for reasons of reproducibility. Schematics of the gaseous mercury sampling train are depicted in ***Fig.4.7***, while the list of chemicals and materials employed for this experimental part is given in ***Table 4.11***.

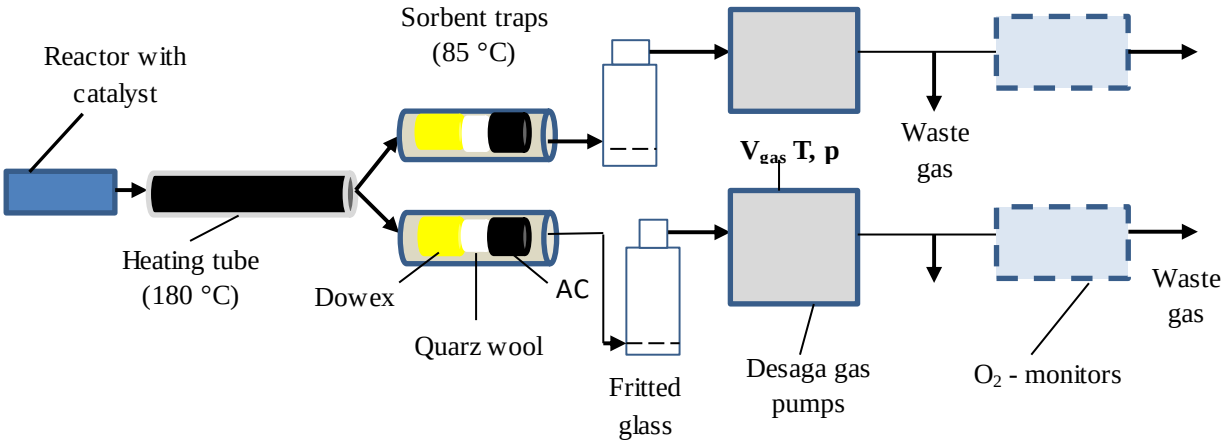

Fig.4.7. *Schematics of the gaseous mercury sampling arrangement*

Table 4.11 *Materials and chemicals employed for sampling of gaseous mercury*

Chemicals/Materials	Producer	Purity	Observations
iodized AC	Carl Roth	95 % Carbon	< 5 % iodine
Dowex 1× 8 resin	Carl Roth		Cl – form
Quartz wool	Carl Roth	p.a	
HCl	VWR	99.98 %	37 %
Deionized water	Own production		≤ 5 µS/cm

Prior to use in the sorbent traps, the Dowex resin was activated in a HCl:H_2O (1:1) mixture at 85 °C for 30 minutes and, then filtered and dried overnight at 120 °C. Activation of Dowex resin by HCl increases the anionic exchanger properties, thereby improving the selective adsorption of Hg^{ox} (more than 98%) [133]. Dowex is a fine mesh resin based on a microporous copolymer of styrene (ST) and divinylbenzene (DVB) with tri-methyl-ammonium as functionalized ionic group. Hg^{ox} is adsorbed on Dowex according to Equation 4.1. Adsorption of $HgCl_2$ on Dowex is temperature limited, with Dowex being unstable at temperatures higher than 150 °C [135].

$$R - N^+(CH_3)_3Cl^- + HgCl_2 \rightarrow R - N^+(CH_3)_3HgCl_3^- \quad (4.1)$$

Iodized activated carbon is an extremely effective medium for adsorbing gaseous Hg^{el} from an air stream. Activated carbon adsorbs Hg^{ox} as well. ***Fig.4.8*** depicts the SEM micrographs of Dowex mesh resin and Activated carbon pellets.

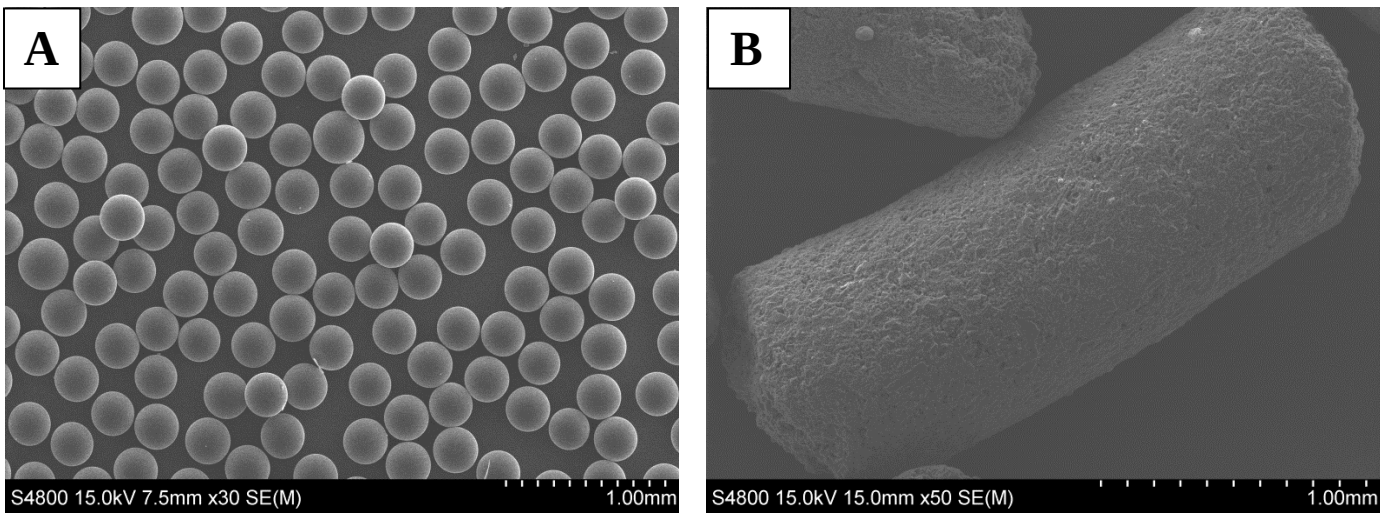

Fig.4.8*. SEM images of Dowex 1 × 8 resin (**A**) and iodized activated carbon pellets (**B**)*

Oxidized Hg is selectively adsorbed by the Dowex layer, while the elemental Hg is adsorbed in the activated carbon layer. The mercury content of Dowex and activated carbon layers was determined by employing the **pyrolytic spectrometer system** from Lumex Ohio (Russia). The system consists of a pyrolytic atomizer PYRO-915 coupled with a Zeeman atomic absorption mercury spectrometer RA-915+ and, permits the direct mercury measurement in the activated carbon and Dowex solid samples. The collected data were used for calculating the mercury oxidation activity ($k_{Hg^{el}/Hg^{ox}}$, in m/h) by employing equation 4.2.

$$k_{Hg^{el}/Hg^{ox}} = -AV \cdot \ln\left(\frac{(1-\eta_{Out})}{(1-\eta_{In})}\right) \tag{4.2}$$

Where, $k_{Hg^{el}/Hg^{ox}}$ is the mercury oxidation activity in a given flue gas (m/h), AV is the area velocity (m/h), $\eta_{Out} = \left(\frac{Hg^{ox}_{Dowex,Out}}{Hg^{el}_{AC,Out} + Hg^{ox}_{Dowex,Out}}\right)$ is the degree of mercury oxidation measured after the catalyst layer, $\eta_{In} = \left(\frac{Hg^{ox}_{Dowex,In}}{Hg^{el}_{AC,In} + Hg^{ox}_{Dowex,In}}\right)$ is the degree of mercury oxidation measured before the catalyst layer (by-pass values), Hg^{ox}_{Dowex} - is the concentration of oxidised mercury measured in the Dowex layer (µg/m^3(STP, dry)), Hg^{el}_{AC} - is the concentration of elemental mercury measured in the AC layer (µg/m^3(STP, dry)). The mercury measurements conducted in by-pass showed that approximately 5 % of the inflow mercury was already in oxidised form. This result is in line with the empty reactor tests (no catalyst present) where 5.3 % of the total mercury was in oxidised state at the outlet of the reactor. Because of the oxidized mercury in the inlet gas, the equation for calculation of the oxidation activity (Equation 4.2) had a bit unusual form compared to the one used elsewhere in the literature [10].

The non-mercury gas components H_2O, SO_2 and NO were continuously measured using a multi component BINOS analysis system from Emerson Process (formerly Leybold-Heraeus GmbH) equipped with a hot (200 °C) photometric cell. A paramagnetic OXYNOS analyser was employed for measuring the O_2 concentration. All of these devices were regularly calibrated with conventional certified reference gases.

4.3.2. DeNOx reaction

DeNOx activity of reference SCR and Au/TiO_2-coated SCR catalysts was determined at temperature of 390 °C and NH_3/NO molar ratios of 1 and 1.2. DeNOx activity was calculated according to the first order reaction equation.

$$k_{DeNOx} = -AV \cdot \ln\left(1 - \frac{\left(NO_{inlet} - NO_{outlet}\right)}{NO_{inlet}}\right), \text{ m/h} \qquad (4.3)$$

The model flue gas was generated by mixing two different gas streams. First stream introduced N_2, SO_2, NO and, NH_3 by means of MFCs, while the second stream introduced water vapours and air by the HovaCal system from IAS Schmaeh (Germany). After exiting the reactor, the model flue gas phase was semi-continuously measured using a multi component BINOS analysis system from Emerson Process (formerly Leybold-Heraeus GmbH) equipped with a hot (200 °C) photometric cell. A paramagnetic OXYNOS analyser was employed for measuring the O_2 concentration. All of these devices were regularly calibrated with conventional certified reference gases. ***Fig.4.9*** depicts the experimental set-up employed for DeNOx tests.

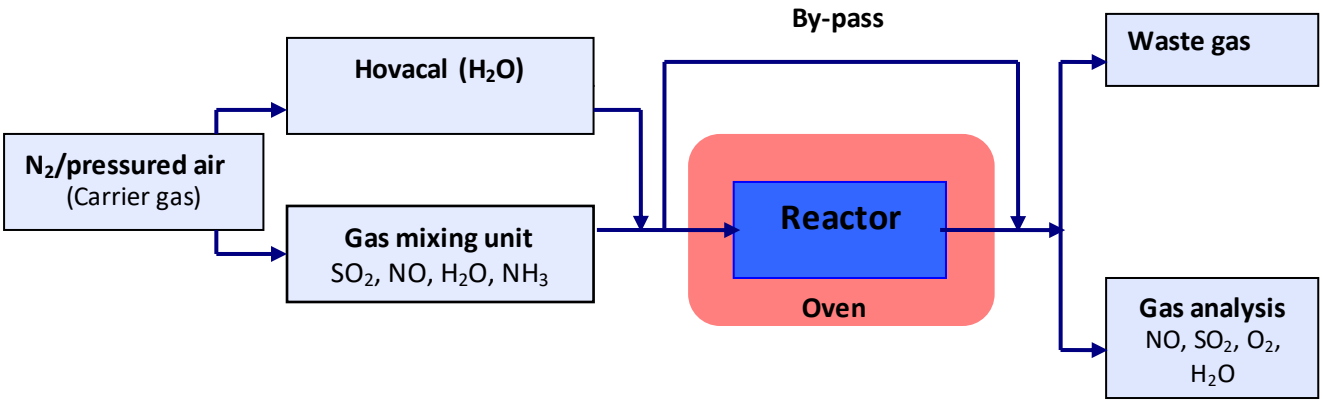

Fig.4.9. *Schematics of the experimental set up employed for DeNOx tests*

4.3.3. SO_2/SO_3 conversion

SO_2/SO_3 conversion investigations were performed with the aim to determine the amount of SO_3 produced over the uncoated SCR catalysts and Au/TiO_2-coated SCR catalysts. The model flue gas was generated by mixing two different gas streams. Nitrogen and pressured air were used as carrier gas. The SO_2 and NO were added to the carrier gas by

means of MFCs with a controlled flow rate so that the concentrations given in ***Table 4.8*** would be reached. A second gas stream introduced water vapour in the model flue gas by employing the HovaCal evaporator system from IAS Schmaeh, Germany. After exiting the reactor, the model flue gas phase was continuously measured in order to determine the SO_2 and NO concentration. An infrared analyzer, HT-Binos 1001 (Rosemount, Germany) was used to measure the SO_2 concentration of the model flue gas. NO concentration was measured by employing the HT-Binos 1004 (Rosemount, Germany). The area velocity (AV) was of approximately 21 m/h.

SO_2 and SO_3 concentrations in the simulated flue gas were measured downstream of the catalyst in accordance with VDI method number 2462 [20]. SO_3 concentration was determined by controlled condensation of sulphuric acid aerosols in a glass condenser at 85 °C.

Prior to the SO_2 to SO_3 conversion tests, the catalyst samples were conditioned for 48 – 72 hours under the model flue gas conditions. After conditioning the catalyst samples, a number of two to three SO_2/SO_3-conversion tests with an elapsed time of at least one hour between the end of one test and start of the next test were conducted. In order to measure the SO_2 to SO_3 conversion rate in the presence of honeycomb catalysts, a gas sampling train was attached to the experimental set-up and connected directly to the reactor. The SO_2/SO_3 sampling train consists of a Graham condenser with glass frit, 3 Desaga sampling glasses and a Desaga pump. Schematics of the experimental set-up are given in ***Fig.4.10***.

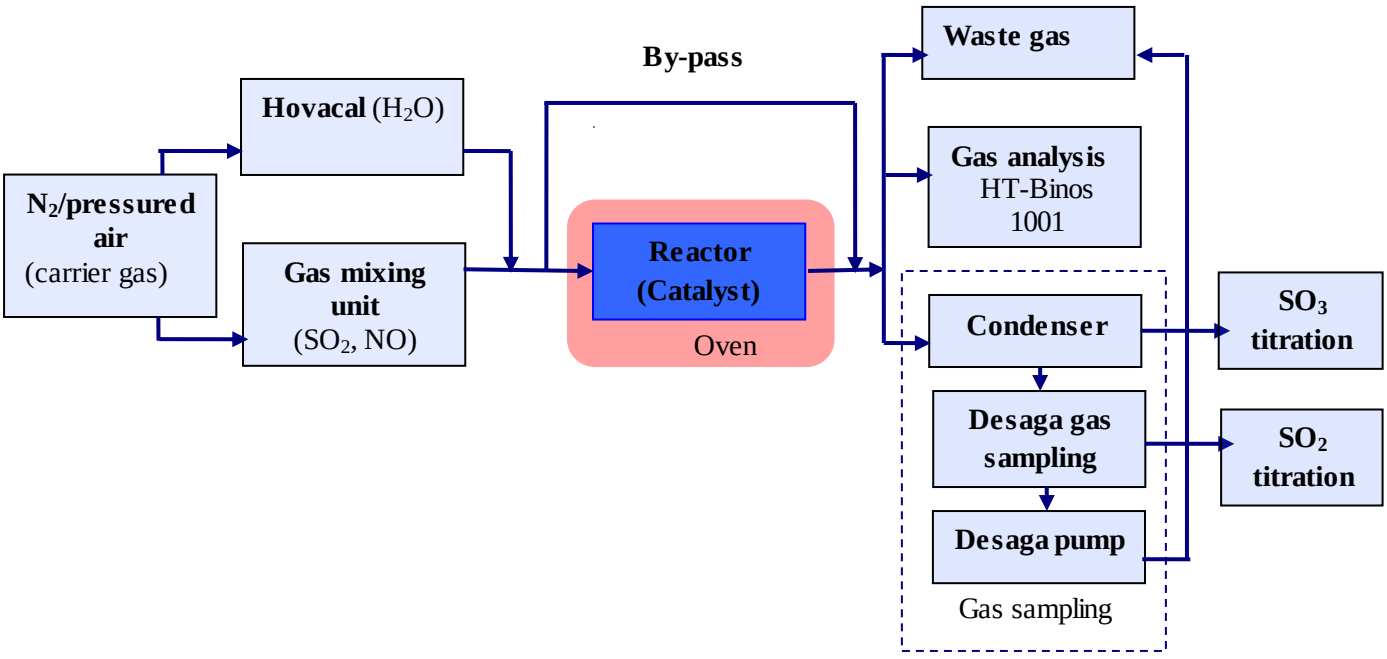

Fig.4.10. *Schematics of the experimental set-up employed for SO_2/SO_3 conversion tests*

The Graham condenser was connected at the outlet of the experimental reactor. The condenser was operated at 85 °C, which is above the water dew point and below the sulfuric acid dew point. Under these conditions, the sulfuric acid aerosols were condensed in the Graham condenser and collected on the glass frit. Desaga gas sampling system was connected to the Graham condenser and a 3 L_N/min model flue gas was sucked through the Graham condenser and the three sampling glass bottles by a Desaga pump. The first two gas sampling bottles were filled with 30 mL water peroxide (3%) each, while the third sampling bottle was used as a condense trap. A total of 120 L model flue gas was sampled for each test. Detailed schematics of the gas sampling train are depicted in ***Fig.4.11***. Materials and chemicals used for SO_2/SO_3 conversion tests are given in ***Table 4.12.***

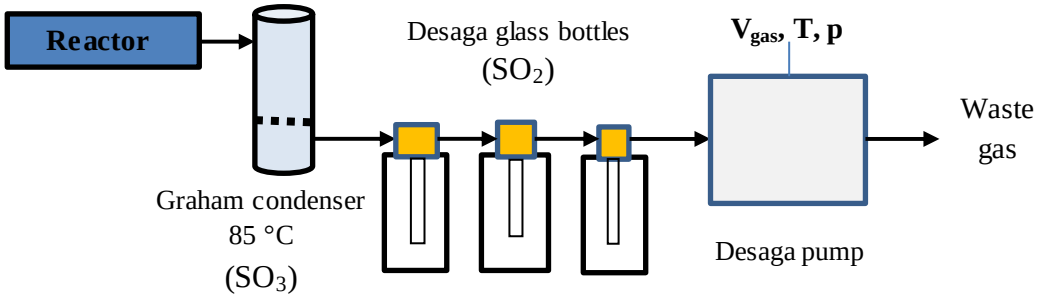

Fig.4.11. *SO_2/SO_3 gas sampling train*

Table 4.12 *Materials and chemicals employed for SO_2/SO_3 conversion tests*

Chemicals/Materials	Producer	Purity	Observations
H_2O_2	Merck	p.a	35 %
NaOH 0.1 M	Sigma Aldrich	p.a	standard solution
$Ba(ClO_4)_2$ 0.005 M	Sigma Aldrich	p.a	in isopropanol/water
$(CH_3)_2CHOH$	Sigma Aldrich	p.a	
Thorin	Fisher	p.a	indicator
Bromphenol	Sigma Aldrich	p.a	indicator
Deionized water	Own production		≤ 5 µS/cm

With: p.a – pro analysis

For SO_3 analysis, the sulfuric acid which was condensed in the Graham condenser is washed out with 50 mL deionized water. The collected liquid sample is then filled in a 250 mL glass and filled until the sign with 2-Propanol. From this solution, 3 samples of 50 mL

each were pipetted in Erlenmeyer glasses. For the determination of sulfuric ion concentration, the as prepared liquid samples were titrated with barium perchlorate (0.005 mol/L) in 2-Propanol-Water 80/20 solution in the presence of a Thorin indicator (3 – 5 drops) by employing a burette with 0.02 mL scale. The addition of barium perchlorate solution was continued until the solution changed its colour from lemon yellow to light pink. The amount of SO_3 in the solution was calculated by employing equation 4.4

$$Y \text{ mg } SO_3 = X \text{ mL } (BaClO_4)_2 \cdot C((BaClO_4)_2) \cdot M(SO_3) \cdot f \qquad (4.4)$$

where: C – concentration of barium perchlorate solution (0.005 mmol/mL)

M (SO_3) – molar mass of sulphur trioxide (M = 80.0642 mg/mmol)

f – sample factor (from 250 mL solution, 50 mL are taken for each titration → 250/50 = 5)

For the analysis of SO_2 concentration in the gas, the liquid (H_2O_2 3 vol.-%) is transferred from the Desaga sampling glasses into a 200 mL glass and filled until the sign with distilled water. From this solution, 3 samples of 20 mL each were filled in Erlenmeyer glasses. The acid-base titration of the solution was performed with NaOH solution 0.1 M and in the presence of Bromphenol blue indicator (3 - 4 drops). The addition of NaOH 0.1 M was continued until the solution changed its color from yellow to violet blue, the color change takes place in the 3.0 – 4.6 pH-range. Equation 4.5 was used to calculate the amount of SO_2 in the sample and consequently in the model flue gas.

$$Y \text{ mg } SO_2 = X \text{ mL } (NaOH) \cdot C(NaOH) \cdot M(SO_2) \cdot f \qquad (4.5)$$

where: C (NaOH) – concentration of sodium hydroxide solution (0.1 mmol/mL)

M (SO_2) – molar mass of sulphur dioxide (M = 64 mg/mmol)

f - sample factor (from 200 mL solution, 20 mL are taken for each titration → 200/20 = 10 · 0.5 = 5)

The SO_2 to SO_3 conversion rate (K_{SO_2/SO_3}) was calculated with equation 4.6:

$$K_{SO_2/SO_3} = \frac{C_{SO_3}[ppm]}{\left(C_{SO_2}[ppm] + C_{SO_3}[ppm]\right)} \cdot 100, (\%) \qquad (4.6)$$

CHAPTER 5

Preparation and characterization of Au/TiO_2-coated SCR-DeNOx catalysts

In this chapter, the different stages involved in the preparation of Au/TiO_2-coated SCR catalysts are discussed in detail. Firstly, the synthesis and characterization of powdered Au/TiO_2 catalysts is discussed. The chemistry of the Au-based solution is of great importance for obtaining gold nano-particles coated on the support (TiO_2). The catalyst powders were further employed for the preparation of Au/TiO_2 based suspensions. Therefore, a detailed discussion on the quality and properties of the as prepared suspensions follows. In the last part of the chapter, the preparation and characteristics of Au/TiO_2-coated SCR-DeNOx monolithic catalysts are given in detail.

5.1. Synthesis and characterization of Au/TiO_2 catalyst powders

5.1.1. Chemistry of Au-based solution

The Au/TiO_2 catalysts powders were synthesized by employing the deposition precipitation method [102, 136]. The deposition-precipitation method involves dissolving $HAuCl_4 \cdot 3H_2O$ in distilled water, carefully adjusting the solution's pH and then adding the TiO_2 powder which acts as support for the Au from the solution. During maturation at 70 °C and pH higher than 7, all Au^{3+} complexes found in the solution become strongly attached to the TiO_2 particles surface [137]. At room temperature and a pH value $\leq$ 2, the main species

found in an aqueous solution is $AuCl_4^-$. Above pH 6, the $AuCl_4^-$ ions found in solution are hydrolyzed to $AuCl_{4-x}(OH)_x$ species (with x = 1 ÷ 3) [136], while at pH value higher than 8, the completely hydrolyzed $Au(OH)_4^-$ ion is the predominant species [138]. The extent of hydrolysis in aqueous hydrogen tetrachloroaurate solution is pH and temperature dependent. At room temperature, the following reactions occur in the solution [138]:

$$[AuCl_4]^- + H_2O \Leftrightarrow [AuCl_3(H_2O)] + Cl^- \quad (5.1)$$

$$[AuCl_3(H_2O)] \Leftrightarrow [AuCl_3(OH)]^- + H^+ \quad (5.2)$$

Once with increasing the pH and temperature of the solution, the concentration of $AuCl_4^-$ decreases, leading to the formation of different hydrolyzed gold species:

$$[AuCl_3(OH)]^- + H_2O \Leftrightarrow AuCl_2(H_2O)(OH) + Cl^- \quad (5.3)$$

$$AuCl_2(H_2O)(OH) \Leftrightarrow [AuCl_2(OH)_2]^- + H^+ \quad (5.4)$$

$$[AuCl_2(OH)_2]^- + H_2O \Leftrightarrow [AuCl(OH)_3]^- + H^+ + Cl^- \quad (5.5)$$

$$[AuCl(OH)_3]^- + H_2O \Leftrightarrow [Au(OH)_4]^- + H^+ + Cl^- \quad (5.6)$$

Since it is known that the pH control is critical in determining the gold particle size [136, 138], the solution's pH was closely monitored by employing the ***WTW pH / Cond 340i*** pH-meter with SenTix® 41 sensor. During the heating process, the pH value dropped to 5, requiring further addition of NH_4OH 0.1 M to readjust the solution's pH to 7 – 8. The addition of TiO_2 support to the hydrogen tetrachloroaurate solution causes a slight pH drop, requiring further addition of NH_4OH 0.1 M. In order to avoid local high concentrations of precipitating agent which may lead to the precipitation of $Au(OH)_3$ in the solution, the pH adjustment was done by adding small quantities of NH_4OH 0.1 M solution.

After maturating for 1 hour at 70 °C, the suspension was filtered so that the solid (Au/TiO_2 catalyst) was separated from the liquid phase. Since it is believed that the presence of residual chlorine in the catalysts causes the gold nanoparticles to form large agglomerates during drying and calcination processes, several washings were performed. A clear liquid resulted after filtration and washing steps was analyzed to determine the Cl^- and Au contents. The chloride content in the clear liquid resulted after filtration and washing was determined by employing the ***Corning Chloride Analyzer 926***.

Fig.5.1 depicts the chloride content analysis of the clear liquids resulted after filtration and washing of 1 and 2 wt.-% Au/TiO_2 catalysts. A significant amount of Cl^- was removed during vacuum filtration process, which it varied with the initial concentration of $HAuCl_4$ solution. The measurements show that the chloride content drops with each washing step. Based on these results it can be stated that the chlorine is successfully removed from the Au/TiO_2 catalysts only after, at least, four washings are performed.

Gold contents of the filtration and washing liquids were determined by means of Inductively Coupled Plasma Mass Spectroscopy (ICP-MS) according to DIN EN ISO 11885 protocol on an ***Elan DRC II system*** (Perkin Elmer) with detection limit of 0.01 mg/L. The results of quantitative analysis, carried out by ICP-MS means are given in ***Table 5.1***. The initial hydrogen tetracloroaurate solution has a calculated theoretical gold content of 402.4 mg/L. Following the addition of TiO_2 to the hydrogen tetracloroaurate solution, the gold content of the solution dramatically decreases due to the strong interaction of gold with the surface of TiO_2 particles. This strong gold-TiO_2 interaction is proven by the low gold content of the clear liquid after filtration. Further washing the Au/TiO_2 catalysts with hot water caused the removal of an even lower amount of gold from the catalyst.

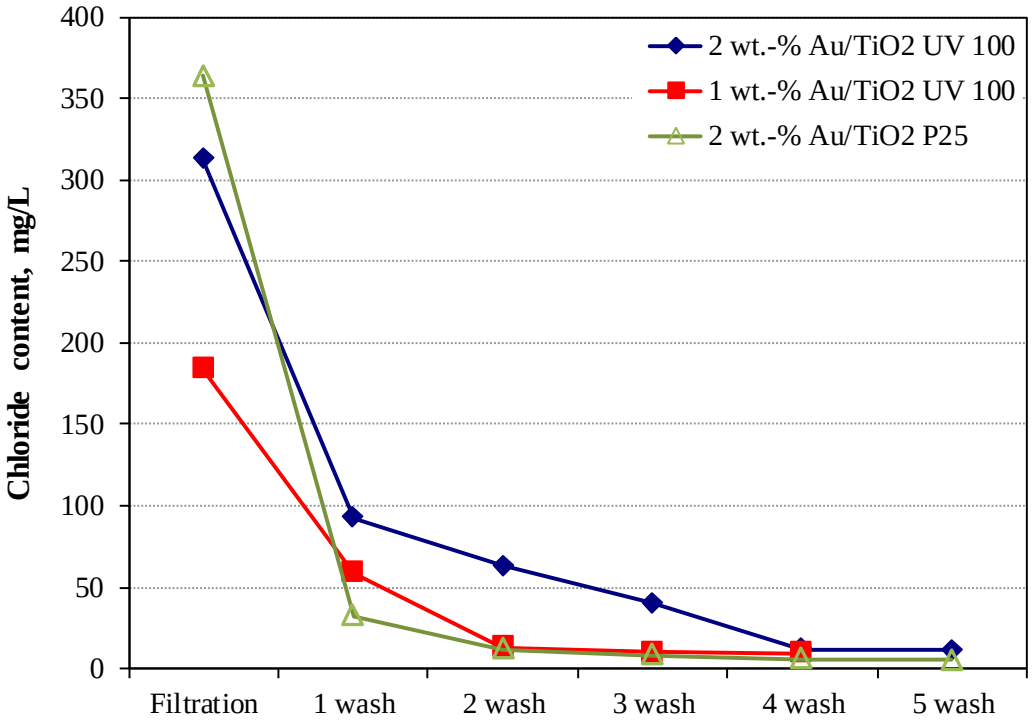

Fig. 5.1. *Chloride content in the filtrate and washing liquids for 1 and 2 wt% Au/TiO_2 catalysts*

Table 5.1 *Gold content analysis of clear liquid after filtration and washing of 2 wt.-% Au/TiO_2 P25 catalysts*

Theoretical Au content in the initial solution (mg/L)	Au content in the liquid after filtration (mg/L)	Au content in the liquid after 5 washings (mg/L)
402.4	0.656	0.132

5.1.2. Physical-chemical characterization of Au/TiO_2 powdered catalysts

The physical-chemical properties of a catalyst are of great importance for its future catalytic activity. Therefore, several characterization methods, including DR-UV-Vis, SEM, XRD and, EDX were employed with the aim of obtaining a better insight into the physical-chemical characteristics of the as prepared nano-Au/TiO_2 catalyst powders. The results of these investigations are briefly discussed below.

5.1.2.1. Diffuse reflectance UV-Vis (DR UV-Vis) analysis

Fig. 5.2 depicts the DR-UV-Vis spectra for TiO_2 powders and 2 wt.-% Au/TiO_2 catalysts calcined at 400 °C in air flow for 4 hours. Au/TiO_2 catalyst samples exhibit a shift in the absorption spectrum with a broad band located at around 550 nm, caused by the presence of Au nanoparticles in the catalyst matrix. This band gap appears due to surface plasmon resonance (SPR) of the metallic nano-gold particles with dimensions higher than 5 nm [139].

Some authors [140, 141] suggest that these band gaps are the result of collective oscillations of free conduction-band electrons induced by interactions with incident electro-magnetic radiation whose wavelength is higher than the size of Au particles. Therefore, the position, size and shape of the SPR band are caused by several factors, such as size, shape and surface area of Au nanoparticle, gold loadings and interaction of Au particles with the TiO_2 support [142]. It has been proposed in the literature that the band gap from 520 to 680 nm is generated by the presence of gold particles with dimensions between 5 and 80 nm. Moreover, the as-prepared Au/TiO_2 catalyst samples are purple in colour, which is consistent with the specific adsorption characteristics of Au nano-particles. The 190 – 350 nm band gaps are characteristic to the TiO_2 supports.

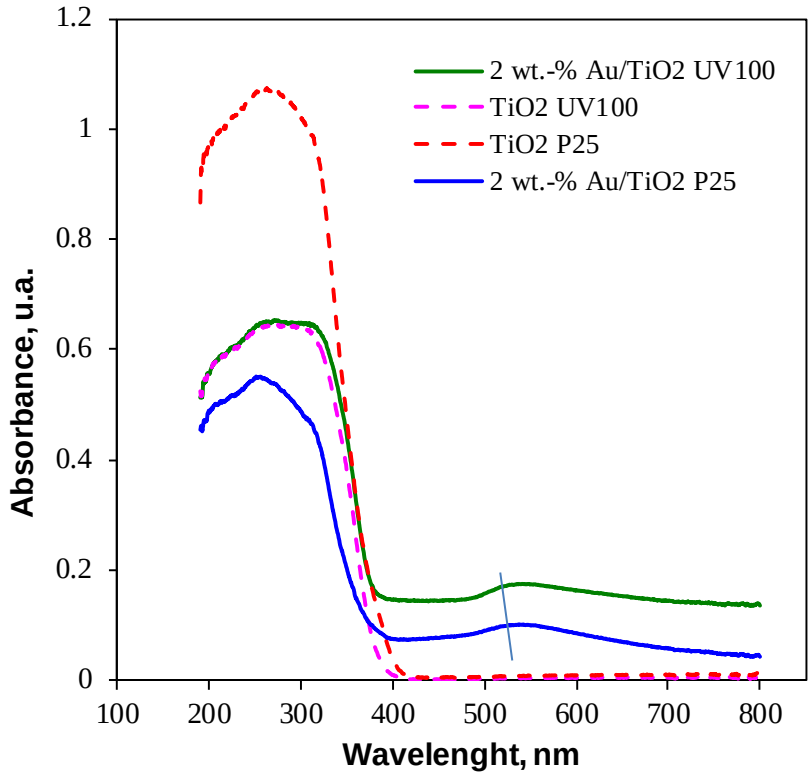

Fig. 5.2 *DR-UV-Vis spectra for TiO_2 and 2 wt.-% Au/TiO_2 catalyst powders prepared by deposition precipitation method*

5.1.2.2 X-ray diffraction (XRD) analysis

X-ray diffractograms (XRD) were obtained for the 1 and 2 wt.-% Au/TiO_2 (P25 and Hombikat UV100) catalysts prepared by deposition-precipitation method. Calcined and uncalcined catalysts samples were investigated as well. The purpose of this study was to identify the crystalline phases (gold, TiO_2 anatase and rutile) and, to determine the influence of calcination process on the gold particles (reduction of Au^{3+} to Au^0) and on the TiO_2 substrate (possible phase transformation from anatase to rutile which might occur at high calcination temperatures). ***Fig.5.3*** and ***Fig.5.4*** depict the XRD patterns of 2 wt.-% Au/TiO_2 P25 catalyst calcined and uncalcined. Both XRD patterns display similar diffraction peaks characteristic to anatase and rutile phases found in the commercially available TiO_2 P25, suggesting that the TiO_2 support remained stable during the precipitation of gold and calcination process. This aspect is clearly observed in the XRD patterns of uncalcined and calcined 2 wt.-% Au/TiO_2 UV100 catalysts as well, where only the TiO_2 anatase characteristic peaks appear (see ***Appendix 5.1***). The TiO_2 Hombikat UV100 powder is made

exclusively of anatase phase as mentioned by the producer (see product information on www.sachtleben.de).

The XRD patterns of uncalcined Au/TiO_2 P25 samples show no characteristic peaks for crystalline gold. However, the XRD patterns reveal the presence of two crystalline phases attributed to TiO_2 anatase and TiO_2 rutile. The absence of gold characteristic peaks can be attributed to the presence of very small and highly dispersed gold particles (less than 5 nm) or to the presence of non-crystalline gold (Au^{3+}) which could not be detected by XRD analysis [141]. Following the calcination process at 400 °C, Au^{3+} is reduced to metallic Au^0. At high calcination temperatures gold particles tend to agglomerate forming gold clusters. Both calcined Au/TiO_2 catalysts samples display the characteristic diffraction peaks of gold at 2θ angle: 38.1; 44.4; 64.5; 77.4; 82; 98.1; 110.8 and 115 assigned to different planes of the face centered cubic (FCC) crystalline gold (1 1 1), (2 0 0), (2 2 0), (3 1 1), (2 2 2), (4 0 0), (3 3 1) and (4 2 0) according to the JCPDS card No. 01-1174.

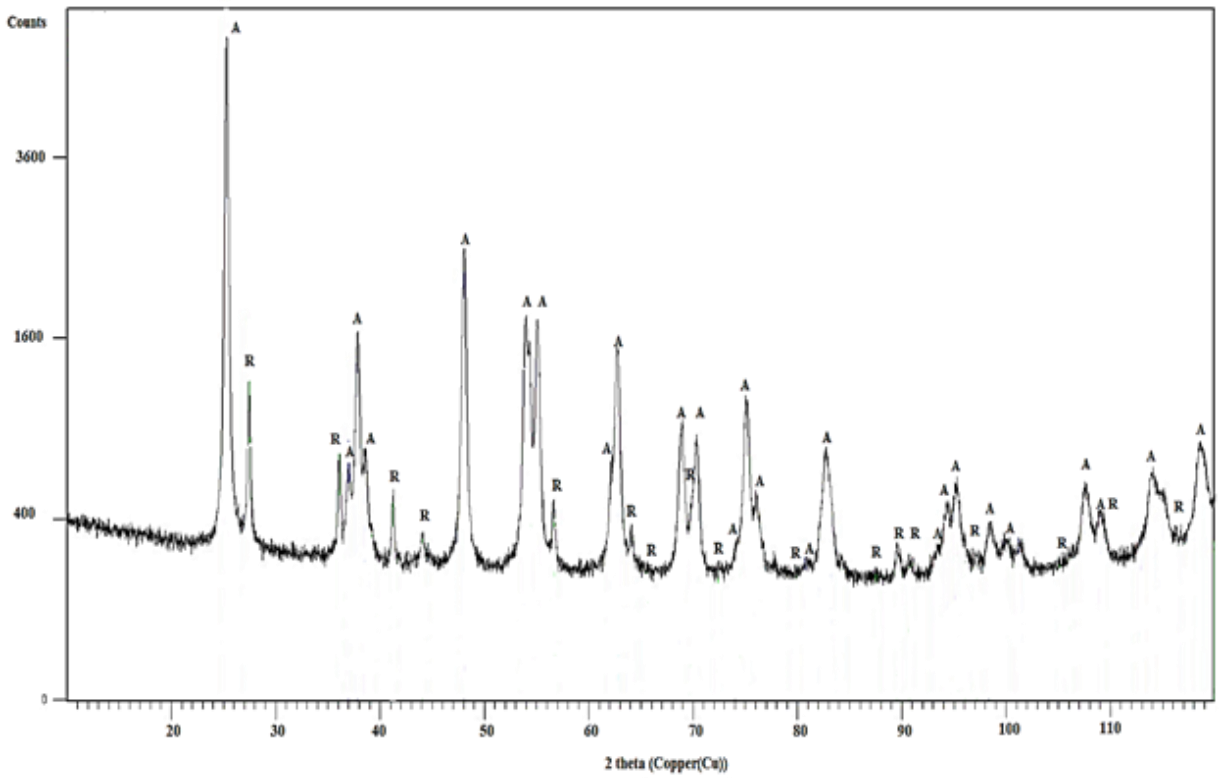

Fig.5.3. *XRD patterns for 2 wt.-% Au/ TiO_2 P25 uncalcined sample (where: A – anatase; R – rutile)*

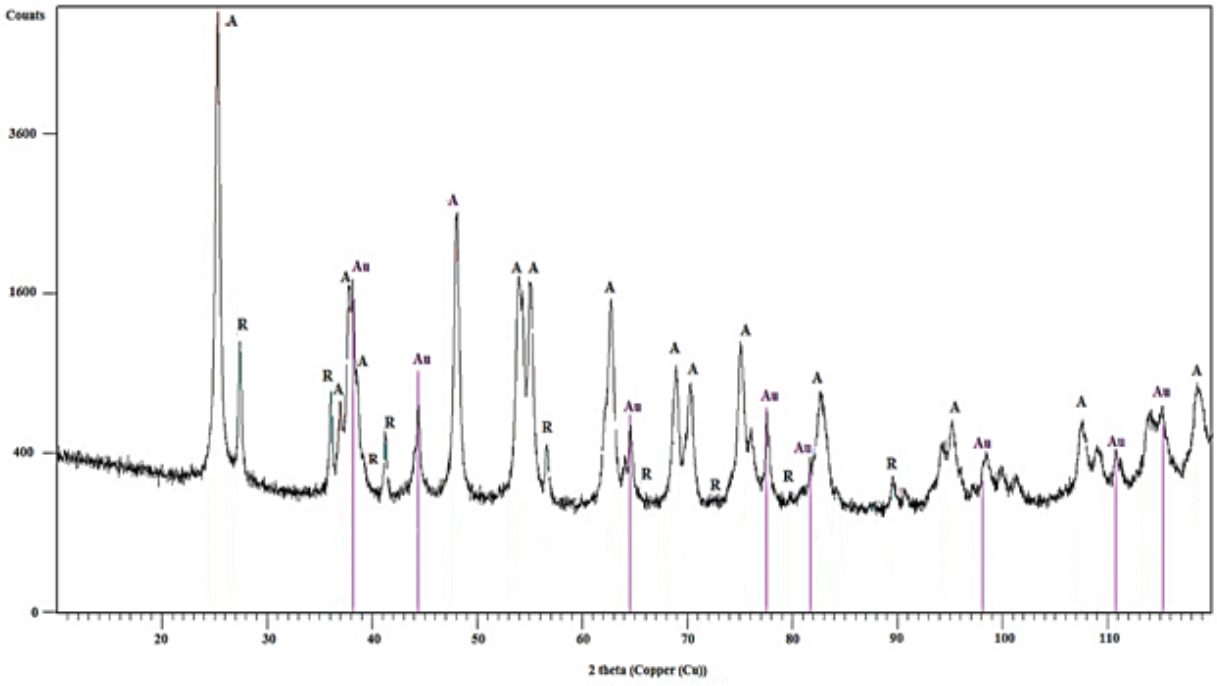

Fig.5.4. *XRD patterns for 2 wt.-% Au/ TiO_2 P25 calcined sample (where: A – anatase; R – rutile; Au – gold)*

5.1.2.3. Elemental composition by Energy dispersive analysis of the X-Rays (EDX)

The elemental composition of 2 wt.-% Au/TiO_2 (TiO_2 P25 and TiO_2 UV100) catalyst powders was determined by employing energy dispersive analysis of X-ray method. The overall results concerning the elemental composition of the 2 wt% Au/TiO_2 calcined catalysts are summarized in ***Table 5.2***, while the EDX spectra of the catalysts are depicted in ***Fig.5.5***. The gold content at the surface of Au/TiO_2 P25 and Au/TiO_2 P25 UV100 catalysts samples are 2.34 wt.-% and 2.26 wt.-%, respectively. These values are similar to the calculated values of Au in the final catalyst. The EDX spectra of Au/TiO_2 powdered catalysts display the characteristic peaks of titanium, oxygen, aluminum and, gold elements.

Table 5.2 *Elemental composition of 2 wt% Au/TiO_2 catalysts determined by EDX analysis*

Elemental composition / Sample type	Au (wt.-%)	Ti (wt.-%)	O (wt.-%)	Al (wt.-%)
2 wt.% Au/TiO_2 P25	02.34	67.48	29.07	01.10
2 wt.% Au/TiO_2 UV100	02.26	79.74	16.80	01.20

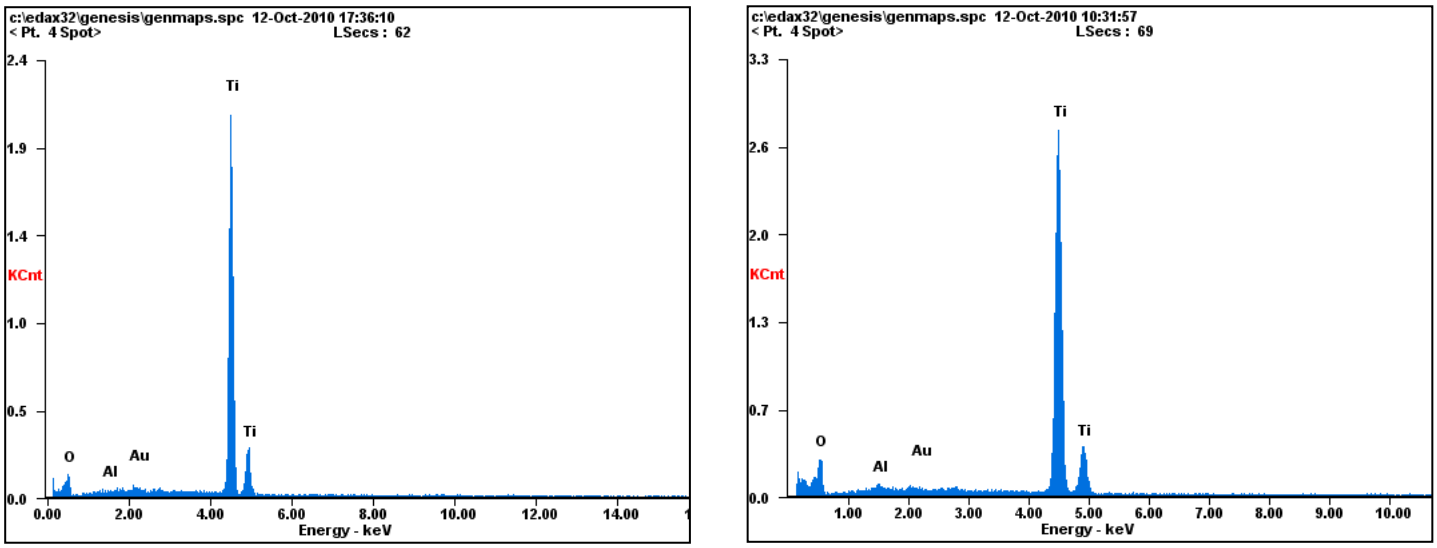

Fig.5.5. *EDX spectra for 2 wt.-% Au/TiO_2 P25 (left) and 2 wt.-% Au/TiO_2 UV100 (right) catalyst*

5.1.2.4. Field Scanning electron microscopy (FE-SEM) analysis

Field Scanning Electron Microscopy was employed to identify the morphological characteristics of the 2 wt.-% Au/TiO_2 catalyst powders and of the TiO_2 substrates (P25 and Hombikat UV100). FE-SEM images of TiO_2 P25 and 2 wt.-% Au/TiO_2 P25 catalysts powders are given in ***Fig 5.6***. Commercially available titanium dioxide (P25 and Hombikat UV100), employed as supports for the synthesis of Au/TiO_2 catalysts consists of tightly packed aggregates composed of primary particles with sizes ranging from 1 to 300 nm.

The washing, drying and calcining procedures applied to Au/TiO_2 catalysts led to the formation of agglomerates with sizes in the micrometer range. This was confirmed by SEM characterization of Au/TiO_2 catalysts powders. The TiO_2 P25 support and the 2 wt.-% Au/TiO_2 P25 catalyst powders exhibit similar sponge like morphology, where the TiO_2 primary particles are strongly packed forming agglomerates in the micrometer range. In the micrograph images of the Au/TiO_2 catalysts, relatively large gold crystallites are visible. These crystallites were formed at the high calcination temperature due to sintering of small gold particles. Similar results were observed on the SEM micrographs of 2 wt.-% Au/TiO_2 Hombikat UV100 catalysts (see ***Appendix 5.2***).

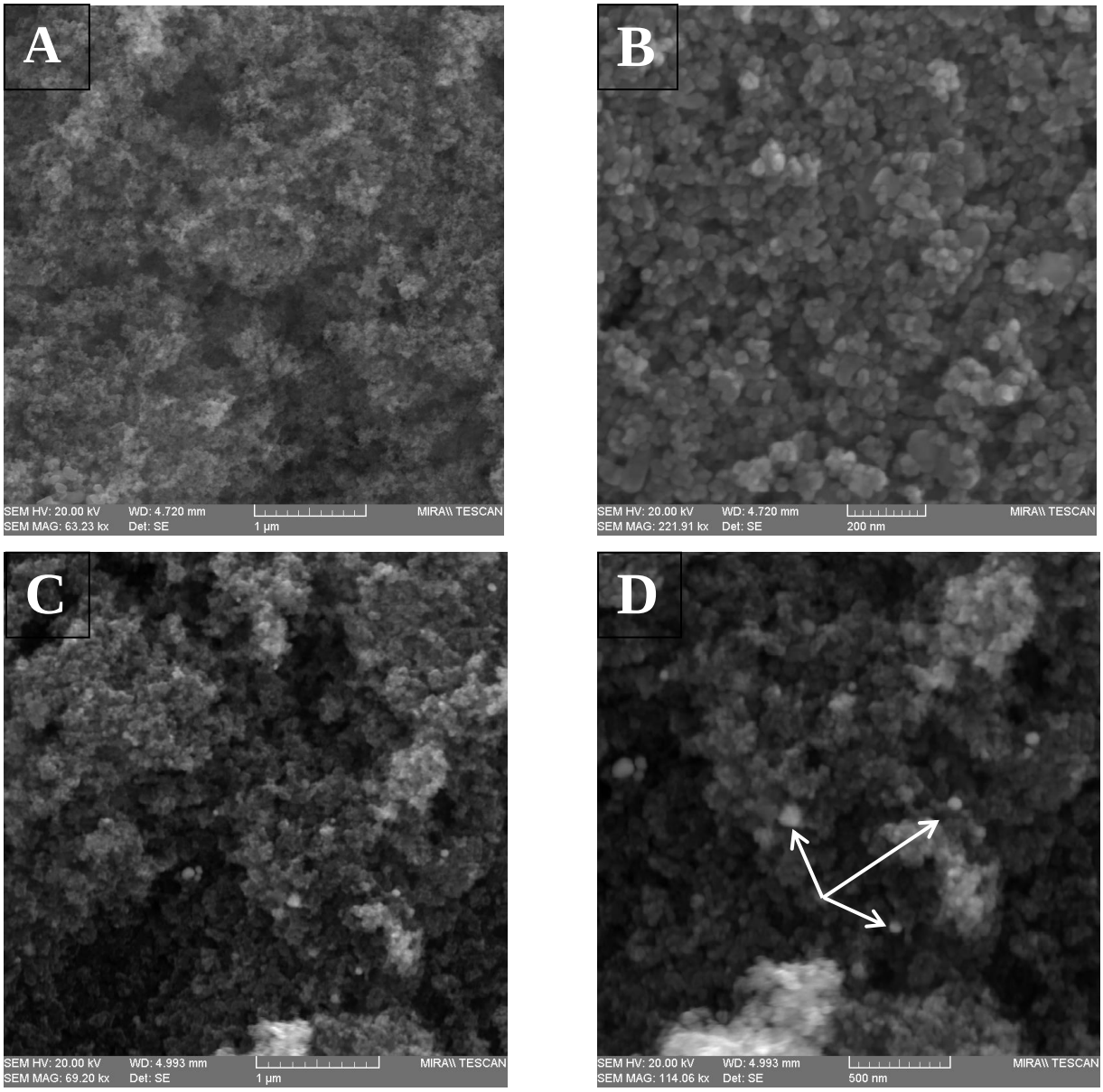

Fig.5.6. *Scanning electron micrographs for:* ***A*** *and* ***B*** *– TiO_2 P25;* ***C*** *and* ***D*** *– 2 wt.-% Au/ TiO_2 P25 calcined catalyst.*

5.2. Preparation and characterization of stable Au/TiO_2 suspensions

Two different types of Au/TiO_2-based suspensions (noted Type I and Type II) were prepared according to the methods described in ***Chapter 4, section 4.1.2***. Type I suspensions were prepared by employing Au/TiO_2 catalyst powders which were dispersed in an aqueous medium and stabilized by the addition of a dispersing agent, namely ammonium polyacrylate (NH_4-PA). Type II suspensions were obtained by dissolving in deionized water a calculated amount of $HAuCl_4 \cdot 3H_2O$ to obtain 1 and 2 wt% Au in the final catalysts and, carefully adjusting the pH to 7 – 8. The TiO_2 support in the form of Aerodisp W 740 X stable

suspension with 40 wt.-% solid content was added to the gold solution. During the maturation period, the gold from the solution was coated on the TiO_2 particles surface. The following sections present and discuss the results on the stability and properties of the as-prepared suspensions.

5.2.1. Stability and properties of Au/TiO_2-based suspensions

Rheological properties, particle size distribution in the suspension, and iso-electric point of the dispersed particles are indicative of the suspension's stability and characteristics. Also, the properties of suspension directly influence the quality and catalytic activity of the coated Au/TiO_2 layers obtained by employing the respective suspension for coating purposes.

5.2.1.1. Iso-electric point (IEP) of Au/TiO_2-based suspensions

A typical measurement of zeta potential variation as a function of pH value for the 2 wt.-% Au/TiO_2 Type I and II based suspensions with 2 wt.-% solid content is plotted in **Fig.5.7**. The zeta potential was measured in the 1.5 ÷ 9 pH-ranges. By analyzing the zeta potential values, it was possible to identify the iso-electric point of the dispersed particles. Isoelectric point (i.e.p) is the pH value where the zeta potential is zero. At the i.e.p there are no electrostatic repulsive forces in the system, such that the van der Waals forces are totally dominant and the particles tend to agglomerate [143]. The isoelectric point for Type I suspensions was identified at pH 2.2, while the isoelectric point of Type II suspensions was found at pH 3.6 – 4.1. This scatter in isoelectric point values can be attributed to the different methods employed for preparation as well, to the different dispersing agents employed. Even though the producer of Aerodisp suspension does not give detailed information regarding the dispersing agents employed for stabilizing the TiO_2 particles, it is safe to assume that there is a significant difference in terms of composition between the own-made TiO_2 suspensions and the commercially available Aerodisp suspension. It has to be noted that the isoelectric point values for suspended TiO_2 particles reported in the literature vary greatly, ranging from pH 2 up to 8.9 [144, 145, 146]. These differences are mainly due to TiO_2 modifications (i.e. anatase, rutile etc), the presence of impurities on the TiO_2 particles surface, dispersing medium and dispersing agents employed for suspensions preparation.

Based on the zeta potential results depicted in ***Fig.5.7***, it could be concluded that for Type I suspensions stabilized by addition of 0.35 wt.-% NH_4PA a stable region occurs in the 4 – 9 pH range, where the measured zeta potential was between - 35 and - 50 mV. For the case of Type II suspensions, the stable plateau starts at pH 6 with zeta potential values between -

30 and - 40 mV. Type II suspensions were stable at pH value lower than 2 as well, with zeta potential of dispersed particles higher than + 30 mV. Zeta potential for 1 wt.-% Au/TiO_2-based suspensions exhibits a similar trend as the measured values for 2 wt.-% Au/TiO_2 –based suspensions (see ***Appendix 5.3***).

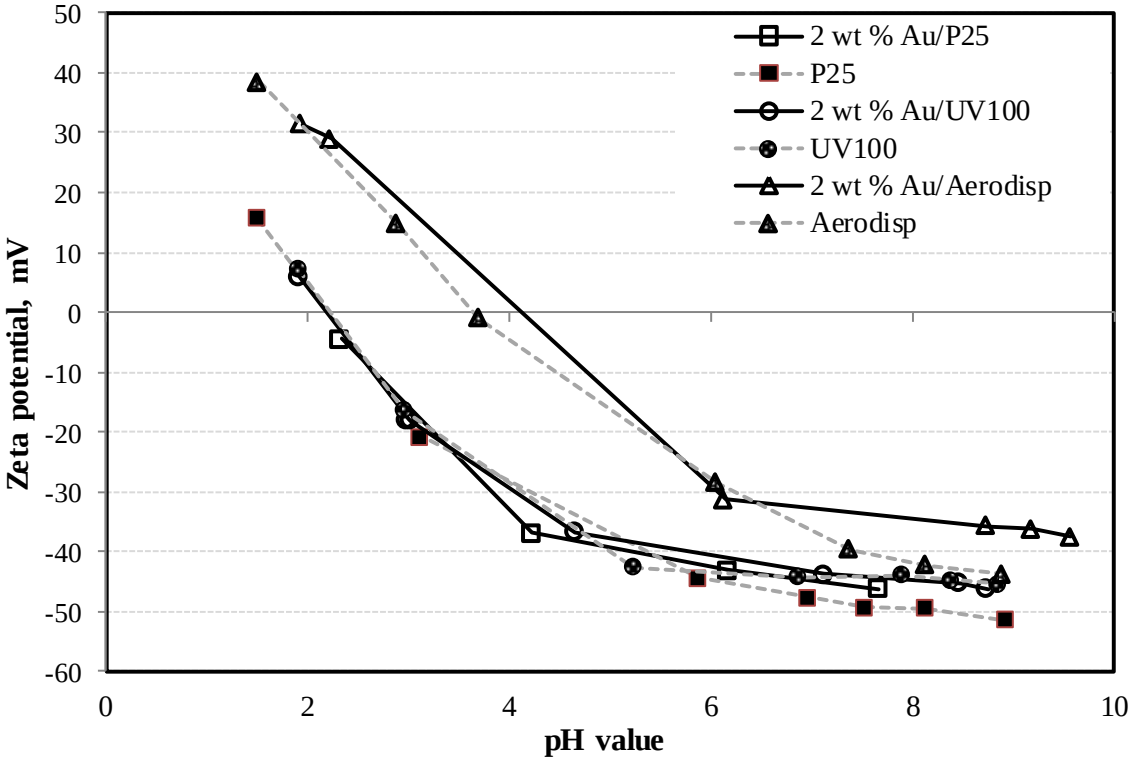

Fig.5.7. *Zeta potential versus pH-value for type I and type II suspensions with 2 wt.-% solid content*

5.2.1.2. Particle size distribution and viscosity of the Au/TiO_2 suspensions

Table 5.3 presents the measured viscosities and particle size distribution by intensity and volume for all types of suspension studied. All the suspensions exhibit similar rheological properties, with viscosities between 1.61 and 1.72 mPa·s at the selected measurement conditions (30 °C and 100 s^{-1} shear rate). However, the particles size distribution in the suspensions varies with the type of TiO_2 support and gold loadings of the catalysts. The presence of Au nanoparticles alters the size distribution of the TiO_2 supports. ***Fig.5.8*** shows how the size distribution changes from unimodal (for TiO_2 and 1 wt.-% Au/TiO_2) to bimodal once the Au content increases to 2 wt.-%. The particle size distribution by intensity for 2 wt.-% Au/TiO_2 P25 suspensions was bimodal with the small and large particle peaks located at

183 nm and 2360 nm, respectively. Details on the particle size distribution by intensity measured for Type I and Type II suspensions are given in ***Appendix 5.5***.

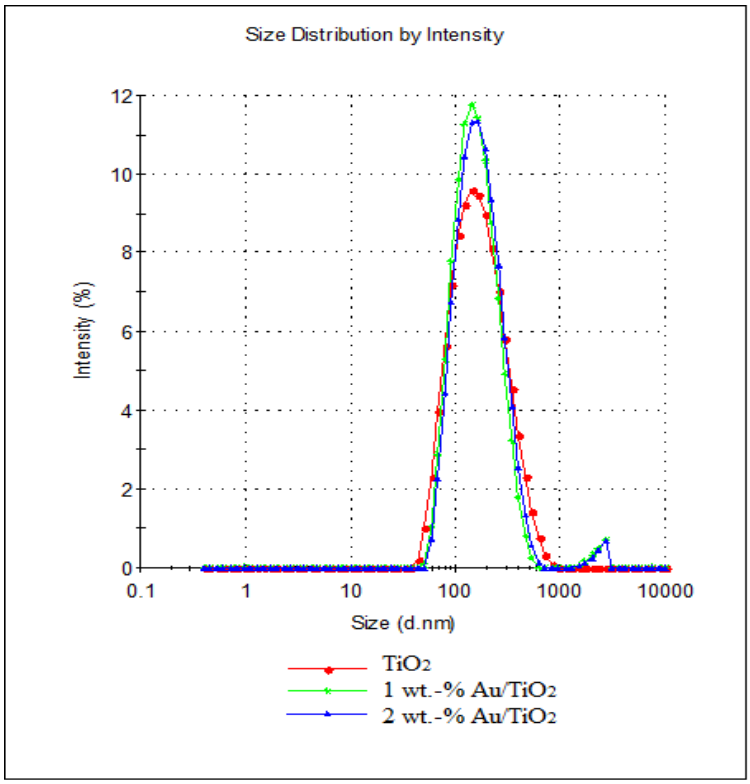

Fig.5.8. *Particle size distribution by intensity in the Type I suspensions Au/TiO_2 P25 (by DLS means)*

For the dispersed Au/TiO_2 UV100 particles, the size distribution by intensity was unimodal with peaks at 589 nm (2 wt.-% Au/TiO_2 UV100 suspension) and 629 nm (1 wt.-% Au/TiO_2 UV100 suspension), while the dispersed TiO_2 UV100 exhibits a bimodal distribution. These results clearly show that probe sonication performed for Type I suspensions did not lead to a complete breakage of Au/TiO_2 aggregates down to their primary size (lower than 50 nm), results which are similar to those reported in previous works [144, 145]. A similar trend was observed for the case of 1 wt.-% Au/Aerodisp dispersion where bimodal distributions were observed with low and high intensity peaks at 13 nm and 175 nm, respectively. It must be noted that the average particle size of Type II suspension Au/Aerodisp are considerably smaller than that ofType I suspensions.

Table 5.3 *Average particles size distribution and viscosities of Au/TiO_2 suspensions*

Suspension	Mean particles size by intensity (nm)		Mean particles size by volume (nm)		Viscosity (mPa·s)
	Peak 1	Peak 2	Peak 1	Peak 2	
Type I					
2 wt.-% Au/P25	(183)*	(2360)*	-	-	1.62
1 wt.-% Au/P25	496 (181)*	-	460	-	1.61
TiO_2 P25	378 (190)*	-	383	-	1.70
2 wt.-% Au/UV100	589	-	573	-	1.73
1 wt.-% Au/UV100	629	-	498	735	1.72
TiO_2 UV100	130	761	1320	817	1.64
Type II					
2 wt.-% Au/Aerodisp	-	-	-	-	1.62
1 wt.-% Au/Aerodisp	13	175	14	-	-
TiO_2 Aerodisp	148	-	150	-	1.63

*values in brackets were obtained by dynamic light scattering (DLS) means

5.3. SCR-DeNOx monoliths coated with thin Au/TiO_2 layers

The Au/TiO_2 coated SCR-DeNOx monolithic catalysts were prepared by employing the dip-coating procedure described in ***chapter 4.1.3.*** ***Fig.5.9*** depicts the calculated mass of Au/TiO_2 coated on the surface of the SCR-DeNOx monolithic catalysts. Whereas ***Fig. 5.10*** gives a visual impression of the colour change caused by the coating. The mass of Au/TiO_2 coatings was determined by weighing the SCR monoliths before and after dip-coating procedure. The mass of Au/TiO_2 was calculated as follows: $m_{coating} = m_{coated_SCR} - m_{uncoated_SCR}$

By dip-coating the SCR monoliths in Au/TiO_2 suspensions with 2 wt.-% solid content, a very low amount of Au/TiO_2 was coated on their surface, leading to the formation of a very thin layer on the surface of the SCR catalysts. This was specifically designed so that the thin Au/TiO_2 layer would increase the activity towards Hg^{el} oxidation reaction without hindering the initial catalytic activity of the SCR monolithic substrate. It can be observed that the coatings obtained by employing type I Au/TiO_2 P25 suspensions have the lowest mass,

whereas the type II Au/TiO_2 Aerodisp suspensions led to a significantly higher mass of the coated layers. One could explain these results by relating to the suspensions stability and particles size distribution. For instance, the Aerodisp based suspensions exhibit a higher stability with relatively small particles, therefore it is assumed that the smaller particles enter the porous structure of the SCR catalyst hence the higher mass of the coated Au/TiO_2 layer. The particles in type I suspensions form agglomerates which cover only the outer surface of SCR catalyst, causing a much lower amount of Au/TiO_2 to be coated. The specific geometrical surface coverage (in µg $Au/TiO_2/mm^2$ of SCR surface) was calculated by employing the mass of Au/TiO_2 coating and the geometrical surface of the SCR samples. The results are given in ***Appendix 5.6***.

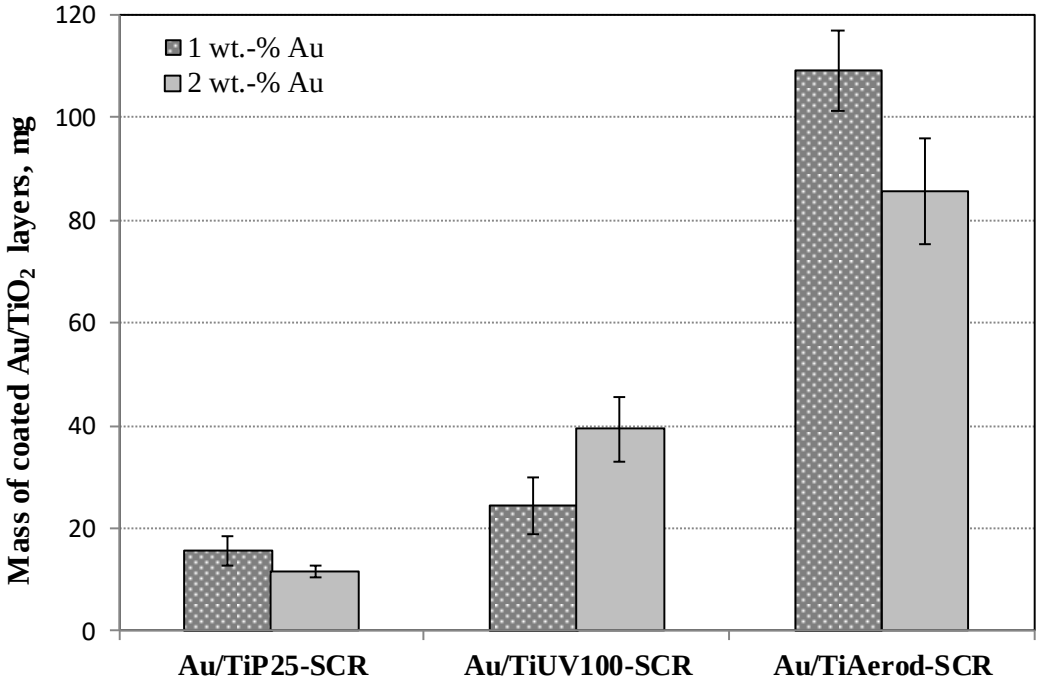

Fig.5.9. *Mass of Au/TiO_2 layers coated on the SCR-DeNOx monolits surface (average geometrical surface area of ~ 0.0161 m^2)*

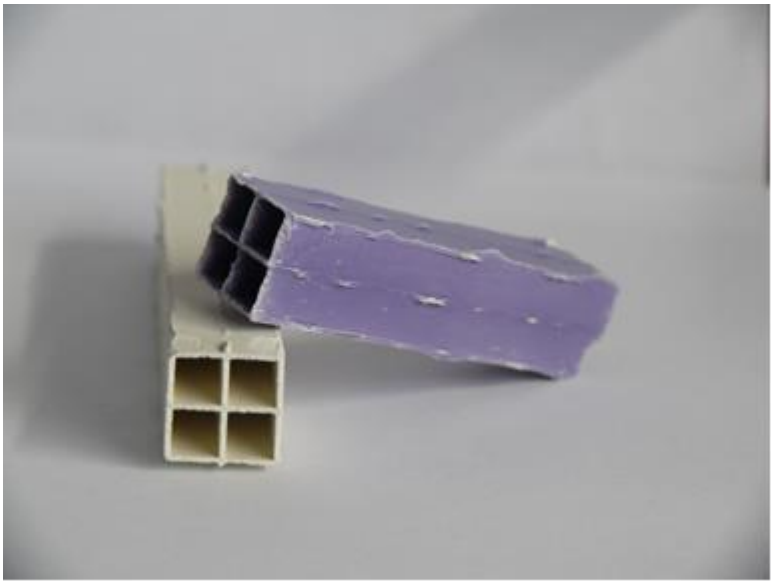

Fig.5.10. *Uncoated SCR-DeNOx (light cream) and 2Au/TiAerod-SCR monoliths (purple)*

5.3.1. Characterization of Au/TiO_2-coated SCR-DeNOx monoliths

The physical-chemical properties of the as-prepared Au/TiO_2-coated SCR-DeNOx catalysts offer valuable information on the structure and composition of the above mentioned catalysts. These properties play an essential role in the catalytic activity. The structural properties as well as the chemical composition could offer important information on the mercury oxidation reaction.

5.3.1.1. Scanning Electron Microscopy (SEM) analysis

Fig.5.11 depicts the SEM micrographs for the surface of uncoated SCR and 2Au/TiP25-SCR monoliths. As can be observed in ***Fig.5.11.A*** the uncoated SCR monolith has a relatively smooth surface at higher resolution with visible porous structure (***Fig.5.11.B***). When looking at the coated SCR monolith surface, ***Fig.5.11.C***, it can be noted that the Au/TiO_2 layers consist of irregularly shaped agglomerates. A zoom in on one of these agglomerates, ***Fig.5.11.D***, reveals that the gold coated TiO_2 particles with sizes under 100 nm form a tightly packed sponge-like structure. Similar morphology was observed for the prepared Au/TiO_2 catalyst powders (***Fig.5.6***) where the primary particles formed tightly packed agglomerates [3].

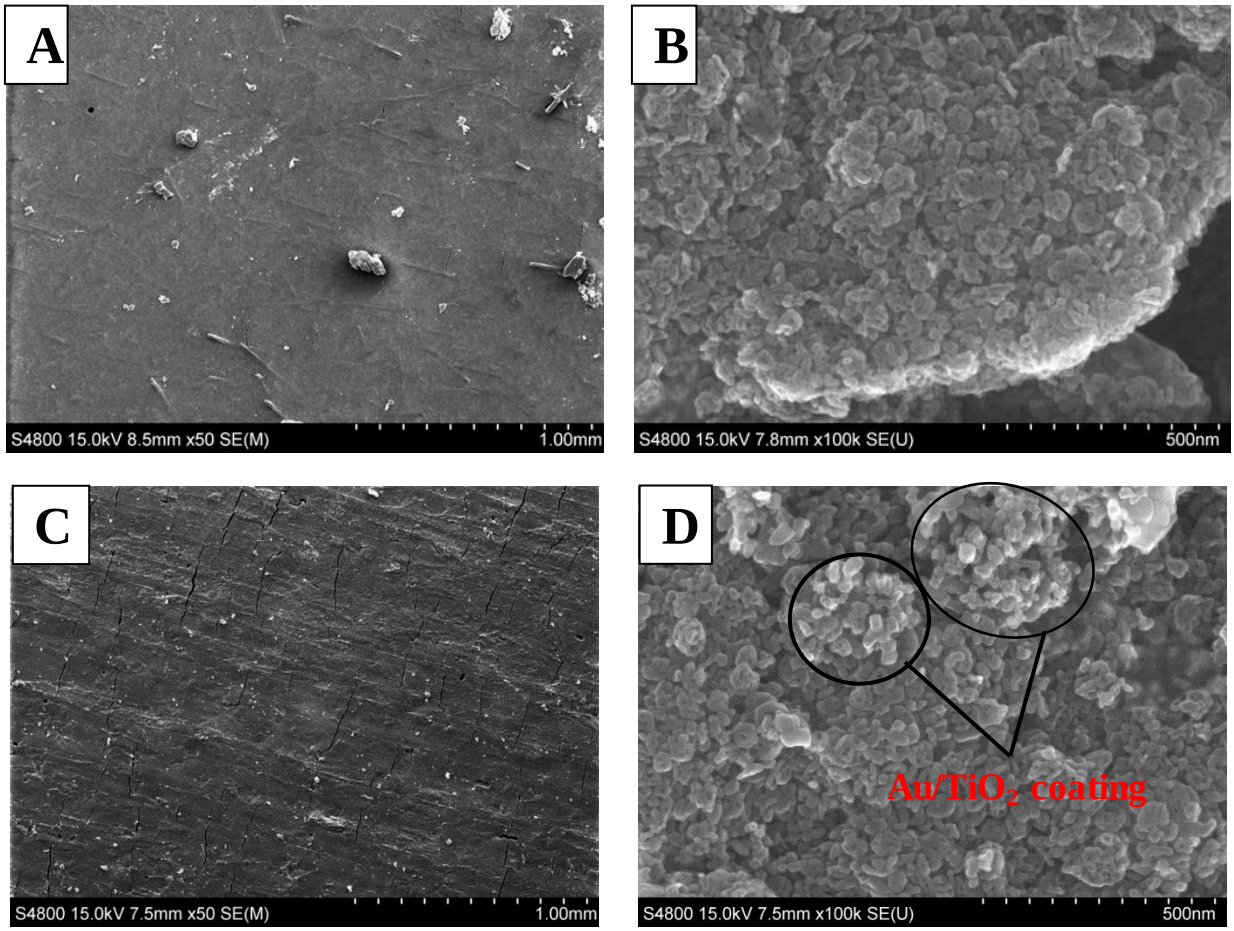

***Fig.5.11**. Scanning electron micrographs for: **A** – uncoated SCR; **B** – uncoated SCR at high resolution; **C** – 2Au/TiP25-SCR; **D** - 2Au/TiP25-SCR at high resolution.*

5.3.1.2. EDX analysis

The actual composition measured at the surface of uncoated and Au/TiO_2-coated SCR catalysts is given in ***Table 5.4***. The surface of SCR uncoated catalysts consists of Ti, O, Al, Si, Ca, and W elements, whereas the Au/TiO_2-coated SCR samples contain an extra element, Au namely. More details on the elemental composition at the surface of uncoated and Au/TiO_2-coated SCRs are given in ***Appendix 5.7***; ***5.8*** and ***5.9***.

The measurements show that the actual gold loading values are relatively close to the theoretical calculated ones. The dispersion degree of Au element at the surface was investigated for the case of calcined and uncalcined Au/TiAerod-SCR samples by EDX elemental mapping method. The gold mapping results given in ***Fig.5.12*** show a relatively

uniform gold distribution at the surface of both uncalcined and calcined Au/TiAerod-SCR catalyst samples.

Contrary to the presumption that during the calcination process Au particles sinter forming large gold cluster, the EDX mapping results show similar surface gold distributions for uncalcined and calcined samples. Therefore, it can be concluded that the catalyst calcination at 400 °C does not cause significant changes in gold distribution at the surface of the coated catalysts.

Table 5.4 *Elemental composition of SCR uncoated and Au/TiAerod-SCR catalysts by EDX method*

Element / ***Sample***	***Ti*** *(wt %)*	***O*** *(wt %)*	***Al*** *(wt %)*	***Si*** *(wt %)*	***Ca*** *(wt %)*	***W*** *(wt %)*	***Cl*** *(wt %)*	***Au*** *(wt %)*
Uncoated SCR	70.8±5.3	17.5±4.6	2.4±0.5	4.2±1	0.8±0.4	4.7±0.7	-	-
1Au/TiAerod-SCR	73.1±5.3	21.9±4.8	4.6±0.9	2±0.8	-	-	-	1.2 ± 0.2
2Au/TiAerod-SCR	85.1±7.2	10.1±8.1	1.61±0.5	1.37±0.95	-	-	1.63*	1.76 ± 0.6

*the presence of Cl in the Au/Aerodisp coatings is due to the fact that the Au/Aerodisp suspensions were prepared by skipping the washing of the Au/Aerodisp catalysts

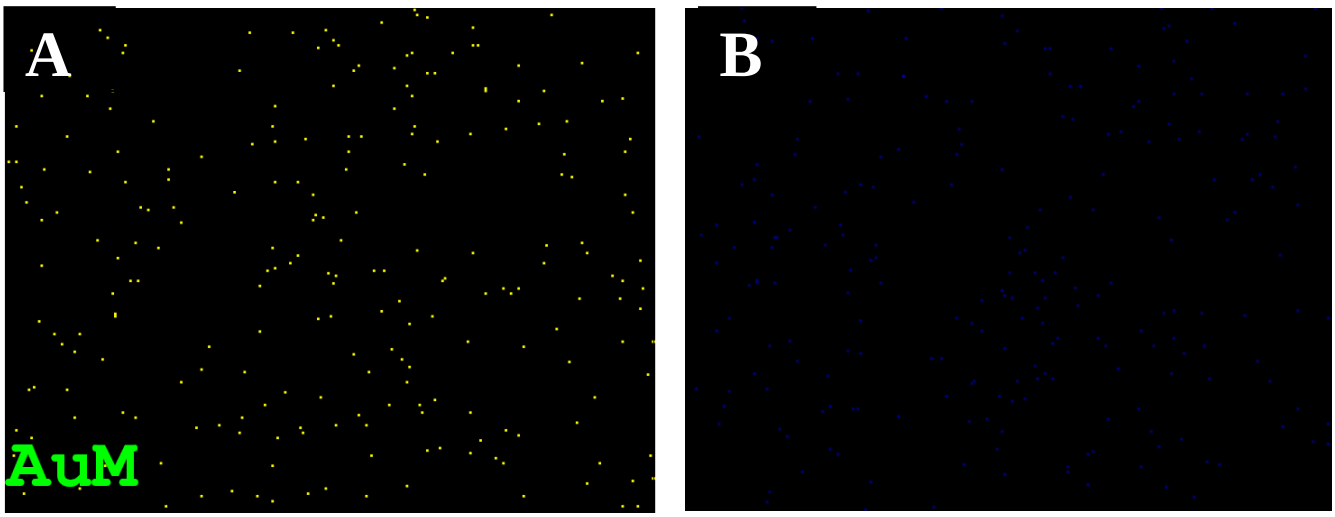

Fig.5.12. *Mapping of gold element distribution on the SCR surface at 5 μm resolution:* ***A*** *– 2Au/TiAerod-SCR uncalcined and* ***B*** *- 2Au/TiAerod-SCR calcined*

5.3.1.3. Surface study by Digital Microscope (DM)

Digital Microscope analysis was employed to investigate the surface quality and surface characteristics of Au/TiO_2 coatings at micrometer scale. By employing the 3D option of the Digital Microscope, it was possible to assess the surface topography of the uncoated and Au/TiO_2-coated SCR catalysts. All the investigated catalysts samples exhibit a rough surface with visible peaks and indentations, see ***Fig.5.13***. The SCR-DeNOx monolithic catalysts are extruded ceramic based honeycombs consisting of TiO_2, V_2O_5, WO_3 and glass fibers are added for improving the mechanical strength. When studying the surface of uncoated and coated SCR catalysts, the glass fibers can be observed. Applying the thin Au/TiO_2 layers on the surface of SCR catalyst did not cause major changes to the surface topography of the SCR substrate at this scale. The most significant change observed is color wise, the uncoated SCR has a light cream color, whereas the Au/TiO_2-coated SCR surface has a purple hue caused by the presence of Au nano-particles on its surface, see also ***Fig.5.10***.

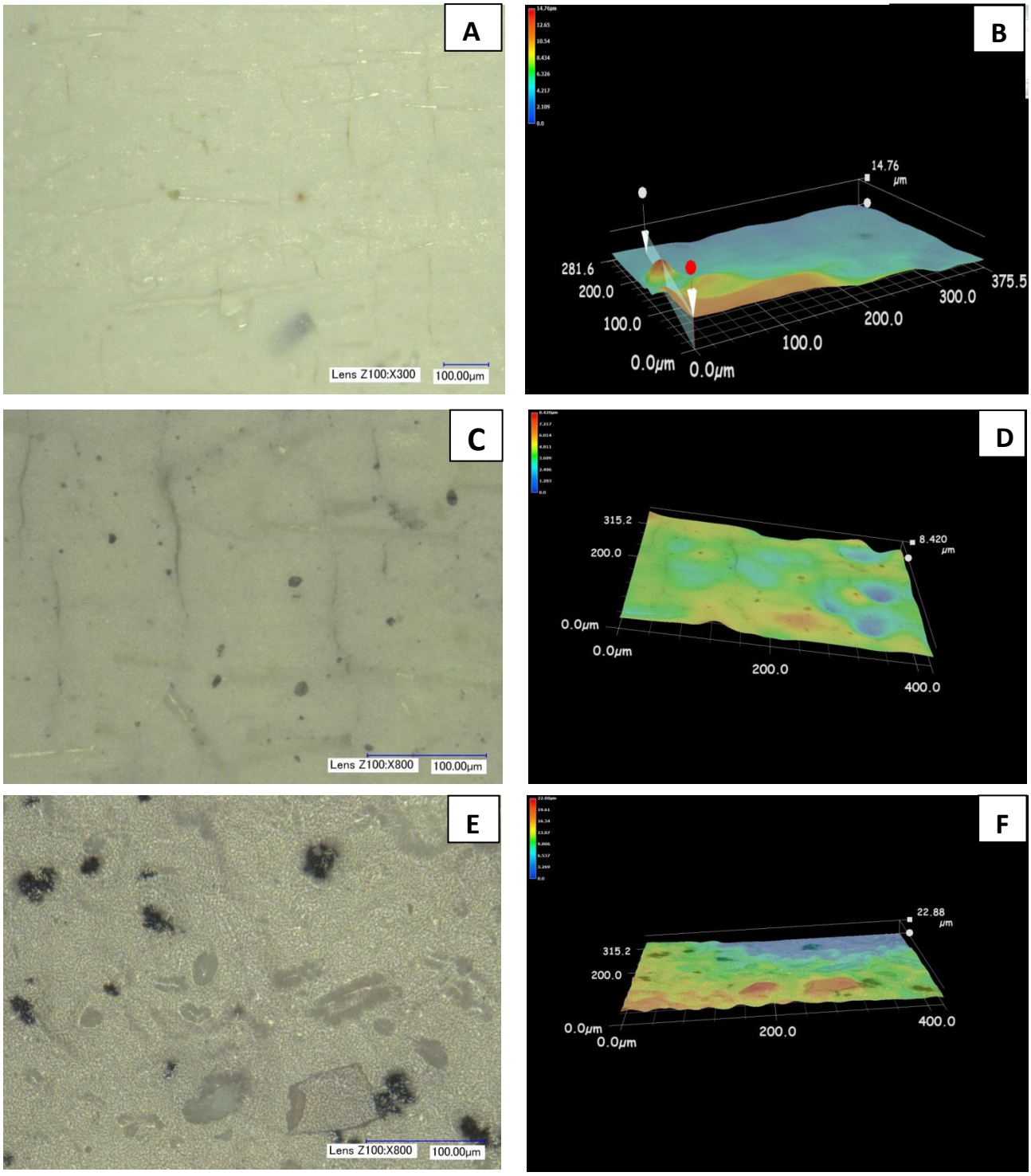

Fig.5.13. *Digital microscope images and their corresponding 3D profiles for:* ***A*** *and* ***B*** *– uncoated SCR surface,* ***C*** *and* ***D*** *– 2Au/TiP25-SCR surface, and* ***E*** *and* ***F*** *– 2Au/TiAerod-SCR surface*

5.3.1.4. Textural properties by N_2 absorption

The textural properties of uncoated and Au/TiO_2 coated SCR monoliths were investigated by employing N_2 absorption method. ***Table 5.5*** presents the textural properties (BET surface area, pore volume and pore diameter) for the selected catalyst samples. As can be observed, all samples present similar BET surface areas, pore volumes and pore sizes. These results indicate that applying a thin Au/TiO_2 layer to the surface of SCR monolithic catalyst did not cause significant changes in the textural properties of the commercial SCR monolith.

Table 5.5 *Textural properties of uncoated SCR-DeNOx and of Au/Aerodisp-coated SCR-DeNOx catalyst samples*

Catalyst type	BET surface (m^2/g)	Pore volume (cm^3/g)	Pore diameter (nm)
uncoated SCR	61.5	0.22	13.14
TiAerod-SCR	69.9	0.23	13.34
1Au/TiAerod-SCR	62.8	0.23	12.18
2Au/TiAerod-SCR	63.21	0.23	14.63

5.3.2. Stability of Au/TiO_2 coated layers

When considering the use of Au/TiO_2-coated SCR-DeNOx catalysts at industrial scale, a very important aspect that must be taken into consideration is their long-term stability and activity under industrial conditions. Several tests ("air-blow tests") were conducted aiming to determine the long-term stability of Au/TiO_2 coated layers under high volume flows. For this purpose, the coated and uncoated SCR-DeNOx catalysts were placed in a specially designed reactor and a 16 m^3/h air-flow (equivalent to a linear velocity of 26 m/s) was passed through the reactor for one hour. Should be mention that the linear velocity in the SCR industrial reactors varies between 4 and 8 m/s. After the air-blow tests the catalyst samples were dried at 120 °C/overnight and then placed in a desiccator to cool. Their weight was measured before and after the air-blow test, determining the weight loss that occured during the air-blow test. The studied samples show very little weight loss after the air-blow tests, which is indicative of Au/TiO_2 coated layers stability.

5.4. Conclusions

In this chapter, all the stages related to the preparation and characterization of the Au/TiO_2-coated SCR-DeNOx monolithic catalysts are presented. The preparation of Au/TiO_2-SCR catalysts consists of three main steps: synthesis of Au/TiO_2 powdered catalysts, preparation of Au/TiO_2 stable suspensions, and coating of commercially available SCR-DeNOx monoliths with a thin Au/TiO_2 layer by dipping in the as prepared Au/TiO_2 suspensions.

The Au/TiO_2 powdered catalysts were prepared by deposition-precipitation method. Two different commercially available TiO_2 powders were employed as supports for the gold nano-particles. Obtaining gold nano-particles requires careful control and adjustment of preparation parameters, such as temperature, pH, washing etc. The prepared catalysts were calcined and characterized by employing DR-UV-Vis, XRD, EDX, SEM methods. The investigations concluded that by employing the deposition-precipitation method it was possible to obtain Au/TiO_2 catalysts with gold nano-particles with dimensions below 100 nm.

A comprehensive study on the preparation and characterization of Au/TiO_2 based suspensions was conducted with the aim of establishing the most suitable way to achieve stable suspensions with 2 wt% solid content. To this end, two types of suspensions were prepared. Type I suspensions were obtained by dispersing and stabilizing Au/TiO_2 powders in an aqueous medium, while Type II suspensions were prepared by dissolving a calculated amount of $HAuCl_4 \cdot 3H_2O$ in deionised water and adding the TiO_2 support in the form of a stable commercial Aerodisp W 740 X suspension. The investigations showed that both type of suspensions exhibit fairly good stability. The characteristic properties of the suspensions were studied and the rheological properties, the particle size distributions and iso-electric points were determined. All suspensions exhibit relatively similar rheological properties with viscosities between 1.61 and 1.72 mPa·s at the selected measurement conditions. The particle size distributions in the suspensions vary greatly with the type of suspension as well as the type of TiO_2 support employed for the preparation of Au/TiO_2 powders, with Type II suspensions providing smaller particles size. The zeta potential measurements showed Type I suspensions to be stable in the 4 – 9 pH rage, whereas the Type II suspensions exhibit stability at pH lower than 2 and higher than 6.

The last part of this chapter describes the coating of SCR-DeNOx monolithic catalysts obtained by dip-coating method. The surface characteristics of Au/TiO_2-coated SCR-DeNOx monoliths were investigated by means of SEM, EDX and Digital Microscope. This part of the

experimental investigation has shown that by dip-coating with respective suspensions, Au/TiO_2-nano-particles can be applied to the surface of structured SCR-DeNOx catalysts. The gold content at the surface of the coated SCR monoliths was shown to be similar to that of Au/TiO_2 powdered catalysts employed for coating, while the gold distribution was relatively uniform.

CHAPTER 6

Catalytic activity of Au/TiO_2-coated SCR-DeNOx catalysts

The scope of this part of the experimental investigations was to assess the catalytic activity of the as-prepared Au/TiO_2-coated SCR-DeNOx monolithic catalysts. The investigations chiefly focused on elemental mercury oxidation activity; and DeNOx and SO_2/SO_3 conversions activities were selectively studied in order to determine to which degree these "standard" properties of SCR catalysts are affected by the Au/TiO_2 coatings. To this end, the experimental tests were performed by employing small honeycomb-shaped SCR and Au/TiO_2-coated SCR catalyst samples prepared as described in ***Chapter 5***. The catalytic activities of monolithic samples were studied in laboratory-scale set-ups under simulated flue gas conditions typical for hard coal-fired power plants.

6.1. Assessment of Hg^{el} oxidation activity

As mentioned above, the oxidation of elemental mercury over the Au/TiO_2-coated SCR catalysts compared to the reference SCR catalyst (uncoated) was the reaction investigated in detail. The catalytic tests were performed under simulated flue gas conditions as given in ***Table 4.8,*** where the concentration of Hg^{el} varied between 60 and 130 $\mu g/m^3$. Based on the premisis that the prepared Au/TiO_2-coated SCR catalysts are designed for use as a final catalyst layer in an industrial SCR reactor, the inhibitory effect of NH_3 on mercury oxidation activity is no longer of great concern here, therefore the effect of NH_3 was not studied. Since in previous investigations it was shown that carbon dioxide had only a

negligible effect on mercury oxidation [10], CO_2 was omitted in the simulated flue gas as well.

The influence of several parameters, such as HCl content (10 and 100 mg/m^3), reaction temperature (180 – 390 °C) and gold loadings (1 and 2 wt.-% Au) on mercury oxidation reaction was studied in greater detail. The experimental results were obtained by employing the experimental set-up given in ***Fig.4.5***. The mercury oxidation activity of the Au/TiO_2-coated catalysts was determined by employing the dry mercury sorbent-trap method. An example of the variability of experimental results obtained by employing the dry mercury sorbent trap is given in ***Table 6.1***. It can be noted that the presented experimental results show no great variability, being reproducible within ±1%.

Table 6.1 Example of results reproducibility for Hg^{el} oxidation degree (%) data obtained by employing Dowex/AC sorbent traps method

2Au/TiUV100-SCR (sample I)			**2Au/TiUV100-SCR (sample II)**		
Hg Sampling 1	Sorbent trap A	92.2 %	Hg Sampling 1	Sorbent trap A	92.1 %
	Sorbent trap B	91.7 %		Sorbent trap B	93.3 %
Hg Sampling 2	Sorbent trap A	91.0 %	Hg Sampling 2	Sorbent trap A	91.9 %
	Sorbent trap B	91.0 %		Sorbent trap B	92.3 %
Hg Sampling 3	Sorbent trap A	91.6 %	Hg Sampling 3	Sorbent trap A	94.5 %
	Sorbent trap B	92.1 %		Sorbent trap B	92.3 %
Average oxidation, %		91.6 ± 0.52	Average oxidation, %		92.7 ± 0.99

Sorbent traps A and B were placed in parallel; Hg^{el} oxidation degree (%) $= \left(\frac{Hg^{ox}_{Dowex}}{\left(Hg^{ox}_{Dowex} + Hg^{el}_{AC}\right)} \right) \bullet 100$;

reaction temperature 320 °C and 100 mg/m^3 HCl, variability given as Standard Deviation (±).

6.1.1. Effect of different Au/TiO_2 coatings type on Hg^{el} oxidation activity

This part of the experimental investigation aims to determine which type of Au/TiO_2 coating has the highest impact on the Hg^{el} oxidation activity of the SCR catalyst selected as a support. The reaction temperatures of 180 and 390 °C and HCl concentrations of 10 and 100 mg/m^3 were selected. ***Fig.6.1.a*** and ***Fig.6.1.b*** depict the Hg^{el} oxidation activities of the uncoated SCR catalyst and those of SCR catalysts covered with different Au/TiO_2 coatings containing 2 wt.-% Au. It is obvious that the presence of Au/TiO_2 coatings at the surface of SCR catalyst significantly enhanced the overall Hg^{el} oxidation activity of the substrate.

The most visible influence of Au/TiO_2 coatings on Hg^{el} oxidation activity was observed at 180 °C. At this temperature, the selected SCR-uncoated reference catalyst exhibited a relatively low Hg^{el} oxidation activity, which was expected considering that the selected commercial SCR-DeNOx catalyst for hot site conditions was designed with a V_2O_5 content below 1 %. By applying a thin Au/TiO_2 coating, the Hg^{el} oxidation activity at 180 °C and 100 mg/m^3 HCl was boosted from about 18 m/h for the uncoated SCR-catalyst to 38 m/h for the 2Au/TiAerod-SCR catalyst (***Fig.6.1.a***). When increasing the reaction temperature to 390 °C, the uncoated SCR catalyst showed a much higher mercury oxidation activity of 29 m/h. Although, at this high reaction temperature, the Hg^{el} oxidation activity increased as a consequence of coating with Au/TiO_2, the effect is significantly lower when compared with that measured at 180 °C [3].

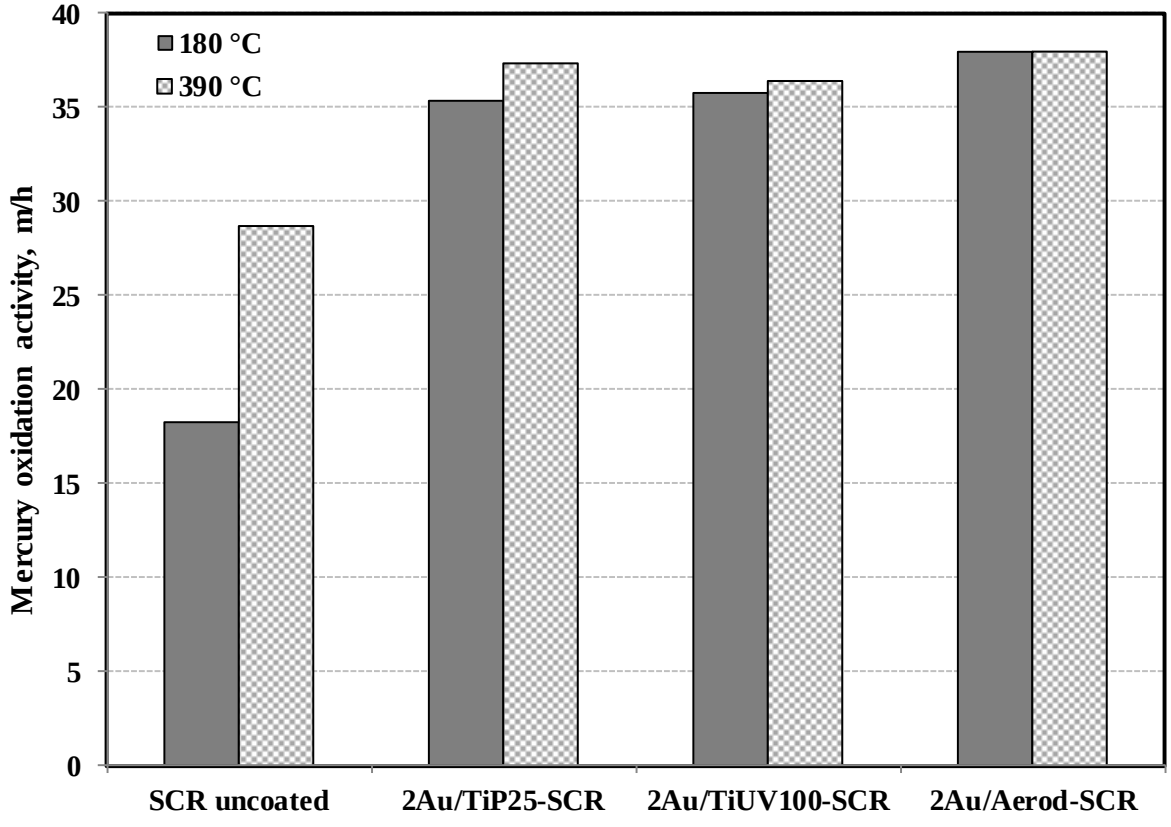

Fig.6.1.a. *Effect of Au/TiO_2 coatings on Hg^{el} oxidation activity at 180 and 390 °C and 100 mg/m^3 HCl*

Decreasing the HCl content from 100 to 10 mg/m^3 resulted in a significant decrease in mercury oxidation activity at high reaction temperature (390 °C). This effect can be observed for all types of catalysts, including the uncoated reference catalyst, with measured mercury oxidation activities below 7 m/h (see ***Fig.6.1.b***). However, at lower reaction temperature (180 °C), the Au/TiO_2-coated and uncoated SCR catalyst samples maintain a

high oxidation activity, similar to that when the HCl content of the simulated flue gas was 100 mg/m^3.

From these results, it is obvious that the effect of Au/TiO_2 coatings on the Hg^{el} oxidation activity is somewhat limited at higher temperatures. The lower performance of Au/TiO_2 coatings at 390 °C may be explained by the decreased Hg adsorption/amalgamation by Au at higher temperatures [147]. The importance of the mercury being adsorbed on the gold surface for the oxidation process has already been pointed out in literature [148]. When it comes to the effect of the different Au/TiO_2 coatings on the oxidation activity, no significant differences were detected [3].

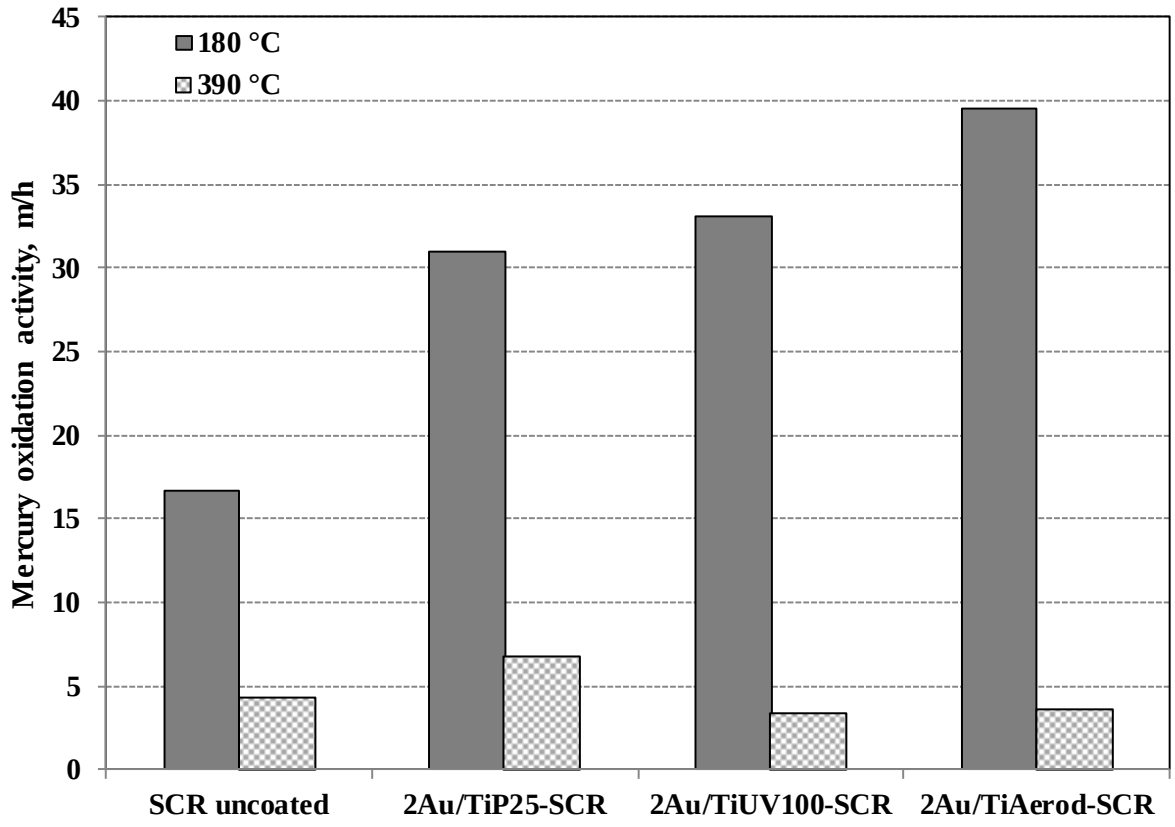

Fig.6.1.b. *Effect of Au/TiO_2 coatings on Hg^{el} oxidation activity at 180 and 390 °C and 10 mg/m^3 HCl*

6.1.2. Effect of reaction temperature and HCl concentration on Hg^{el} oxidation activity

Mercury oxidation activities of uncoated and Au/TiO_2-coated SCR-DeNOx catalysts were determined under the simulated flue gas conditions given in ***Table 4.8*** and the temperature range 180-390 °C, which is from cold-site to hot-site power plant conditions. The HCl content of the simulated flue gas was 10 and 100 mg/m^3. The evaluated catalysts cover a wide range of activities from 3 m/h up to 52 m/h, see ***Figs. 6.2.a*** and ***6.2.b***. These variations in Hg^{el} oxidation activities are due to the type of catalyst, reaction temperature and HCl

content of the flue gas. It can be seen that coating the surface of the commercial reference SCR-DeNOx catalyst with Au/TiO_2 led to a significant enhancement of the Hg^{el} oxidation activity in the temperature interval of 180-320 °C. The oxidation activity of all the investigated catalyst samples reached a maximum at around 320 °C irrespective of the HCl content of the flue gas. Further increasing the temperature up to 390 °C caused the Hg^{el} oxidation activity to decrease. This decrease in the Hg oxidation activity of uncoated SCR catalysts at hot site temperatures was noted by other authors as well [65, 73, 80]. Studies in literature on a wider temperature range for V_2O_5-WO_3/TiO_2 SCR-DeNOx resulted in a maximum activity between 300 and 400 °C [77]. From this it appears that the decreasing mercury oxidation rate of commercial SCR-DeNOx catalysts at high temperatures seems to be a common feature of the SCR system [3].

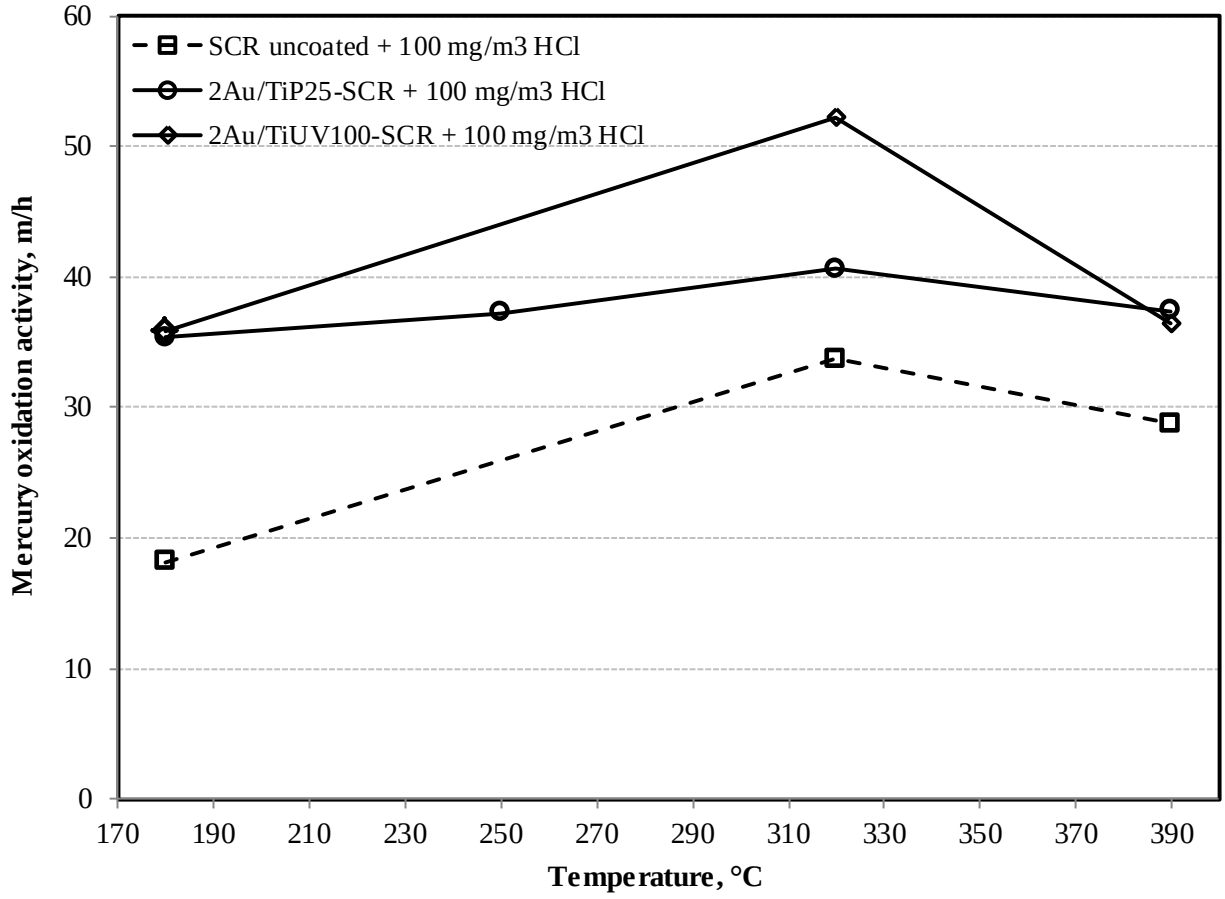

Fig.6.2.a. *Effect of reaction temperature on Hg^{el} oxidation of uncoated and Au/TiO_2-coated SCR-DeNOx monoliths at 100 mg/m^3 HCl.*

When analysing the results of Hg^{el} oxidation activities for HCl concentration of 10 mg/m^3 (***Fig. 6.2.b***), a few surprising findings can be outlined. Firstly, in the temperature interval 180-320 °C, Hg^{el} oxidation activities were relatively close to those for HCl concentrations of 100 mg/m^3. After increasing the temperature further, a decrease in Hg^{el} oxidation activity is observed for all types of catalysts investigated in flue gases with 100 as well as 10 mg/m^3 HCl. However, this drop in activity is much stronger in flue gas with the low HCl content of 10 mg/m³. Here, all of the mercury oxidation activities shown in ***Fig. 6.2.b*** are below 7 m/h at 390 °C [3].

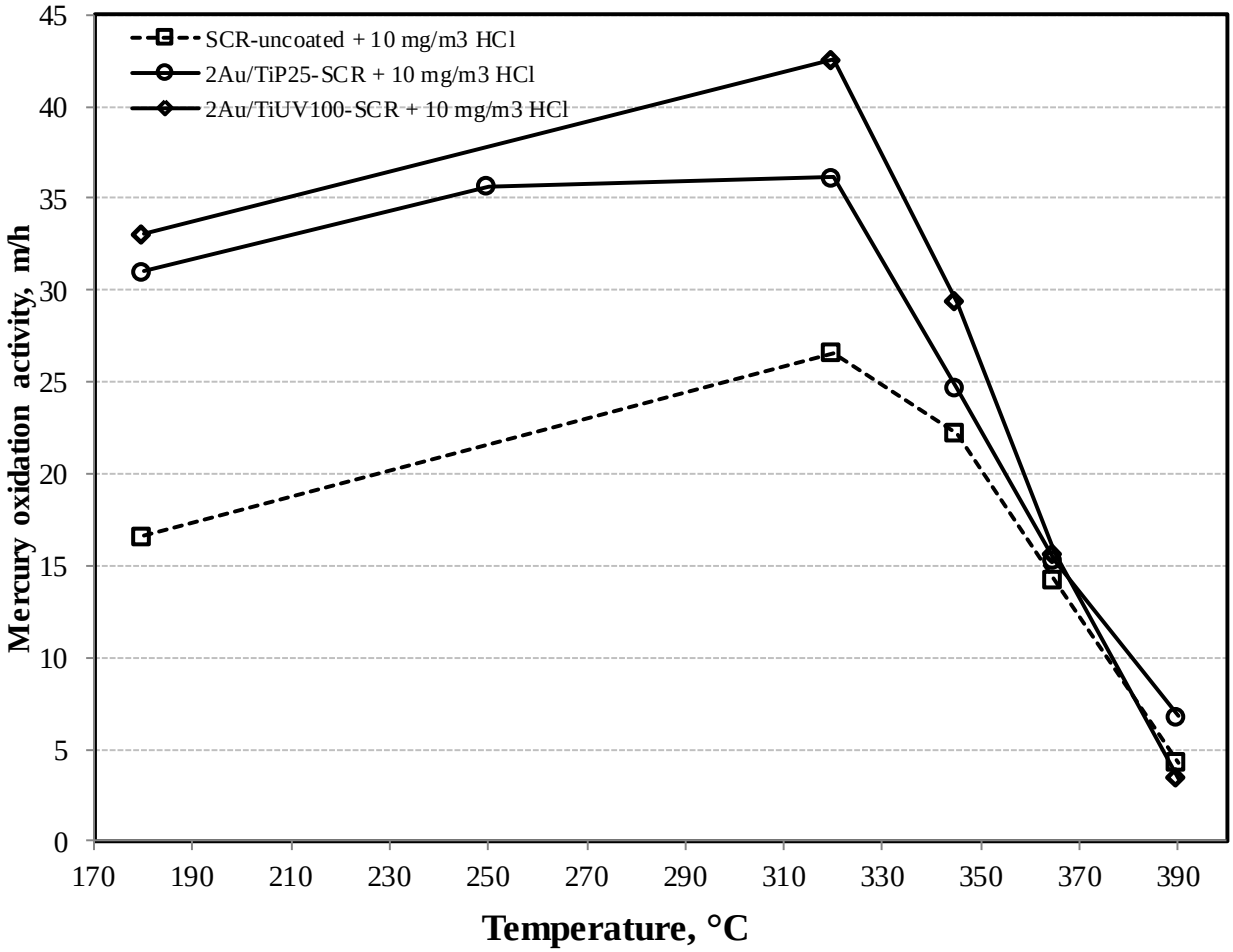

Fig.6.2.b. *Effect of reaction temperature on Hg^{el} oxidation of uncoated and Au/TiO_2-coated SCR-DeNOx monoliths at 10 mg/m^3 HCl.*

From ***Fig. 6.2.b*** it can be seen that at temperatures higher than 350 °C gold-coatings of the reference SCR-DeNOx catalysts no longer improved mercury oxidation appreciably. At these high temperatures and low HCl concentrations in the flue gas, it is possible to conclude that mercury oxidation is caused almost exclusively by the SCR substrate and not appreciably by gold coatings applied to the surface. Obviously, the effect of the gold also depends, to a significant extent, on the adsorption of a chlorine species on its surface, as has already been

predicted by theoretical considerations [149]. Higher temperatures decrease the adsorption and consequently surface concentration of the chlorine species [3].

6.1.3. Effect of gold loadings on Hg^{el} oxidation activity

Since the previous experimental results show that gold coatings have the highest impact on Hg^{el} oxidation under cold site conditions, it seemed appropriate to select 180 °C temperature to investigate the effect of gold loadings on Hg^{el} oxidation. **Table 6.2** depicts the effect of 1 and 2 wt.-% gold loadings on the Hg^{el} oxidation activity of Au/TiO_2-coated SCR catalysts. When the HCl concentration of the flue gas is 100 mg/m^3, a negligible difference is observed in Hg oxidation activity as a function of the amount of gold loadings. Similar results were obtained when the HCl concentration was only 10 mg/m^3. In all cases the coated catalysts show activity of approximately twice that of the uncoated reference catalyst. It appears that the lower gold loadings investigated do not cause a significant decrease in Hg^{el} oxidation activity at 180 °C reaction temperature. These findings are encouraging from an economic point of view when considering the cost of gold as a coating material [3].

Table 6.2 *Effect of gold loadings (1 and 2 wt.-% Au) on Hg^{el} oxidation activity over Au/TiO_2-coated SCR-DeNOx monoliths at 180 °C and, 100 and 10 mg/m^3 HCl*

Catalyst type	k_{Hg}, *m/h* (100 mg/m^3 HCl)	$k_{Hg\ coated}/k_{Hg\ uncoated}$ (100 mg/m^3 HCl)	k_{Hg}, *m/h* (10 mg/m^3 HCl)	$k_{Hg\ coated}/k_{Hg\ uncoated}$ (10 mg/m^3 HCl)
2Au/TiP25-SCR	35.4	1.95	31	1.87
1Au/TiP25-SCR	33.4	1.84	30.2	1.82
2Au/TiUV100-SCR	35.8	1.97	33.1	1.99
1Au/TiUV100-SCR	35.06	1.93	33.6	2.02
2Au/TiAerod-SCR	38	2.09	38.4	2.3
1Au/TiAerod-SCR	40.2	2.21	39.8	2.4

$k_{Hg\ uncoated} = 18.2 \pm 1.35$ at 100 mg/m^3 HCl and, $k_{Hg\ uncoated} = 16.6 \pm 1.92$ at 10 mg/m^3 HCl

6.1.4. Effect of Hg^{el} initial concentration

As previously mentioned, the initial Hg^{el} concentration of the simulated flue gas varied between 60 and 130 $\mu g/m^3$ (STP, dry), raising the question of how these variations affect the mercury oxidation activity of the tested catalysts. These variations in Hg^{el} concentration were caused by the high sensitivity of the permeation unit (Hg^{el} source) towards

small changes of the gas pressure in the system. ***Table 6.3*** shows the Hg^{el} oxidation efficiencies for different catalysts as the Hg^{el} concentrations of the simulated flue gas varied. It can be noted that the variation of Hg^{el} concentration in the flue gas caused only a slight change in mercury oxidation activity.

Table 6.3 *Effect of Hg^{el} initial concentration on mercury oxidation activity*

Catalyst type	***T= 320 °C and 100 mg/m³ HCl***	
	inlet Hg^{el} concentration *$\mu g/m^3$ (STP, dry)*	***Hg^{el} oxidation efficiency*** *(%)*
SCR-uncoated (sample I)	119.3	77.7
SCR-uncoated (sample II)	89.3	82.4
2Au/TiUV100-SCR (Sample I)	90.7	91.6
2Au/TiUV100-SCR (Sample II)	95	92.9
2Au/TiP25-SCR (Sample I)	68	87.9
2Au/TiP25-SCR (Sample II)	79.4	82.7

6.1.5. Possible mechanistic pathways for mercury oxidation on Au/TiO_2-coated SCR catalysts

When discussing the potential mechanism for the oxidation of Hg^{el} on the Au/TiO_2-coated SCR catalysts surface an important aspect must be taken in account, namely the presence of two different active sites (Au- and V_2O_5-active sites) on the catalysts surface. Au and V_2O_5 active-sites are known to adsorb mercury on their surface [8, 91]. Surface experimental studies conducted on the SCR catalysts suggested that V_2O_5-active sites oxidize elemental mercury via Langmuir-Hinshelwood mechanism with both adsorbed Hg^{el} and HCl species reacting to form weakly adsorbed $HgCl_2$ which is subsequently desorbed from the catalyst surface [2]. A recent density functional theory (DFT) modelling study [149] suggests that the Hg^{el} oxidation on Au (111) surfaces in the presence of chlorine species may occur in a step by step process ($Hg \rightarrow HgCl \rightarrow HgCl_2$) via a Langmuir-Hinshelwood mechanism where Hg^{el} and Cl_2 (or HCl) species are separately adsorbed on the gold surface [3]. Cl_2 and HCl gaseous molecules are readily adsorbed onto the Au^0 surface and further dissociated to chlorine atoms (Cl) and hydrogen atoms (H) [2, 91, 98].

Therefore, we can assume that the elemental mercury oxidation in the presence of HCl on the Au/TiO_2-coated SCR catalysts surface occurs most likely via two separate Langmuir-Hinshelwood mechanisms where both Hg^{el} and HCl species from the flue gas are adsorbed in parallel onto the Au and V_2O_5-active sites. The adsorbed Hg^{el} and HCl further react to form $HgCl_2$ which is readily desorbed from the catalyst surface. A schematic representation of the possible Hg^{el} oxidation mechanism occurring at the surface of Au/TiO_2-coated SCR catalysts is given in ***Fig.6.3***.

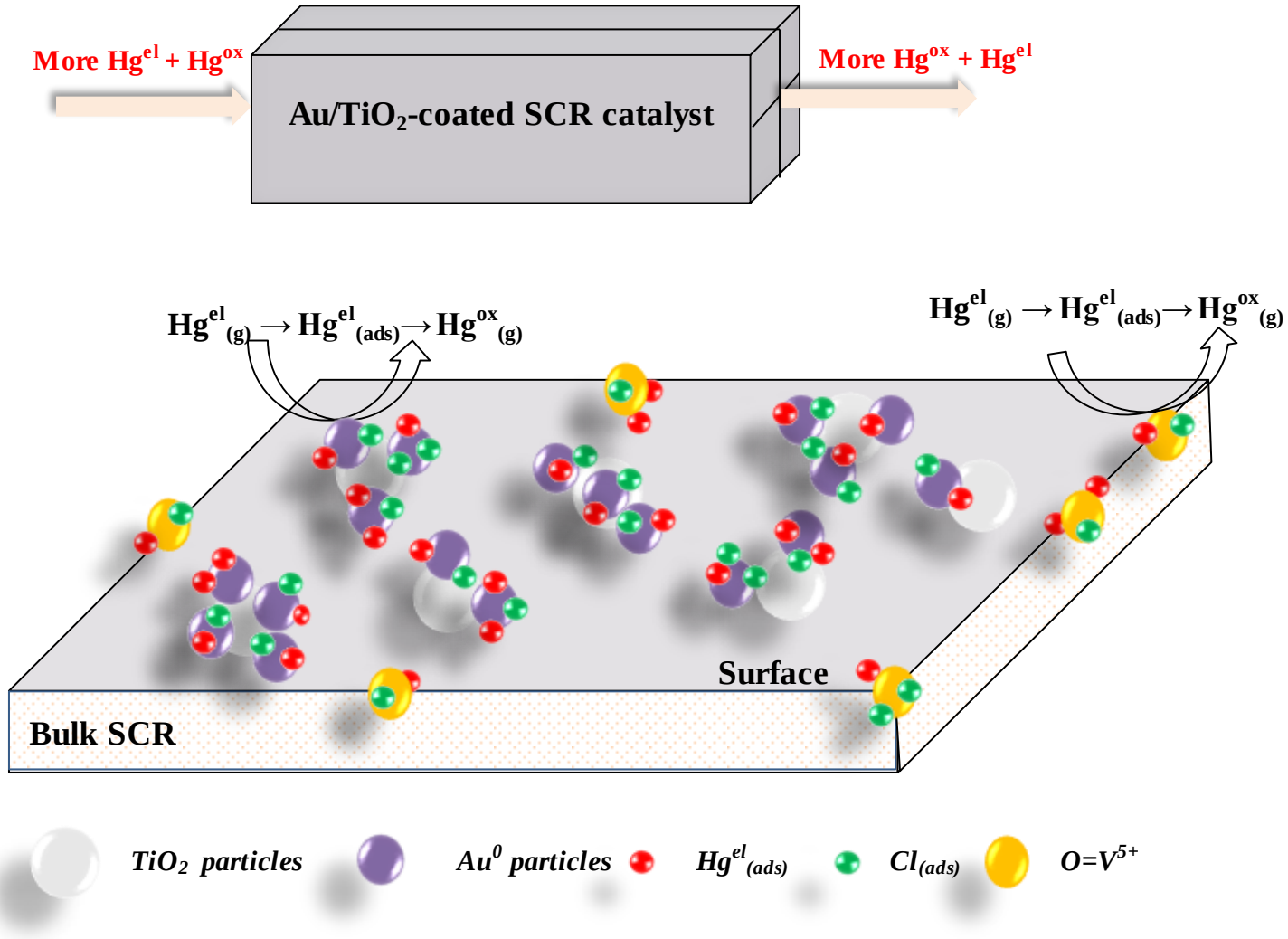

Fig.6.3. *Schematics of Hg^{el} oxidation mechanism at the surface of Au/TiO_2-coated SCR catalysts*

The parallel adsorption and oxidation of Hg^{el} on the V_2O_5 and Au^0 active sites at the SCR-DeNOx catalysts surface are expressed by equations (6.1 – 6.6) [149, 150].

$$Hg^{el}_{(g)} + SCR(O = V^{5+}) \leftrightarrow \left(Hg_{(ads)} \cdots O - V^{4+}\right) \quad (6.1)$$

$$V_2O_5 + 2HCl \rightarrow 2VO_2Cl_{(ads)} + H_2O \quad (6.2)$$

$$\left(\boldsymbol{V^{4+} - Cl_{(ads)}}\right) + \left(\boldsymbol{Hg_{(ads)} \cdots O - V^{4+}}\right) \leftrightarrow \left(\boldsymbol{V^{4+} - O \cdots HgCl_{(ads)} \cdots V^{4+}}\right) \quad \textbf{(6.3)}$$

$$Hg^{el}_{(g)} + Au^0 \leftrightarrow \left(Hg_{(ads)} - Au^0\right) \quad (6.4)$$

$$HCl_{(g)} + Au^0 \leftrightarrow \left(Cl_{(ads)} - Au^0 - H_{(ads)}\right) \quad (6.5)$$

$$\left(\boldsymbol{Hg_{(ads)} - Au^0}\right) + \left(\boldsymbol{Cl_{(ads)} - Au^0 - H_{(ads)}}\right) \leftrightarrow \left(\boldsymbol{H_{(ads)} - Au^0 \cdots HgCl_{(ads)} \cdots Au^0}\right) \quad \textbf{(6.6)}$$

The temperature dependence of these two reactions is different. It is known that the V_2O_5-based mercury oxidation mechanism is inhibited by ammonia and the DeNOx reaction [10, 151]. Nothing so far is known, that the Au might show similar inhibition effects. Further studies are needed to verify this hypothesis [3].

6.2. DeNOx activity of Au/TiO_2-coated SCR catalysts

NOx reduction tests were performed at 390 °C and in the presence of NH_3/NO ratios of 1 and 1.2, respectively. The Au/TiO_2-coated SCR catalysts were tested as fresh and aged (one week aged) in order to establish the effect of a short aging period on its DeNOx activity. The catalytic tests were performed under simulated flue gas conditions given in ***Table 4.8***. It must be noted that the NOx reduction tests were performed in the absence of Hg^{el} and HCl from the simulated flue gas. Hg^{el} and HCl compete with the DeNOx reaction for the available active sites and oxygen. However, it has to be considered from a mass balance point of view that in flue gases the Hg^{el} levels are in ppb-range, therefore this competition will be small [3].

6.2.1. Influence of NH_3/NO ratio on DeNOx activity

In this experimental study, the influence of NH_3/NO molar ratio of 1 and 1.2 on DeNOx activity was investigated for all types of catalysts (see ***Table 4.7***). The experimental results are given in separate graphs for each type of catalysts as follows: ***Fig.6.4.a*** for Au/TiUV100-SCR catalysts, ***Fig.6.4.b*** for Au/TiP25-SCR and, ***Fig.6.4.c*** for Au/TiAerod-SCR catalysts.

The experimental results depicted in these figures clearly show that the applied Au/TiO_2 coatings did not cause any significant change in the DeNOx activity of the SCR-DeNOx monolithic catalyst employed as a support. Also, the variation in NH_3/NO molar

ratios did not cause major differences in DeNOx activity of the SCR-uncoated and Au/TiO_2-coated SCR catalysts under the conditions investigated.

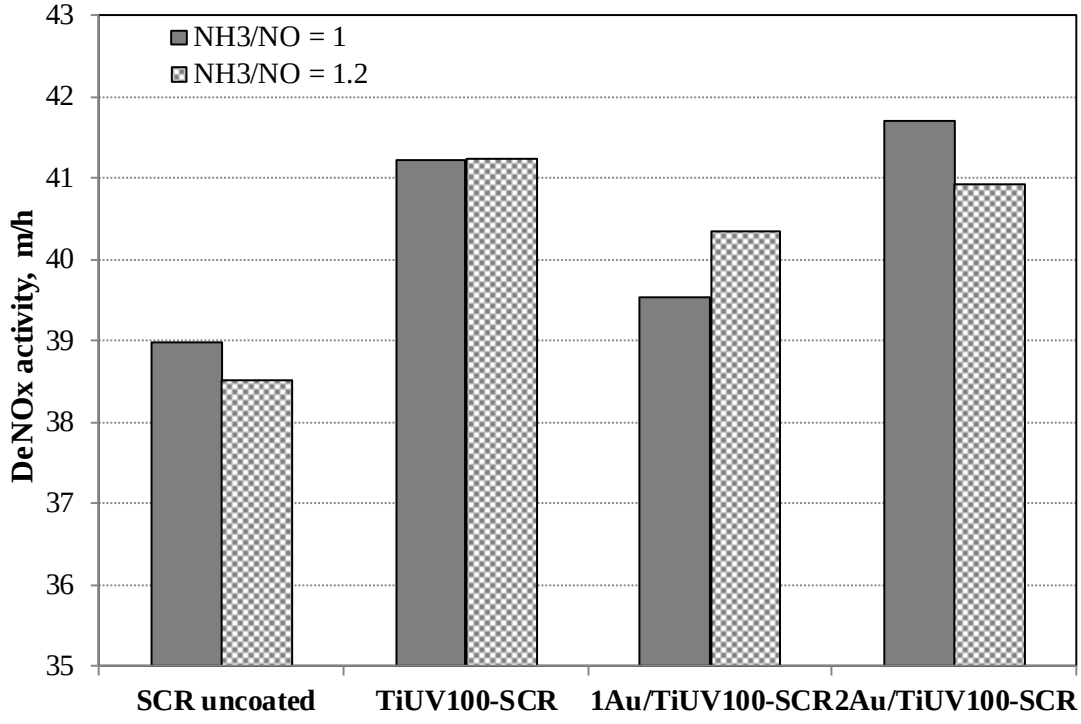

Fig.6.4.a. *DeNOx activity of Au/TiO_2-UV100-coated SCR-DeNOx catalysts at 390 °C*

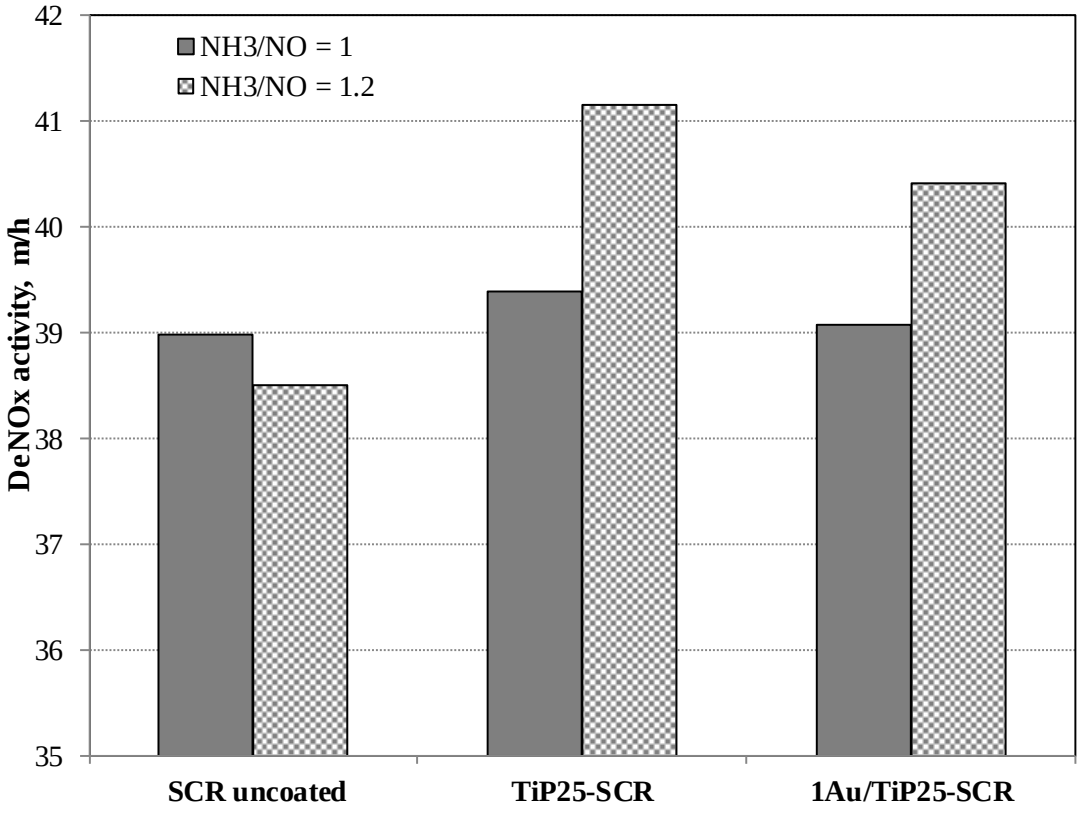

Fig.6.4.b. *DeNOx activity of Au/TiO_2-P25-coated SCR-DeNOx catalysts at 390 °C*

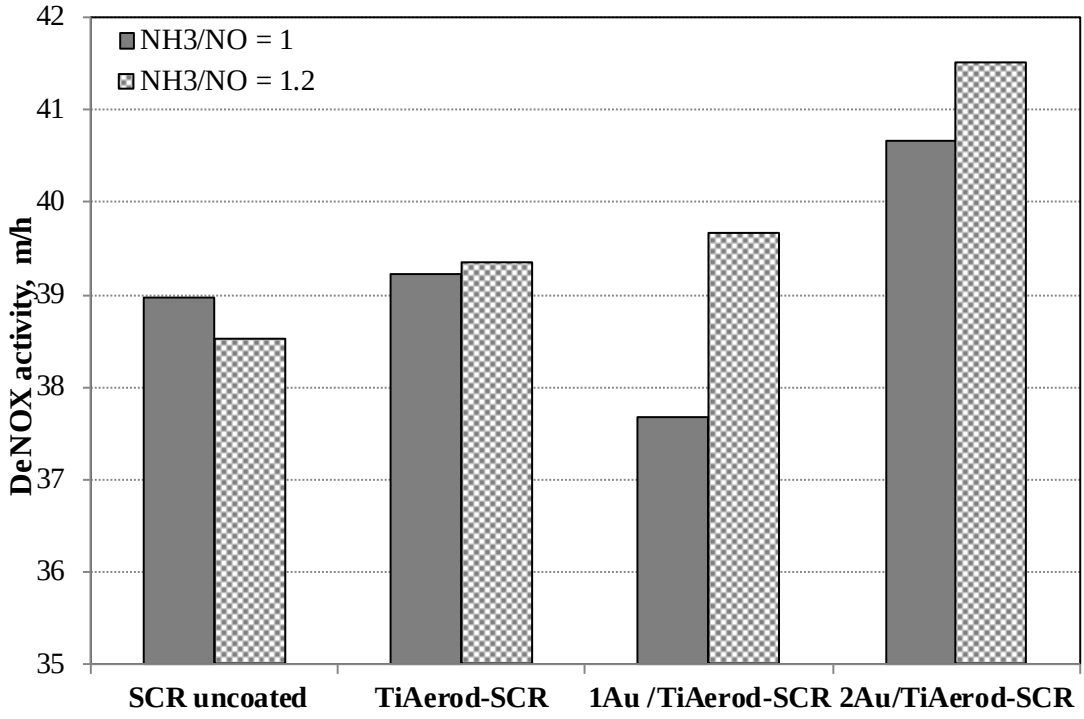

Fig.6.4.c. *DeNOx activity of Au/TiO_2-Aerodisp-coated SCR-DeNOx catalysts at 390 °C*

6.2.2. Influence of the ageing process on DeNOx activity

In order to establish whether a short ageing process (one week) has any influence on the DeNOx activity of SCR-uncoated and Au/TiO_2-coated SCR catalysts, fresh and one week aged catalyst samples were investigated at 390 °C and NH_3/NO molar ratio of 1.2. ***Fig.6.5*** depicts the experimental results obtained in this study. The fresh catalysts exhibit a slightly higher DeNOx activity than the aged catalyst samples. However, it must be noted that the catalysts in this study were aged for only one week. It is expected that longer operation periods might cause more significant decreases in DeNOx activity, hence the need for regeneration of catalytic activity applied at industrial level. The loss of catalytic activity is not affected only by the age of the catalyst but also by the flue gas history (flue gas composition, operation temperature and the presence of fly ash).

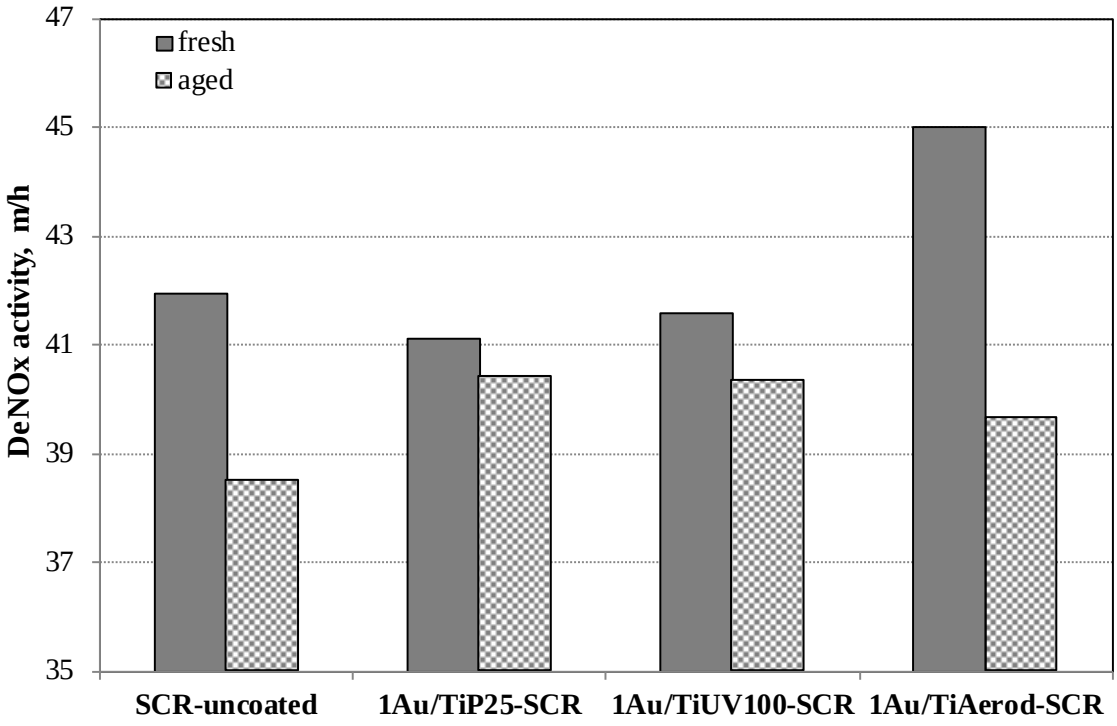

Fig.6.5. *DeNOx activity of fresh and aged Au/TiO_2-coated SCR-DeNOx catalysts at 390 °C and NH_3/NO = 1.2*

6.3. SO_2/SO_3 conversion activity of Au/TiO_2-coated SCR catalysts

SO_2/SO_3 conversions tests were performed at 390 °C and in the absence of NH_3, Hg^{el} and HCl from the simulated flue gas. The catalytic tests were performed under simulated flue gas conditions given in ***Table 4.8*** and by employing Au/TiO_2-coated SCR catalysts aged for one week. Compared to the DeNOx and mercury reactions, which are relatively fast reactions, the SO_2/SO_3 conversion is a slow chemistry-controlled reaction which takes place within the whole porous catalyst. In practice, the SO_2 from flue gas diffuses into the SCR catalyst's porous structure and is oxidised to SO_3 in the presence of O_2. The presence of sulphur trioxide leads to the formation of undesirable sulphuric acid mist in the flue gas, causing corrosion on the plant equipment and plume opacity of power plants [3].

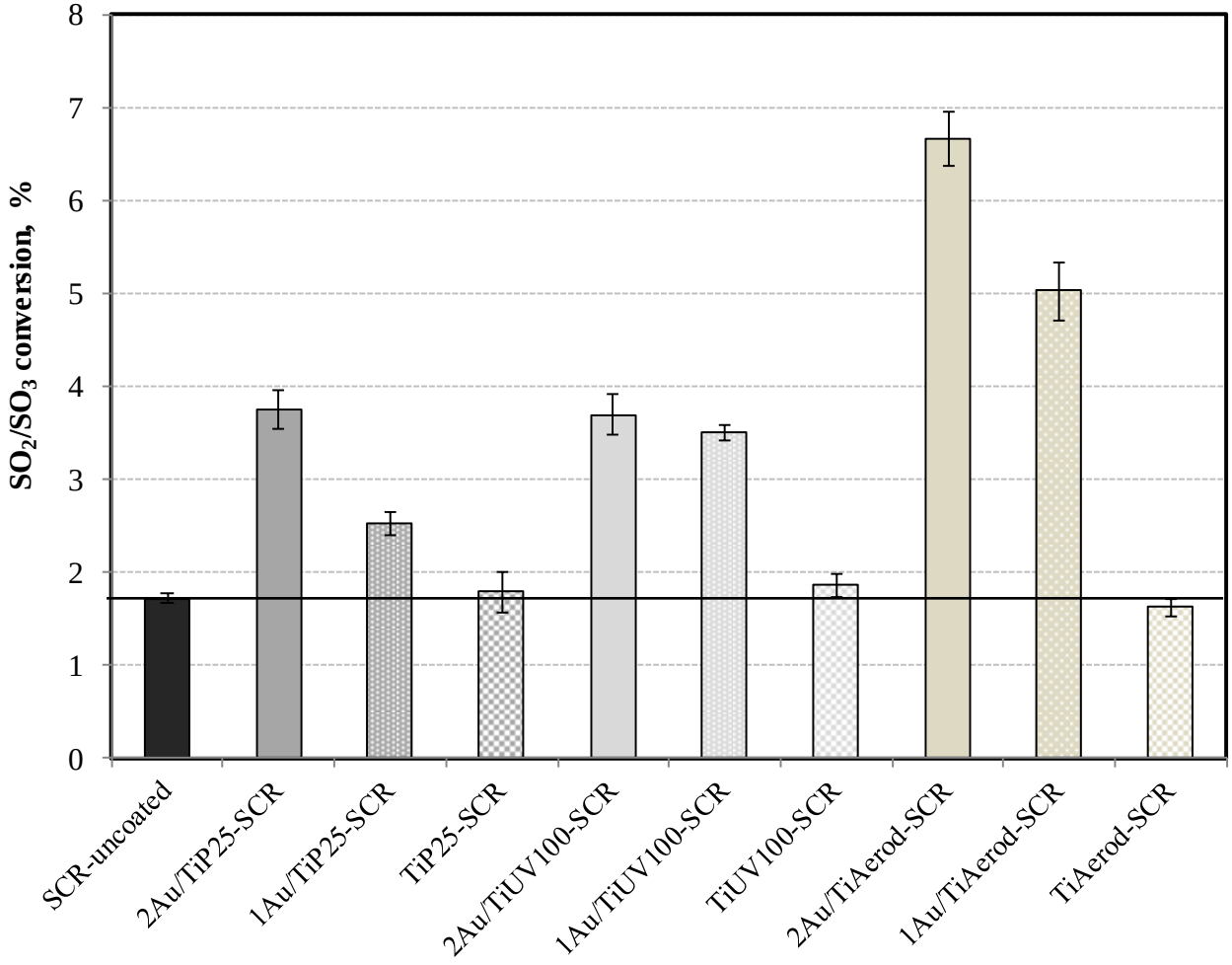

Fig.6.6. *SO_2/SO_3 conversion of uncoated and gold coated SCR-DeNOx catalysts at 390 °C*

In order to establish the extent to which the presence of gold in the coatings increases the SO_2/SO_3 conversion rate, all types of catalyst prepared (see ***Table 4.7***) were tested for this reaction. ***Fig.6.6*** depicts the SO_2/SO_3 conversion results. The uncoated SCR catalyst showed a SO_2/SO_3 conversion rate of 1.72 % under the chosen reaction parameters. When looking at the additional experimental results, it can be observed that the presence of Au/TiO_2 layers on the SCR monoliths surface led to an increase in SO_2/SO_3 conversion. Significant increase in conversion of SO_2 to SO_3 was measured when the gold loads of the coated layers were 2 wt.-%, reaching a maximum value of 6.66 % for the 2Au/TiAerod-SCR catalyst. It should be noted that the type II dispersion with Aerodisp contains 50 % dissolved gold. The dissolved gold will also have coated the inner surface of the porous catalyst, not only the outer surface as in the case of Au/TiO_2 particles. SO_2/SO_3 conversion followed the order: **SCR-uncoated < 2Au/TiUV100-SCR < 2Au/TiP25-SCR < 2Au/TiAerod-SCR.** By comparison, 1 wt.-% Au in the coating led to a significantly lower conversion rate [3].

The gold-based coatings investigated consist of relatively low amounts of gold whereas the TiO_2 substrate is the major component. The question of how much influence is exerted by the TiO_2 on SO_2/SO_3 conversion arises. With this purpose in mind, the conversion of SO_2 to SO_3 for TiO_2 coated samples was also investigated. The presence of TiO_2 on the surface of SCR catalysts seems to have caused only a small increase for the SCR samples coated with type I suspensions (TiP25-SCR and TiUV100-SCR) without gold coating and a slight decrease for TiO_2 coatings obtained by type II suspension (TiAerod-SCR) (see ***Fig. 6.6***). These findings seem to indicate that the oxidation activity of the gold mainly affects the SO_2/SO_3 conversion. It should be noted that the SO_2/SO_3 conversion rate over SCR catalysts has been shown to be influenced by a number of factors, such as reaction temperature, SO_2 concentration, H_2O content [66, 152, 153]. A major factor is that a much lower SO_2/SO_3 conversion rate is expected once the reaction temperature decreases [3].

6.4. Conclusions

The laboratory-scale experiments showed that Au/TiO_2 coating of commercial V_2O_5-WO_3/TiO_2 SCR-DeNOx catalyst improved its mercury oxidation capabilities. This enhancement of oxidation activity, however, is dependent on the reaction temperature and the HCl concentration of the flue gas. The maximum mercury oxidation activity of the gold-coated and the reference SCR-DeNOx substrate occurs between 300 and 350 °C. It appears that Au/TiO_2 coatings are most active in the temperature interval 180 - 320 °C under cold site conditions of a power plant, with increases in mercury oxidation activity by a factor of 2. Another very interesting finding is that at 180 °C varying the HCl concentration in the flue gas between 10 and 100 mg/m³ and/or gold loadings of the coated layers between 1 and 2 wt.-% did not lead to significant changes in mercury oxidation activity. A dramatic decrease in oxidation activity was observed once the reaction temperature was increased to above 350 °C with the HCl content as low as 10 mg/m^3 [3].

From the experimental observations it appears that the oxidation of mercury on the surface of the gold is a reaction between adsorbed mercury and adsorbed chlorine species as proposed in the literature [149]. Most likely, the mercury oxidation at the surface of Au/TiO_2-coated SCR catalysts proceeds via two parallel Langmuir-Hinshelwood mechanisms. At temperatures below 320 °C, the absorbed HCl-derived species are sufficiently available and do not affect the rate-limiting step. However, at temperatures above 320 °C the adsorption of chlorine will decrease, becoming a rate limiting factor. It should also be noted that increasing

the operating temperatures to above 400 °C will increasingly shift the thermodynamic equilibrium from the oxidised to the elemental mercury [3].

Another important aspect of this investigation was that the NOx activity of the prepared catalysts was only slightly changed by the applied Au/TiO_2 coatings, at least under hot-site conditions of 390 °C. The conversion of SO_2/SO_3 over SCR catalysts also has a major impact on the catalyst design and use in industrial SCR units. The reference SCR catalyst converted SO_2 to SO_3 to a certain degree at 390 °C, but its conversion activity was increased by coating with Au/TiO_2. Results clearly showed that at 390 °C, the Au on the SCR catalysts surface was responsible for the increase in SO_2/SO_3 conversion. This increase varied with the Au load and coating type [3].

When looking at the economics of implementing Au/TiO_2-coated SCR catalysts in industrial SCR units, it must be considered that the gold based coatings investigated in this work consist of relatively low amounts of gold (1 or 2 wt% Au) with the TiO_2 substrate being the major component. The Hg oxidation in SCR reactors takes place mostly at the outlet of the reactor, making the developed Au/TiO_2-coated SCR catalysts most suitable for use as a last catalyst layer. An analysis on the cost increase of SCR catalysts as a result of Au/TiO_2 coating when considering only the material cost of gold (gold salt employed for Au/TiO_2 coatings preparation) showed that cost increase varies with the coating type and gold loadings (see ***Appendix 6.1***). The calculated cost increase of SCR catalysts followed the order: ***Au/TiO_2 P25-coated SCR < Au/TiO_2 UV100-coated SCR < Au/TiO_2 Aerodisp-coated SCR***.

General Conclusions

The Ph.D thesis approches the topic of catalytic oxidation of elemental mercury from coal fired flue gases. The catalytic oxidation of elemental mercury proceeds according to the reaction below:

$$Hg^0 + \text{oxidizing species} \xrightarrow{catalyst,\ T\,°C} Hg^{2+} + \text{reduced species}$$

Hydrogen halides (HCl, HBr) are the most common starting compounds for oxidation of elemental mercury in flue gases. Oxidized mercury can be found in flue gases as $HgCl_2$, $HgBr_2$, $HgSO_4$, HgO etc.

The objective of the present thesis has been to improve the mercury oxidation activity of a commercial SCR-DeNOx monolithic catalyst by applying a thin Au/TiO_2 layer on its surface. The focus has been placed on the preparation and characterization of Au/TiO_2-coated SCR-DeNOx catalysts and, investigation of the catalytic activity of the aforementioned catalysts for mercury oxidation, DeNOx and SO_2/SO_3 conversion reactions. The catalytic activities of the monolithic samples were studied in laboratory-scale set-ups under simulated flue gas conditions typical to hard coal-fired power plants.

The present work is structured in two main parts. First part discusses the state of knowledge in the area of catalytic oxidation of elemental mercury, while in the second part the own contributions are presented and discussed. The mercury oxidation activity of the SCR-DeNOx catalysts is an important co-benefit. Therefore, increasing this activity by impregnating/coating the SCR catalyst surface with a thin metal layer, in this case Au/TiO_2, is a new and interesting research avenue. For this purpose, a commercially available SCR-DeNOx honeycomb shaped catalyst was coated with a thin Au/TiO_2 layer by employing the dip-coating method. The experimental research presented in this work followed a number of

objectives, as described in ***Chapter 3***. Based on the experimental results obtained during each stage of this research it is possible to formulate the following ***Concluding Remarks***:

- The preparation of Au/TiO_2-coated SCR catalysts consisted of three main parts, as follows: synthesis of Au/TiO_2 powdered catalysts by deposition-precipitation, preparation of Au/TiO_2 stable suspension by employing Au/TiO_2 catalysts and, coating of SCR monoliths with a thin Au/TiO_2 layer by employing the dip-coating method.
- The deposition-precipitation method employed for the preparation of powdered Au/TiO_2 catalysts leads to the formation of gold nano-particles with sizes below 100 nm.
- The two different type of suspensions (Type I and II) prepared in this work showed sufficient stability. Their characteristic properties were studied and, the rheological properties, the particle size distributions and iso-electric points were determined. All the suspensions have similar rheological properties at the selected measurement conditions, while their particle size distribution and iso-electric points vary with the type of suspension and type of TiO_2 support.
- The experimental investigation has shown that by dip-coating with respective suspensions, Au/TiO_2 nano-particles can be applied to the surface of monolithic SCR-DeNOx catalysts.
- The characterization results of the as prepared catalysts indicate that coating of the SCR monoliths with Au/TiO_2 caused no significant changes in the morphological and textural properties of the SCR substrate.
- Experimental investigations showed that by applying a thin Au/TiO_2 layer to the surface of a commercial SCR-DeNOx monolithic catalyst improves considerably its activity for mercury oxidation.
- A number of catalyst and reaction parameters affect the mercury oxidation activity (reaction temperature, HCl content and concentration, gold loadings).
- When comparing the mercury oxidation activities of Au/TiO_2 coated SCR catalysts obtained by employing different types of suspension (Type I and II) no major difference in catalytic activity was detected.
- The mercury oxidation activities of all catalyst samples investigated reach a maximum at reaction temperature of about 320 °C. However, HCl content of 100 mg/m^3 led to

higher mercury oxidation activity than the flue gas with a HCl content of only 10 $mg/m^{3.}$

- The Au/TiO_2 coatings are most active in the 180 – 320 °C temperature interval.
- Increasing the reaction temperature up to 390 °C caused the mercury oxidation activity to decrease. A significant decrease was measured once the HCl content of the simulated flue gas was only 10 mg/m^3.
- Mercury oxidation activity at 180 °C reaction temperature was not affected by gold loadings of the coated layer investigated. Increasing the gold loads from 1 wt.% to 2 wt.% did not lead to significantly higher mercury oxidation activity.
- Applying Au/TiO_2 layers to the surface of the commercial SCR catalyst did not affect their activity towards the DeNOx reaction at 390 °C.
- Experimental investigations showed that the commercial reference SCR catalyst converted SO_2 to SO_3 to a certain degree, but the conversion activity increased once the Au/TiO_2 layers were applied to the catalyst surface.
- At 390 °C reaction temperature, SO_2/SO_3 conversion varied with the gold loadings and coating types. Higher gold loads of the coated layers caused higher SO_2/SO_3 conversion. By comparison, 1 wt.-% Au in the coating led to a significantly lower conversion rate.
- The SO_2/SO_3 conversion followed the order: **SCR-uncoated < 2Au/TiUV100-SCR < 2Au/TiP25-SCR < 2Au/TiAerod-SCR.**

Outlook

The experimental results presented in this thesis contribute to the general knowledge regarding the catalytic oxidation of elemental mercury under coal-fired power plant conditions. The Au/TiO_2-coated SCR catalysts were developed and, the testing conditions were selected with the purpose to gain insight into their potential use at industrial scale. However, before testing/implementing this new type of catalyst at industrial scale further investigations and actions are necessary to address the following aspects:

- detailed study of the possible mechanistic pathways of mercury oxidation over the Au/TiO_2-coated SCR catalysts;
- the impact of ammonia and the DeNOx reaction on mercury oxidation over this type of catalysts;

- study of the influence of different flue gas components on mercury oxidation in the presence of Au/TiO_2-coated SCR catalysts;
- the potential impact of gold coatings on the conversion of NO to N_2O in the industrial SCR units;
- the stability and integrity of the Au/TiO_2 coatings under multiple heating-cooling cycles warrants detailed consideration;
- catalysts aging over a longer operation time in a real complex flue gas;
- loss of catalytic activity and catalyst regeneration, etc.

References

[1] Division of Technology, Industry and Economics (DTIE) Chemicals Branch. *Study on Mercury Sources and Emissions and Analysis of the Cost and Effectiveness of Control Measures*. UNEP: Geneva, Switzerland, ***2010***.

[2] Dranga, B.A.; Lazar, L.; Koeser, H. *Oxidation catalysts for elemental mercury in flue gases – A review*. Catalysts ***2012***, *2*, 139 – 170.

[3] Dranga, B.A.; Koeser, H. *Increased co-oxidation activity for mercury under hot and cold site coal power plant conditions – Preparation and evaluation of Au/TiO_2-coated SCR-DeNOx catalysts*. Applied Catalysis B: Environmental ***2015***, *166-167*, 302 – 312.

[4] Rafaj, P.; Bertok, I.; Cofala, J.; Schöpp, W. *Scenarios of global mercury emissions from anthropogenic sources*. Atmospheric Environment ***2013***, *79*, 472 – 479.

[5] US EPA Federal Register. *Mercury and air Toxic Standards (MATS)*. ***2013***, *78*, 24073 – 24094.

[6] M.E.P.C., A.Q.S.I.Q. *Emission Standard of Air Pollutants for thermal Power Plants*. GB 13223-2011, China Environmental Science Press, Beijing, China, ***2011***.

[7] 13th BlmSchV. *Federal Immission Control Ordinance for large combustion plants, and 17th BlmSchV Federal Immission Control Ordinance on waste incineration and co-incineration facilities*. Berlin, Germany, ***2013***.

[8] Straube, S.; Hahn, T.; Koeser, H. *Adsorption and oxidation of mercury in tail-end SCR-DeNOx plants – Bench scale investigations and speciations experiments*. Applied Catalysis B: Environmental ***2008***, *79*, 286 – 295.

[9] Eswaran, S.; Stenger, H.G. *Understanding mercury conversion in selective catalytic reduction (SCR) catalysts*. Energy & Fuels ***2005***, *19*, 2328–2334.

[10] Stolle, R.; Koeser, H.; Gutberlet, H. *Oxidation and reduction of mercury by SCR DeNOx catalysts under flue gas conditions in power plants*. Applied Catalysis B: Environmental ***2014***, *144*, 486 – 497.

[11] Zhao, Y.; Mann, M.D.; Pavlish, J.H.; Mibeck, B.A.F.; Dunham, E.G.; Olson, E.S. *Application of gold catalysts for mercury oxidation by chlorine*. Environmental Science Technology ***2006***, *40*, 1603–1608.

[12] Hrdlicka, J.A.; Seames, W.S.; Mann, M.D.; Muggli, D.S.; Horabik, C.A. *Mercury oxidation in flue gases using gold and palladium catalysts on fabric filters*. Environmental Science Technology ***2008***, *42*, 6677 – 6682.

[13] Pirrone, N.; Mahaffey, R. K. *Where we stand on mercury pollution and its health effects on regional and global scales*, Dynamics of mercury pollution on regional and global scales. Springer Science + Business Media, Inc., USA, ***2005***.

[14] Pascal P. *Nouveau Traite de Chimie Minerale, vol. V*. Editeurs Masson et Cie, Paris, France, ***1962***.

[15] Spacu, P.; Gheorghiu, C.; Brezeanu, M.; Stan, M. *Tratat de Chimie anorganică, vol III*. Editura Tehnică, Bucureşti, Romania, ***1978***.

[16] Calu, N.; Berdan, I.; Sandu, I. *Chimie Anorganică – Metale, vol. II*. Institutul Politehnic, Iaşi, Romania, ***1987***.

[17] Galbreath, K.C.; Zygarlicke, J.C. *Mercury speciation in coal combustion and gasification flue gases*. Environmental Science & Technology ***1996***, *30 (8)*, 2421 – 2426.

[18] Marcu, G. *Chimia Metalelor*. Editura Didactică şi Pedagogică, Bucureşti, Romania, ***1979***.

[19] Pirrone, N.; Cinnirella, S.; Feng, X.; Finkelman, B.R.; Friedli, R.H.; Leaner, J.; Mason, R.; Mukherjee, B.A.; Stracher, G.; Streets, G.D.; Telmer. K. *Global mercury emissions to the atmosphere from natural and anthropogenic sources*. Atmospheric Chemistry and Physics ***2010***, *10*, 5951 - 5964.

[20] United Nations Environment Programme (UNEP). *Global Mercury Assesment 2013:Sources, Emissions, Releases and Environmental Transport*. UNEP Chemicals Branch, Geneva, Switzerland ***2013***.(www.unep.org)

[21] Pirrone, N.; Cinnirella, S.; Feng, X.; Finkelman, B.R.; Friedli, R.H.; Leaner, J.; Mason, R.; Mukherjee, B.A.; Stracher, G.; Streets, G.D.; Telmer. K. *Global mercury emissions to the atmosphere from natural and anthropogenic sources*. Mercury fate and transport in the global atmosphere – Emissions, measurements and models. Springer Science + Business Media, LLC, USA, ***2009***.

[22] UNEP Chemicals Branch. *The global atmospheric mercury assessment: Sources, Emissions and Transport*. Geneva, Switzerland, ***2008***. (www.chem.unep.ch/mercury/)

[23] Pacyna, E.G.; Pacyna, J.M.; Sundseth, K.; Munthe, J.; Kindbom, K.; Wilson, S.; Steenhuise, F.; Maxon, P. *Global emission of mercury to the atmosphere from anthropogenic sources in 2005 and projections to 2020*. Atmospheric Environment ***2010***, *44*, 2487 – 2499.

[24] Sondreal, A.E.; Benson, A.S.; Pavlish, H.J.; Ralston, V.C.N. *An overview of air quality: mercury, trace elements, and particulate matter*. Fuel Processing Technology ***2004***, *85*, 425 – 440

[25] Hutson, D. N. *Mercury capture on fly ash and sorbents: The effects of coal properties and combustion characteristics*. Water Air Soil Pollutants ***2008***, *8*, 323 – 331.

[26] Yudovich, Ya. E.; Ketris, M. P. *Mercury in coal: A review. Part 2, Coal use and environmental problems*. International Journal of Coal Geology ***2005***, *62*, 136-165.

[27] Vosteen, B.W. *Native halogens in coals from US, China and elsewhere – Low chlorine coal need bromide addition for effective mercury capture*. MEC7 – Mercury emissions from Coal – *International Experts Workshop*, Glasgow, June 16-18, ***2010***.

[28] Kilgroe, J.; Senior, C. *Fundamental Science and Engineering of mercury control in coal-fired power plants*. Air Quality IV Conference, Arlington, VA, USA, ***2003***.

[29] Pavlish, H.J.; Hamre, L.L.; Zhuang, Y. *Mercury control technologies for coal combustion and gasification systems*. Fuel ***2010***, *89*, 838 – 847.

[30] Ghorishi, S.B.; Lee, W.C.; Jozewicz, S.W.; Kilgroe, D. J. *Effects of fly ash transition metal content and flue gas HCl/SO_2 ratio on mercury speciation on waste combustion*. Environmental Engineering Science ***2005***, *22 (2)*, 221 – 231.

[31] Ko, B.K.; Byun, Y.; Cho, M.; Namkung, W.; Hamilton, P.I.; Shin, N.D.; Koh, J.D.; Kim, T.K. *Pulsed corona discharge for oxidation of gaseous elemental mercury*, Applied Physics Letters ***2008***, *92*, 251503.

[32] Olson, S.E.; Sharma, K.R.; Pavlish, H.J. *On the analysis of mercuric nitrate in flue gases by GC-MS*. Analytical and Bioanalytical Chemistry ***2002***, *374*, 1045 – 1049.

[33] McLarnon, R.C.; Granite, J.E.; Pennline, W.H. *The PCO process for photochemical removal of mercury from flue gas*. Fuel Processing Technology ***2005***, *87*, 85 – 89.

[34] UNEP Chemicals Branch. *Technical background report to the global atmospheric mercury assessment*. Geneva, Switzerland, ***2008***. (www.chem.unep.ch/mercury/)

[35] Galbreath, K.C.; Zygarlicke, J.C.; Olson, S.E.; Pavlish, H.J.; Toman, L.D. *Evaluating mercury transformation mechanism in a laboratory – scale combustion system*. The Science of the Total Environment ***2000***, *261*, 149 – 155.

[36] Wilson, J.S.; Steenhuisen, F.; Pacyna, M.J.; Pacyna, G.E. *Mapping the spatial distribution of global anthropogenic mercury atmospheric emission inventories*. Atmospheric Environment ***2006***, *40*, 4621 – 4632.

[37] Avramescu, M.-L.; Yumvihoze, E.; Hintelmann, H.; Ridal, J.; Fortin, D.; Lean, R.S.D. *Biogeochemical factors influencing net mercury methylation in contaminated freshwater sediments from the St. Lawrence river in Cornwall, Ontario, Canada*, The Science of the Total Environment ***2011***, *409*, 968 – 978.

[38] United States Environmental Protection Agency (U.S. EPA). *Mercury study report to Congress, volume III, Fate and transport of mercury in the environment.* USA, ***1997***.

[39] Vosteen, W.B.; Straube, S.; Köser, H. *Mercury sorption and mercury oxidation by chlorine and bromine at SCR-DeNOx catalysts – Part A: Oxidation*, 9th Annual EPA, DOE, EPRI, EEI Conference on Clean Air, Global Warming & Renewable Energy, Arizona, USA, ***2006***.

[40] Griffin, R.D. *A new theory of dioxin formation in municipal solid waste combustion*. Chemosphere ***1986***, *15*, 1987-1990.

[41] Niksa, S.; Fujiwara, N. *A predictive mechanism for mercury oxidation on selective catalytic reduction catalyst under coal-derived flue gas*. Journal of Air Waste Management Association ***2005***, *55*, 1866-1875.

[42] He, S.; Zhou, J.; Zhu, Y.; Luo, Z.; Ni, M.; Cen, K. *Mercury oxidation over a vanadia-based selective catalytic reduction catalyst*. Energy Fuels ***2009***, *23*, 253-259.

[43] Kamata, H.; Uueno, S.I.; Naito, T.; Yamaguchi, A.; Ito, S. *Mercury oxidation by hydrochloric acid over a VO_x/TiO_2 catalyst*. Catalysis Communications ***2008***, *9*, 2441-2444.

[44] Li, H.; Wu; Y.C.; Li, Y.; Zhang, J. *Superior activity of MnO_x–CeO_2/TiO_2 catalyst for catalytic oxidation of elemental mercury at low flue gas temperatures*. Applied Catalysis B: Environmental ***2011***, doi:10.1016/j.apcatb.2011.10.021.

[45] Hu, C.; Zhou, J.; Luo, Z.; Cen, K. *Oxidative adsorption of elemental mercury by activated carbon in simulated coal-fired flue gas*. Energy & Fuels ***2011***, *25*, 154-158.

[46] Eom, Y.; Jeon, H.S.; Ngo, A.T.; Kim, J.; Lee, G.T. *Heterogeneous mercury reaction on a selective catalytic reduction (SCR) catalyst*. Catalysis Letters ***2008***, *121*, 219-225.

[47] Liu, Y.; Wang, Y.; Wang, H.; Wu, Z. *Catalytic oxidation of gas-phase mercury over Co/TiO_2 catalysts prepared by sol-gel method*. Catalysis Communications ***2011***, *12*, 1291-1294.

[48] Wen, X.; Li, C.; Fan, X.; Gao, H.; Zhang, W.; Chen, L.; Zeng, G.; Zhao, G. *Experimental study of gaseous elemental mercury removal with CeO_2/γ-Al_2O_3*. Energy & Fuels ***2011***, *25*, 2939-2944.

[49] Kamata, H.; Mouri, S.; Uueno, S.I.; Takano, K.; Watanabe, K.; Yamaguchi, A.; Ito, S. *Mercury oxidation by hydrogen chloride over the CuO based catalysts*. Science Technology Catalysis ***2006***, *172*, 621-622.

[50] Yamaguchi, A.; Akiho, H.; Ito, S. *Mercury oxidation by copper oxides in combustion flue gases*. Powder Technology ***2008***, *180*, 222-226.

[51] Kim, H.M.; Ham, S.W.; Li, J.B. *Oxidation of gaseous elemental mercury by hydrochloric acid over $CuCl_2/TiO_2$ – based catalysts in SCR process*. Applied Catalysis B: Environmental ***2010***, *99*, 272-278.

[52] Liu, Z.; Li, X.; Lee, J.-Y.; Bolin, B.T. *Oxidation of elemental mercury vapor over γ-Al_2O_3 supported $CuCl_2$ catalyst for mercury emission control*. Chemical Engineering Journal ***2015***, *275*, 1-7.

[53] Zhang, A.; Zheng, W.; Song, J.; Hu, S.; Liu, Z.; Xiang, J. *Cobalt manganese oxides modified titania catalysts for oxidation of elemental mercury at low flue gas temperature*. Chemical Engineering Journal ***2014***, *236*, 29-38.

[54] Qiao, S.; Chen, J.; Li, J.; Qu, Z.; Liu, P.; Yan, N.; Jia, J. *Adsorption and catalytic oxidation of gaseous elemental mercury in flue gas over MnO_x/alumina*. Industrial and Engineering Chemistry Research ***2009***, *48*, 3317-3322.

[55] Li, J.; Yan, N.; Qu, Z.; Qiao, S.; Yang, S.; Guo, Y.; Liu, P.; Jia, J. *Catalytic oxidation of elemental mercury over the modified catalyst Mn/α-Al_2O_3 at lower temperatures*. Environmental Science Technology ***2010***, *44*, 426-431.

[56] Xu, Y.; Zhong, Q.; Liu, X. *Elemental mercury oxidation and adsorption on magnesite powder modified by Mn at low temperatures*. Journal of Hazardous Materials ***2015***, *283*, 252-259.

[57] Li, H.; Wu, C.-Y.; Li, Y.; Li, L.; Zhao, Y.; Zhang, J. *Role of flue gas components in mercury oxidation over TiO_2 supported MnO_x-CeO_2 mixed-oxide at low temperature*. Journal of Hazardous Materials ***2012***, *243*, 117-123.

[58] Li, H.; Wu, Y.C.; Li, Y.; Zhang, J. *CeO_2-TiO_2 catalysts for catalytic oxidation of elemental mercury in low-rank coal combustion flue gas*. Environmental Science Technology ***2011***, *45*, 7394-7400.

[59] Li, H.; Wu, Y.C.; Li, L.; Li, Y.; Zhao, Y.; Zhang, J. *Kinetic modelling of mercury oxidation by chlorine over CeO_2-TiO_2 catalysts*. Fuel ***2013***, *113*, 726-732.

[60] Li, H.; Wu, C.-Y.; Li, Y.; Li, L.; Zhao, Y.; Zhang, J. *Impact of SO_2 on elemental mercury oxidation over CeO_2-TiO_2 catalyst*. Chemical Engineering Journal ***2013***, *219*, 319-326.

[61] Kong, F.; Qui, J.; Liu, H.; Zhao, R.; Ai, Z. *Catalytic oxidation of gas-phase elemental mercury by nano-Fe_2O_3*. Journal of Environmental Science ***2011***, *24*, 699-704.

[62] Granger, P.; Parlvulescu, V.I. *Past and present in DeNOx Catalysis – from molecular modeling to chemical engineering*. Elsevier, Amsterdam, (Eds) ***2007***.

[63] Busca, G.; Baldi, M.; Pistarino, C.; Gallardo Amores, J.M.; Sanchez Escribano, V.; Finocchio, E. *Evaluation of V_2O_5-WO_3-TiO_2 and alternative SCR catalysts in the abatement of VOCs*. Catalysis Today ***1999***, *53 (4)*, 525 – 533.

[64] Lazar, L.; Koeser, H.; Balasanian, I.; Bandrabur, F. *Catalytic destruction of aromatic VOCs on SCR-DeNOx commercial catalyst*. Environmental Engineering and Management Journal ***2007***, *6*, 13 – 20.

[65] Zhuang, Y.; Laumb, J.; Liggett, R.; Holmes, M.; Pavlish, J. *Impacts of acid gases on mercury oxidation across SCR catalyst*. Fuel Processing Technology ***2007***, *88*, 929-934.

[66] Schwämmle, T.; Bertsche, F.; Hartung, A.; Brandenstein, J,; Heidel, B.; Scheffknecht, G. *Influence of geometrical parameters of honeycomb commercial SCR-DeNOx-catalysts on DeNOx-activity, mercury oxidation and SO_2/SO_3-conversion*. Chemical Engineering Journal ***2013***, *222*, 274-281.

[67] Lee, B.J.; Lee, M.S.; Lee, Y.I. *The characteristics of catalysts for mercury oxidation in thermal power plants*. Proceedings of World Academy of Science, Engineering and Technology ***2008,*** *34*.

[68] Hong, J.H.; Ham, W.S.; Kim, H.M.; Lee, M.S.; Lee, B.J. *Characteristics of commercial selective catalytic reduction catalysts for the oxidation of gaseous elemental mercury with respect to reaction conditions*. Korean Journal of Chemical Engineering ***2010***, *27*, 1117-1122.

[69] Kamata, H.; Uueno, S.I.; Naito, T.; Yukimura, A. *Mercury oxidation over the $V_2O_5(WO_3)/TiO_2$ commercial SCR catalyst*. Industrial & Engineering Chemistry Research ***2008***, *47*, 8136-8141.

[70] Eswaran, S.; Stenger, H.G. *Effect of halogens on mercury conversion in SCR catalysts*. Fuel Processing Technology ***2008***, *89*, 1153-1159.

[71] Cao, Y.; Gao, Z.; Zhu, J.; Wang, Q.; Huang, Y.; Chiu, C.; Parker, B.; Chu P.; Pan W.P. *Impacts of halogen addition in mercury oxidation, in a slipstream selective catalyst reduction (SCR), reactor when burning sub-bituminous coal*. Environmental Science Technology ***2008***, *42*, 256-261.

[72] Beretta, A.; Usberti, N.; Lietti, L.; Forzatti, P.; Di Blasi, M.; Morandi, A.; La Marca, C. *Modeling of the SCR reactor for coal-fired power plants: Impact of NH_3 inhibition on Hg^0 oxidation*. Chemical Engineering Journal ***2014***, *257*, 170-183.

[73] Madsen, K.; Jensen, D.A.; Frandsen, J.F.; Thogersen, R.J. *A mechanistic study on the inhibition of the DeNOx reaction on the mercury oxidation over SCR catalysts*. Proceedings of Air Quality VIII Conference, Arlington, USA, October 24-27, **2011**.

[74] Rallo, M.; Heidel, B.; Brechtel, K.; Maroto-Valer, M.M. *Effect of SCR operation variables on mercury speciation*. Chemical Engineering Journal ***2012***, *198-199*, 87-94.

[75] Cao, Y.; Chen, B.; Wu, J.; Cui, H.; Smith, J.; Chen, K.C.; Chu, P.; Pan, P.W. *Study of mercury oxidation by a selective catalytic reduction catalyst in a pilot-scale slipstream reactor at a utility boiler burning bituminous coal*. Energy & Fuels ***2007***, *21*, 145-156.

[76] Zhao, L.; Li, C.; Zhang, J.; Zhang, X.; Zhan, F.; Ma, J.; Xie, Y.; Zeng, G. *Promotional effect of CeO_2 modified support on V_2O_5-WO_3/TiO_2 catalyst for elemental mercury oxidation in simulated coal-fired flue gas*. Fuel ***2015***, *153*, 361-369.

[77] Gao, W.; Liu, Q.; Wu, C.-Y.; Li, H.; Li, Y.; Yang, J.; Wu, G. *Kinetics of mercury oxidation in the presence of hydrochloric acid and oxygen over a commercial SCR catalyst*. Chemical Engineering Journal ***2013***, *220*, 53-60.

[78] Lee, W.; Bae, G.N. *Removal of elemental mercury Hg^0 by nanosized V_2O_5/TiO_2 catalysts*. Environmental Science Technology ***2009***, *43*, 1522-1527.

[79] Lee, W.C.; Serre, D.S.; Zhao, Y.; Lee, J.S.; Hastings, W.T. *Mercury oxidation promoted by a selective catalytic reduction catalyst under simulated powder river basin coal combustion conditions*. Journal of Air Waste Management Association ***2008***, *58*, 484-493

[80] Senior, C. *Oxidation of mercury across SCR catalysts in coal-fired power plants burning low rank fuels*. Final Report to U.S.DOE/NETL, U.S. Department of Energy Agreement No. DE-FC26-03NT41728, Reaction Engineering International, ***2004***.

[81] Crocker, R.C.; Benson, A.S.; Laumb, D.J. *SCR catalyst blinding due to sodium and calcium sulphate formation*. *Preprints of Papers -American Chemical Society, Division of Fuel Chemistry* ***2004***, *49*, 169-171.

[82] Staudt, E.J.; Engelmeyer, T.; Weston, H.W.; Sigling, R. *The impact of arsenic on coal fired power plants equipped with SCR*. Presented at ICAC Forum, Houston, February 12-13, ***2002***.

[83] Senior, C.; Lignell, O.D.; Sarofim, F.A; Mehta, A. *Modelling arsenic partitioning in coal-fired power plants*. Combustion Flame ***2006***, *1473*, 209-221.

[84] Senior, C. *Oxidation of mercury across selective catalytic reduction catalysts in coal fired power plants*. Journal of Air Waste Management Association ***2006***, *56*, 23-31.

[85] Yan, N.; Chen, W.; Chen, J.; Qu, Z.; Guo, Y.; Yang, S.; Jinping, J. *Significance of RuO_2 modified SCR catalysts for elemental mercury oxidation in coal-fired flue gas*. Environmental Science Technology ***2011***, *45*, 5725-5730.

[86] Zeng, K.; Stolle, R.; Köser, H. *Quecksilberoxidation am metalleoxiddotierten SCR-DeNOx-Katalysatoren*. ProzessNet Conference, Mannheim, Germany, 08-10 September, ***2009***.

[87] Zhang, X.; Li, C.; Zhang, J.; Zeng, G.; Xie, Y.; Yu, M. *Simultaneous removal of elemental mercury and NO from flue gas by V_2O_5-CeO_2/TiO_2 catalyst*. Applied Surface Science ***2015***, http://dx.doi.org/10.1016/j.apsusc.2015.04.039

[88] Chiu, C.-H.; Hsi, H.-C.; Lin, H.-P. *Multipollutant control of Hg/SO_2/NO from coal-combustion flue gases using transition metal oxide-impregnated SCR catalysts*. Catalysis Today ***2015***, *245*, 2-9.

[89] Poulston, S.; Granite, J.E.; Pennline, W.H.; Myers, R.C.; Stanko, P.D.; Hamilton, H.; Rowsell L.; Smith, J.W.A.; Ilkenhans, T.; Chu, W. *Metal sorbents for high temperature mercury capture from fuel gas*. Fuel ***2007***, *86*, 2201-2203.

[90] Schofield, K. *Fuel-mercury combustion emissions: An important heterogeneous mechanism and an overall review of its implications*. Environmental Science Technology ***2008***, *42*, 9014-9030.

[91] Presto, A.A.; Granite, E.J. *Noble Metal Catalysts for mercury oxidation in utility flue gas*. Platinum Metals Review ***2008***, *52*, 144-154.

[92] Koutsopoulos, S.; Johannessen, T.; Eriksen, K.M.; Fehrmann, R. *Titania-supported Pt and Pt-Pd nanoparticle catalysts for the oxidation of sulfur dioxide*. Journal of Catalysis ***2006***, *238*, 206-213.

[93] Richardson, C. Evaluation of MerCAP for power plant mercury control – *Final project report for US Department of Energy - NETL*, DE-FC26-03NT41993, USA, ***2009***.

[94] Tao, F.M. *A new approach to the efficient basis set for accurate molecular calculations: Applications to diatomic molecules*. Journal of Chemical Physics ***1994***, *100*, 3645-3650

[95] Blythe, M.G.; Braman, C.; Dombrowski, K.; Machalek, T. *Pilot testing of mercury oxidation catalysts for upstream of wet FGD systems – Final Technical Report*. Cooperative Agreement No: DE-FC26-04NT41992, USA, ***2010***.

[96] Blythe, G.; Dombrowski, K.; Machalek, T.; Richardson, C.; Richardson, M. *Pilot testing of mercury oxidation catalysts for upstream of wet FGD systems*. *Final Report*. USA, ***2006.***

[97] Blythe, M.G.; Paradis, J. *Full-scale testing of a mercury oxidation catalyst upstream of a wet FGD system, Final Technical Report*, Cooperative Agreement, No: DE-FC26-06NT42778, USA, ***2010***.

[98] Blythe, G.; Miller, C.; Freeman, B.; Madrid, J. *Full-scale demonstration of oxidation catalyst for enhanced mercury control by wet FGD*. Power Plant Air Pollutant Control "Mega" Symposium, Baltimore, MD, USA, 25-28 August ***2008***.

[99] Delannoy, L.; El Hassan, N.; Musi, A.; Le To, N.N.; Krafft, J-M.; Louis, C. *Preparation of supported gold nanoparticles by a incipient wetness impregnation method*. Journal of Physical Chemistry B ***2006***, *110*, 22471 – 22478.

[100] Tsai, Y-S.; Lin, D-Y.; Fu, T-W.; Lin, D.S. *The activation of supported gold catalysts prepared by impregnation*. Gold Bulletin ***2007***, 40/3.

[101] Haruta, M. *Gold as a novel catalyst in the 21st century: Preparation, working mechanism and applications*. Gold Bulletin ***2004***, *37*, 27 – 36.

[102] Centeno, M.A.; Hidalgo, M.C.; Dominguez, M.I.; Navio, J.A.; Odriozola, J.A. *Titania – supported gold catalysts: Comparision between the photochemical phenol oxidation and gaseous CO oxidation performances*. Catalysis Letters ***2008***, *123*, 198 – 206.

[103] Moreau, F.; Bond, C.G.; Hughes, R.; Moulijn, A.J.; Makkee, M.; Krishna, K.; Silberova, A.A.B. *Preparation of a monolith-supported Au/TiO$_2$ catalyst active for CO oxidation*. Gold Bulletin ***2007***, *40 (4)*, 291 – 294.

[104] Overbury, H.S.; Schwartz, V.; Mullins, R.D.; Yan, W.; Dai, S. *Evaluation of Au size effect: CO oxidation catalyzed by Au/TiO$_2$*. Journal of Catalysis ***2006***, *241*, 56 – 65.

[105] Panayotov, D.A.; Morris, J.R. *Catalytic degradation of a chemical warfare agent simulant: Reaction Mechanisms on TiO$_2$-supported Au nanoparticles*. Journal of Physical Chemistry C ***2008***, *112*, 7496 – 7502.

[106] Sangheeta, P.; Chang, H.-L.; Chen, W.-Y. *Preferential oxidation of CO in H$_2$ stream on Au/TiO$_2$ catalysts: Effect of preparation method*. Industrial & Engineering Chemistry Research ***2009***, *48*, 5666 – 5670.

[107] Wolf, A.; Schüth, F. *A systematic study of the synthesis conditions for the preparation of highly active gold catalysts*. Applied Catalysis A: General ***2002***, *226*, 1 -13.

[108] Tanielyan, K.S.; Augustine, L.R. *Effect of catalyst pretreatment on the oxidation of carbon monoxide over coprecipitated gold catalysts*. Applied Catalysis A: General ***1992***, *85*, 73 – 87.

[109] Sakurai, H.; Tsubota, S.; Haruta, M. *Hydrogenation of CO_2 over gold supported on metal oxides*. Applied Catalysis A: General ***1993***, *102*, 125 – 136.

[110] Khoudiakov, M.; Gupta, C.M.; Deevi, S. *Au/Fe_2O_3 nanocatalysts for CO oxidation: A comparative study of deposition-precipitation and coprecipitation techniques*. Applied Catalysis A: General ***2005***, *291*, 151 – 161.

[111] Scierè, S.; Minicò, S.; Crisafulli, C.; Satriano, C.; Pistone, A. *Catalytic combustion of volatile organic compounds on gold/cerium oxide catalysts*. Applied Catalysis B: Environmental ***2003***, *40*, 43 – 49.

[112] Bamwenda, G.R.; Tsubota, S.; Nakamura, T.; Haruta, M. *The influence of the preparation methods on the catalytic activity of platinum and gold supported on TiO_2 for CO oxidation*. Catalysis Letters ***1997***, *44*, 83 – 87.

[113] Moroz, L.B.; Pyrjaev, A.P.; Zaikovskii, I.V.; Bukhtiyarov, I.V. *Nanodispersed Au/Al_2O_3 catalysts for low-temperature CO oxidation: Results of research activity at the Boreskov Institute of Catalysis*. Catalysis Today ***2009***, *144*, 292 – 305.

[114] Semyannikov, P.P.; Moroz, L.B.; Trubin, V.S.; Zharkova, I.G.; Pyrjaev, A.P.; Smirnov, Y.M.; Bukhtiyarov, I.V. *Chemical vapour infiltration method for deposition of gold nanoparticles on porous alumina supports*. Journal of Structural Chemistry ***2006***, *47 (3),* 458 – 464.

[115] Chen, H.-J.; Lin, N.-J.; Kang, M.-Y.; Yo, Y.-W.; Kuo, N.-C.; Wan, Z.-B. *Preparation of nano-gold in zeolites for CO oxidation: Effects of structure and number of ion exchange sites of zeolites*. Applied Catalysis A: General ***2005***, *291*, 162 – 169.

[116] Zanella, R.; Delannoy, L.; Louis, C. *Mechanism of deposition of gold precursors onto TiO_2 during the preparation by cationic adsorption and deposition-precipitation with NaOH and ureea*. Applied Catalysis A: General ***2005***, *291*, 62 – 72.

[117] Hugon, A.; El Kolli, N.; Louis, C. *Advances in the preparation of supported gold catalysts: Mechanism of deposition, simplification of the procedures and relevance of the elimination of chlorine*. Journal of Catalysis ***2010***, *274*, 239 – 250.

[118] Shen, W.; Liu, F.; Qiu, J.; Yao, B. *The photoinduced formation of gold nanoparticles in a mesoporous titania gel monolith*. Nanotechnology ***2009***, *20*, 105605.

[119] Bond, C.G.; Louis, C.; Thompson, T.D. *Catalysis by gold*, Catalytic Science Series – Vol. 6, Imperial College Press, London, UK, ***2006***.

[120] Pol, G.V.; Gedanken, A.; Calderon-Moreno, J. *Deposition of gold nanoparticles on silica spheres: A sonochemical approach*. Chemistry of Materials ***2003***, *15*, 1111 – 1118.

[121] Perkas, N.; Zhong, Z.; Grinblat, J.; Gedanken, A. *Deposition of gold particles on mesoporous catalyst supports by sonochemical method, and their catalytic performance for CO oxidation*. Catalysis Letters ***2009***, *120*, 19-24.

[122] Uematsu, T.; Fan, L.; Maruyama, T.; Ichikuni, N.; Shimazu, S. *New application of spray reaction technique to the preparation of supported gold catalysts for environmental catalysis*. Journal of Molecular Catalysis A: Chemical ***2002***, *182 – 183*, 209 – 214.

[123] Fan, L.; Ichikuni, N.; Shimazu, S.; Uematsu, T. *Preparation of Au/TiO_2 catalysts by suspension spray reaction method and their catalytic property for CO oxidation*. Applied Catalysis A: General ***2003***, *246*, 87 – 95.

[124] Wen, L.; Fu, K.-J.; Gu, Y.-P.; Yao, X.-B.; Lin, H.-Z.; Zhou, Z.-J. *Monodispersed gold nanoparticles supported on γ-Al_2O_3 for enhancement of low-temperature catalytic oxidation of CO*. Applied Catalysis B: Environmental ***2008***, *79*, 402 – 409.

[125] Benkó, T.; Beck, A.; Geszti, O.; Katona, R.; Tungler, A.; Frey, K.; Guczi, L.; Schay, Z. *Selective oxidation of glucose versus CO oxidation over supported gold catalysts*. Applied Catalysis A: General ***2010***, *388*, 31 – 36.

[126] Choma, J.; Dziura, A.; Jamiola, D.; Nyga, P.; Jaroniec, M. *Preparation and properties of silica-gold core-shell particles*. Colloids and Surfaces A: Physicochemical Engineering Aspects ***2011***, *373*, 167 -171.

[127] Lee, S.; Fan, C.; Wu, T.; Anderson, L.S. *Agglomeration, support effects, and CO adsorption on Au/TiO_2(110) prepared by ion beam deposition*. Surface Science ***2005***, *578*, 5 – 19.

[128] Mallick, K.; Witcomb, J.M.; Scurrell, S.M. *Supported gold catalysts prepared by in situ reduction technique: preparation, characterization and catalytic activity measurement*s. Applied Catalysis A: General ***2004***, *259*, 163 – 168.

[129] Veith, M.G.; Lupini, R.A.; Pennycook, J.S.; Villa, A.; Prati, L.; Dudney, J.N. *Magnetron sputtering of gold nanoparticles onto WO_3 and activated carbon*. Catalysis Today ***2007***, *122*, 248 – 253.

[130] Zheng, X.,;Veith, M.G.; Redekop, E.; Lo, S.C.; Yablonsky, S.G.; Gleaves, T.J. *Oxygen and CO adsorption on Au/SiO_2 catalysts prepared by magnetron sputtering: The role of oxygen storage*. Industrial & Engineering Chemistry Research ***2010***, *49*, 10428 – 10437.

[131] Sayo, K.; Deki, S.; Hayashi, S. *Novel method for preparation of a nanosized gold catalyst supported on TiO_2*. Journal of Colloid and Interface Science ***1999***, *212 (2)*, 597 – 599.

[132] Haruta, M. *Nanoparticles can open a new world of heterogeneous catalysis*. Journal of Nanoparticle Research ***2003***, *5*, 3 – 4.

[133] Metzger, M.; Braun, H. *In-situ mercury speciacion in flue gas by liquid and solid sorption systems*. Chemosphere ***1987***, *16 (4)*, 821 – 832.

[134] Mayer, J.; Hopf, S.; Van Dijen, F.; Baldini, A. *Measurement of low mercury concentrations in flue gases of combustion plants*. VGB PowerTech ***2014***, *(3)*, 64-68

[135] Hocquel, M. *The Behaviour and Fate of Mercury in Coal-Fired Power plants with Downstream Air Pollution Control Devices*. Fortschritt-Berichte VDI VDI Verlag GmbH, Düsseldorf, Grermany, ***2004***.

[136] Haruta, M.; Kobayashi, T.; Sano, H.; Yamada, N. *Novel gold catalysts for the oxidation of carbon monoxide at a temperature far below 0 °C*. Chemistry Letters ***1987***, 405 – 408.

[137] Oros-Ruiz, S.; Zanella, R; Lopez, R.; Hernandez-Gordillo, A.; Gomez, R. *Photocatalytic hydrogen production by water/methanol decomposition using Au/TiO_2 prepared by deposition-precipitation with ureea*. Journal of Hazardous Materials ***2013***, *263P*, 2 – 10.

[138] Moreau, F.; Bond, C.G. *Influence of the surface area of the support on the activity of gold catalysts for CO oxidation*. Catalysis Today ***2007***, *122*, 215 – 221.

[139] Huang, J.; Dai, W.-L.; Li, H.; Fan, K. *Au/TiO_2 as high efficient catalyst for the selective oxidative cyclization of 1,4-butandiol to γ-butyrolactone*. Journal of Catalysis ***2007***, *252*, 69 – 76.

[140] Chiarello, G.L.; Forni, L.; Selli, E. *Photocatalytic hydrogen production by liquid and gas-phase reforming of CH_3OH over flame-made TiO_2 and Au/TiO_2*. Catalysis Today ***2009***, *144 (1-2)*, 69 – 74.

[141] Ortega Mendez, J.A.; Lopez, R.C.; Melian, P.E.; Diaz, G.O.; Rodriguez, D.J.M.; Hevia, F.D.; Macias, M. *Production of hydrogen by water photo-splitting over commercial and synthesised Au/TiO_2 catalysts*. Applied Catalysis B: Environmental ***2014***, *147*, 439 – 452.

[142] Kreibig, U.; Genzel, L. *Optical absorption of small metallic particles*. Surface Science ***1985***, *156 (2)*, 678 – 700.

[143] Greenwood, R.; Kendall, K. *Selection of suitable dispersants for aqueous suspensions of zirconia and titania powders using acustophoresis*. Journal of the European Ceramic Society ***1999***, *19*, 479 – 488.

[144] Mandzy, N.; Grulke, E.; Druffel, T. *Breakage of TiO_2 agglomerates in electrostatically stabilized aqueous dispersions*. Powder Technology ***2005***, *60*, 121 – 126.

[145] Jiang, J.; Oberdörster, G.; Biswas, P. *Characterization of size, surface charge, and agglomeration state of nanoparticle dispersions for toxicological studies*. Journal of Nanoparticle Research ***2009***, *11*, 77 – 89.

[146] Allouni, E.Z.; Cimpan, R.M.; Hol, J.P.; Skodvin, T.; Gjerdet, R.N. *Agglomeration and sedimentation of TiO_2 nanoparticles in cell culture medium*. Colloids and Surfaces B: Biointerfaces ***2009***, *68*, 83 – 87**.**

[147] Levlin, M.; Ikavalko, E.; Laitinen, T. *Adsorption of mercury on gold and silver surfaces*. Fresenius Journal of Analytical Chemistry ***1999***, *365*, 577 – 586.

[148] Lim, D.H.; Aboud, S.; Wilcox, J. *Investigation of adsorption behavior of mercury on Au(111) from first principles*. Environmental Science & Technology ***2012***, *46 (13),* 7260 – 7266.

[149] Lim, D.H.; Wilcox, J. *Heterogeneous mercury oxidation on Au(111) from first principles*. Environmental Science & Technology ***2013***, *47*, 8515 – 8522.

[150] Eom, Y.; Jeon, H.S.; Ngo, A.T., Kim, J., Lee, G.T. *Heterogeneous mercury reaction on a selective catalytic reduction (SCR) catalyst*. *Catalysis Let*ters ***2008***, *121*, 219-225.

[151] Madsen, K. *Mercury oxidation over selective catalytic reduction (SCR) catalysts*, Thesis Technical University of Denmark (DTU), Denmark, ***2011***.

[152] Svachula, J.; Alemany, L.J.; Ferlazzo, N.; Forzatti, P.; Tronconi, E.; Bregani, F. *Oxidation of SO_2 to SO_3 over honeycomb denoxing catalyst.* Industrial & Engineering Chemistry Research ***1993***, *32*, 826 – 834.

[153] Schwämmle, T.; Heidel, B.; Brechtel, K.; Scheffknecht, G. *Study of the effect of newly developed mercury oxidation catalysts on the DeNOx-activity and SO_2-SO_3-conversion*. Fuel ***2012***, *101*, 179-186.

[154] Glodek, A.; Pacyna, J.M. *Mercury emissions from coal-fired power plants in Poland*. Atmospheric Environment ***2009***, 43, 5568 – 5673.

[155] Goodarzi, F.; Goodarzi, N.N. *Mercury in western Canadian subbituminous coal-a weighted average study to evaluate potential mercury reduction by selective minning*. International Journal of Coal Geology ***2004***, 58, 251 – 259.

Appendices

Appendix 1.1 *Physical properties of mercury element*

Physical property	*Value*	*Unit*
Symbol	Hg	
State	liquid	
Colour	silvery white	
Atomic mass	200.59	amu
Atomic number	80	
Atomic radius	0.151	nm
Ionic radius (M^{2+})	0.112	nm
Electronic configuration	[Xe] $4f^{14}5d^{10}6s^2$	
Crystalline structure	rhombohedral	
Density at 25 °C	13.534	g/cm^3
Water solubility at 25 °C	6×10^{-5}	g/L
Heat of fusion	2.29	kJ/mol
1st ionization energy	1007.1	kJ/mol
Boiling point	357	°C
Melting point	- 38.87	°C
Vapour pressure	2.46×10^{-1}	Pa

* http://www.webelements.com/mercury/

Appendix 1.2 *Mercury contents in various coal types from different countries*

Coal type	*Mercury content*	*References*
Anthracite		
Vietnam	< 0.02 – 0.67 g/Mg	[21]
South Korea	< 0.02 – 0.88 g/Mg	[21]
Poland	0.1 mg/kg	[154]
Bituminous		
Germany	0.16 – 0.2 mg/kg	[135]
Egypt	0.04 – 0.36 g/Mg	[21]
Argentina	0.03 – 0.18 g/Mg	[21]
Sub-bituminous		
Romania	0.07 – 0.46 g/Mg	[21]
Columbia	0.02 – 0.17 g/Mg	[19]
Canada	0.008 – 0.121 mg/kg	[155]
Lignite		
Turkey	0.03 – 0.66 g/Mg	[21]
Poland	0.25 mg/kg	[154]

Appendix 1.3 *Physical properties of gold element*

Physical property	***Value***	***Unit***
Symbol	Au	
State	solid	
Colour	golden yellow	
Atomic mass	196.9665	amu
Atomic number	79	
Atomic radius	0.144	nm
Ionic radius: M^{1+}	0.151	nm
M^{3+}	0.099	nm
Electronic configuration	[Xe] $4f^{14}5d^{10}6s^{1}$	
Crystalline structure	face centred cube (fcc)	
Density at 25 °C	19.32	g/cm^3
Heat of fusion	12.55	kJ/mol
1^{st} ionization energy	890.1	kJ/mol
2^{nd} ionization energy	1890	kJ/mol
Boiling point	2856	°C
Melting point	1064.18	°C

* http://www.webelements.com/gold/

Appendix 4.1 *Images of Au/TiO_2 P25 based suspensions stabilized by addition of NH_4-polyacrylate and poly ethylene glycol (PEG)*

Appendix 5.1 *XRD patterns of 2 wt.-% Au/TiO_2 catalysts calcined and uncalcined*

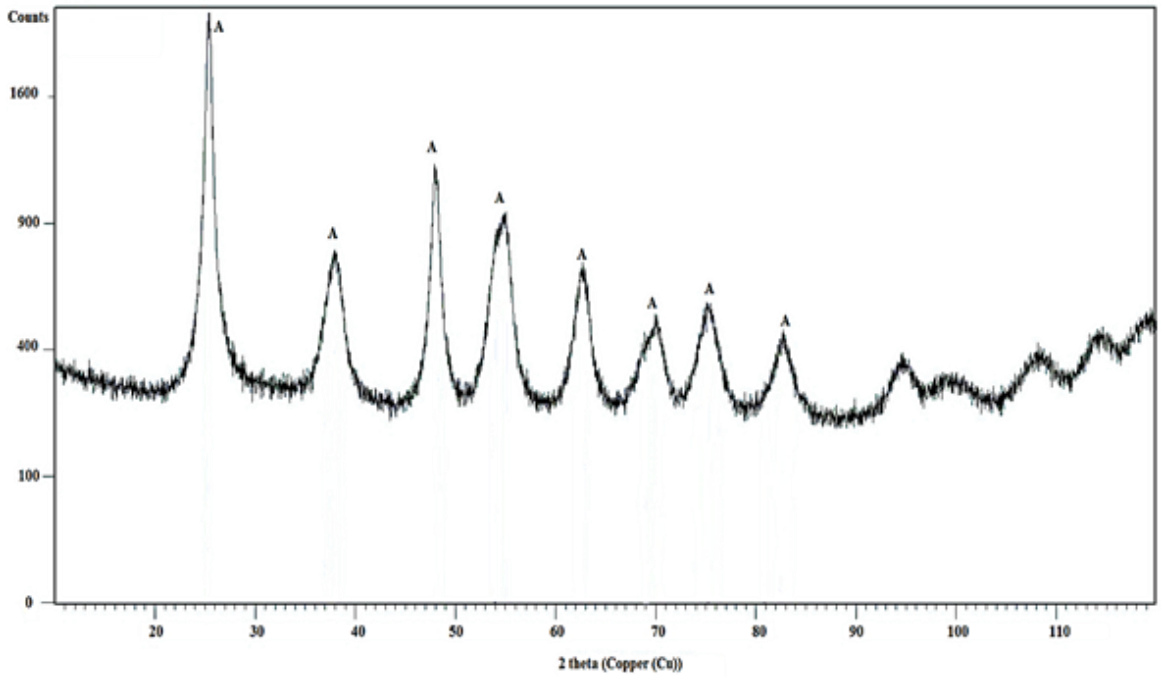

XRD pattern for 2 wt.-% Au/ TiO_2 UV100 uncalcined sample (where: A – anatase)

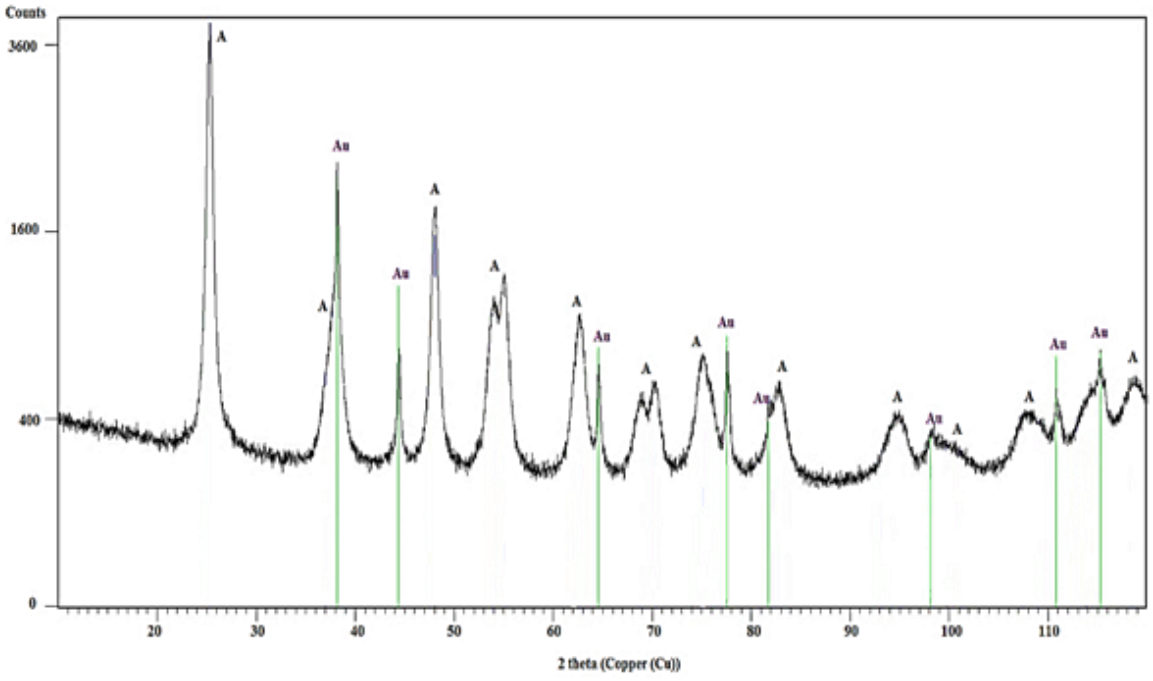

XRD pattern for 2 wt.-% Au/ TiO_2 UV100 calcined sample (where: A – anatase; Au – gold)

Appendix 5.2 *FE-SEM micrographs of TiO_2 UV100 and 2 wt.-% Au/TiO_2 UV100 catalyst powders*

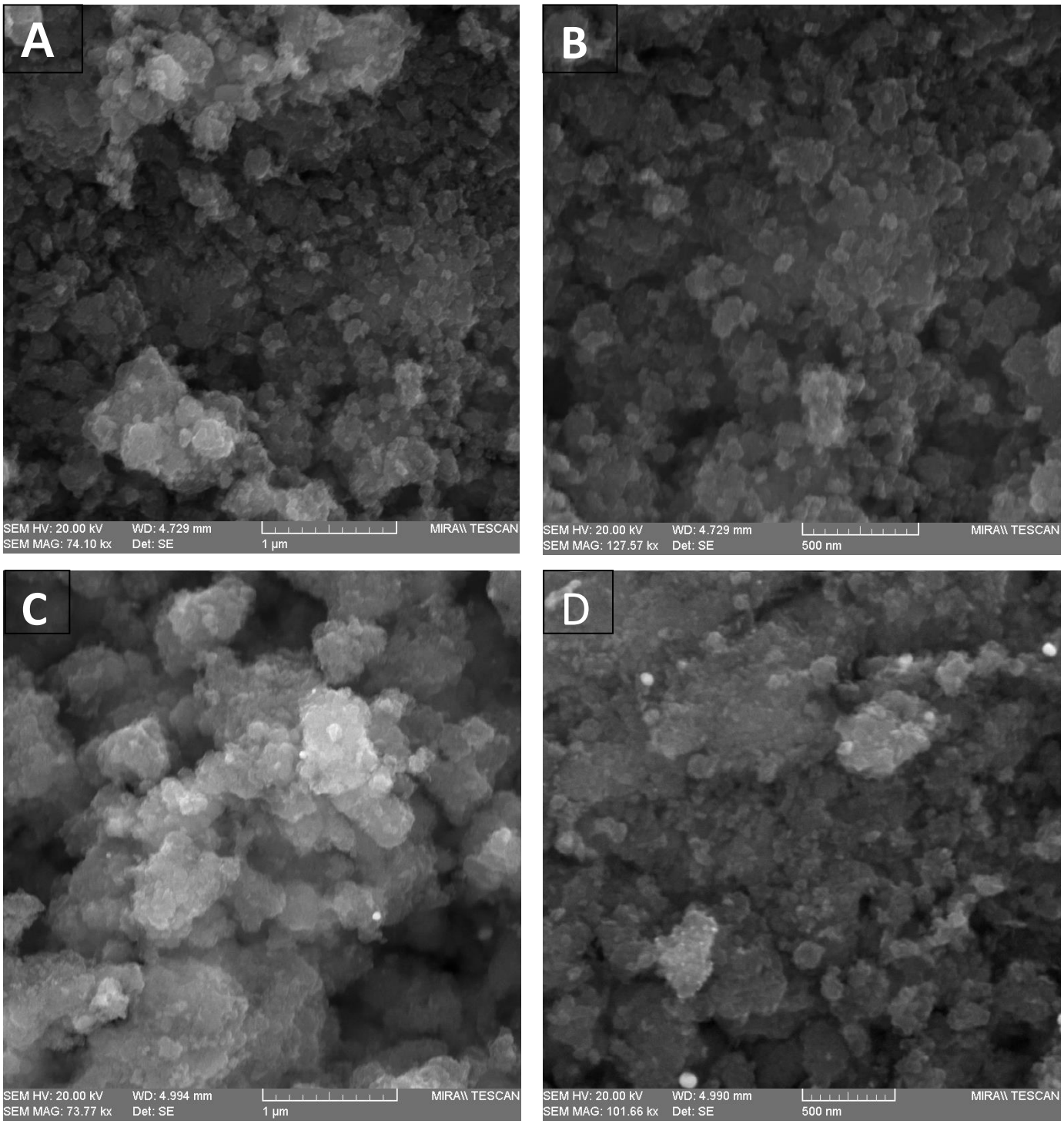

Scanning electron micrographs for: **A** and **B** – TiO_2 Hombikat; **C** and **D** – 2 wt.-% Au/ TiO_2 Hombikat UV100 calcined catalyst

Appendix 5.3 *Zeta potential versus pH for 1 wt.-% Au/TiO_2 based suspensions*

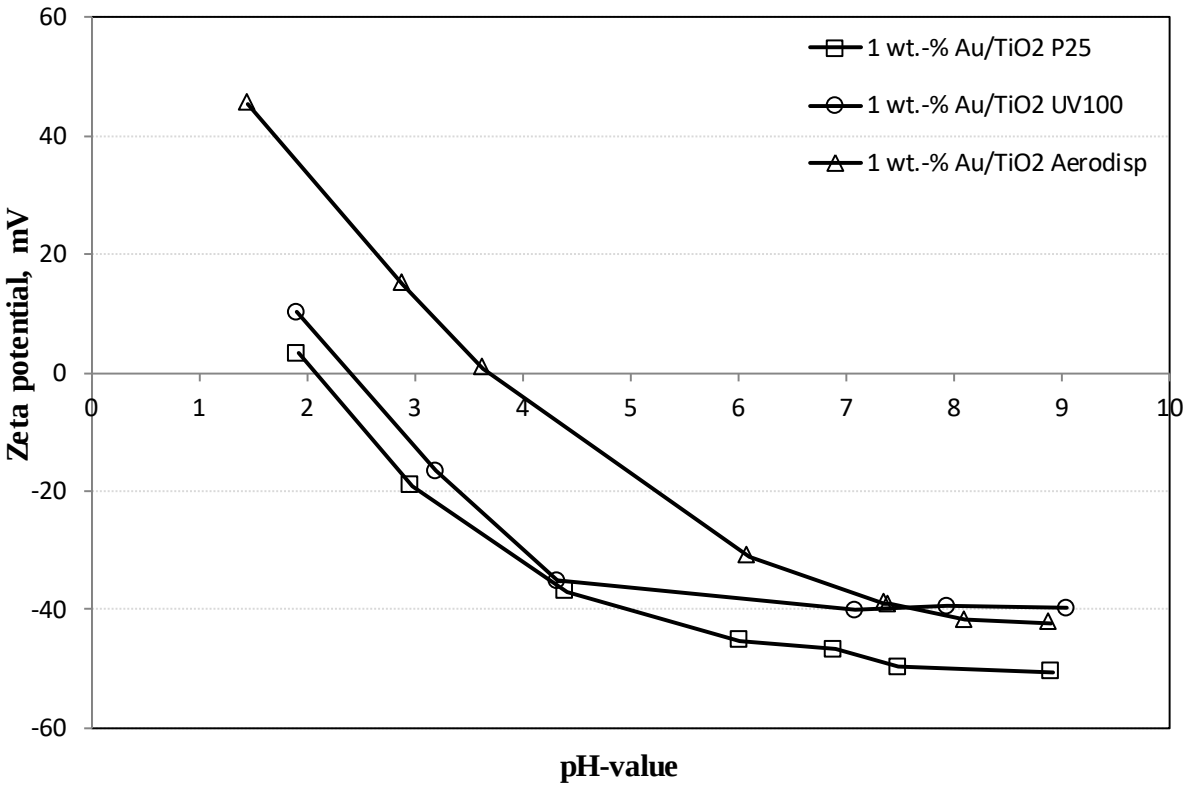

Appendix 5.4 *Example of viscosity measurements for 1 wt.-% Au/TiO_2 P25-based suspension*

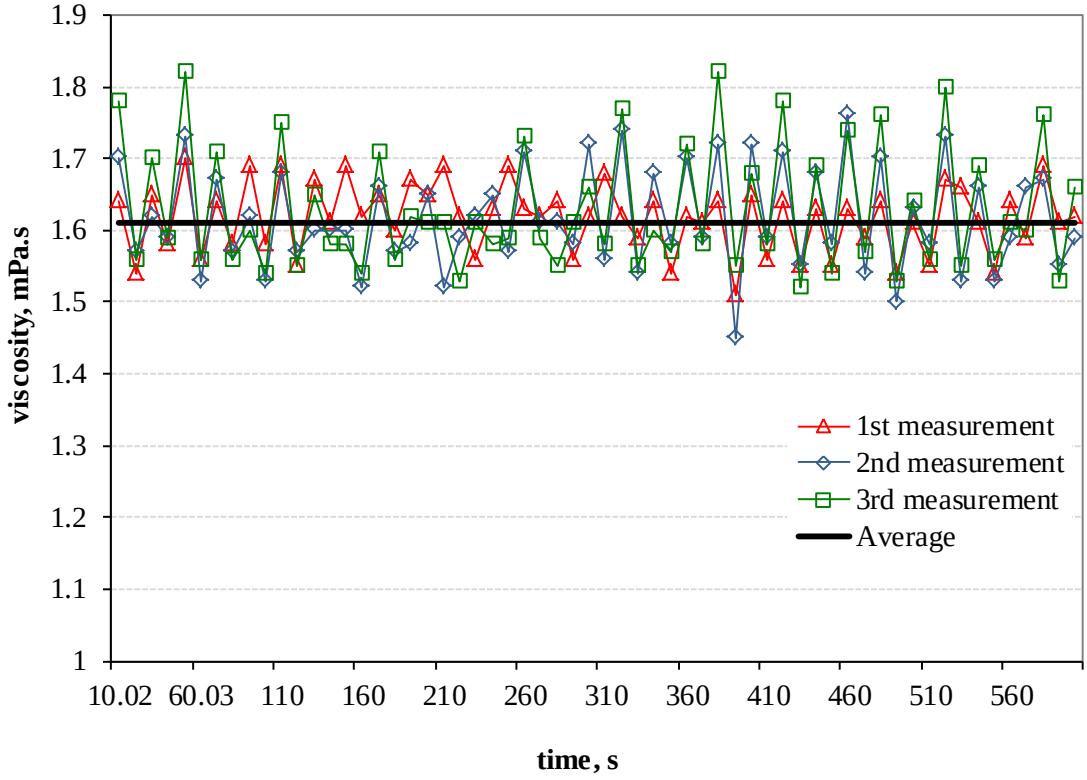

Appendix 5.5 *Particle size distribution by intensity for the Au/TiO_2-based suspensions (measured by Zetamaster S system from Malvern Instruments)*

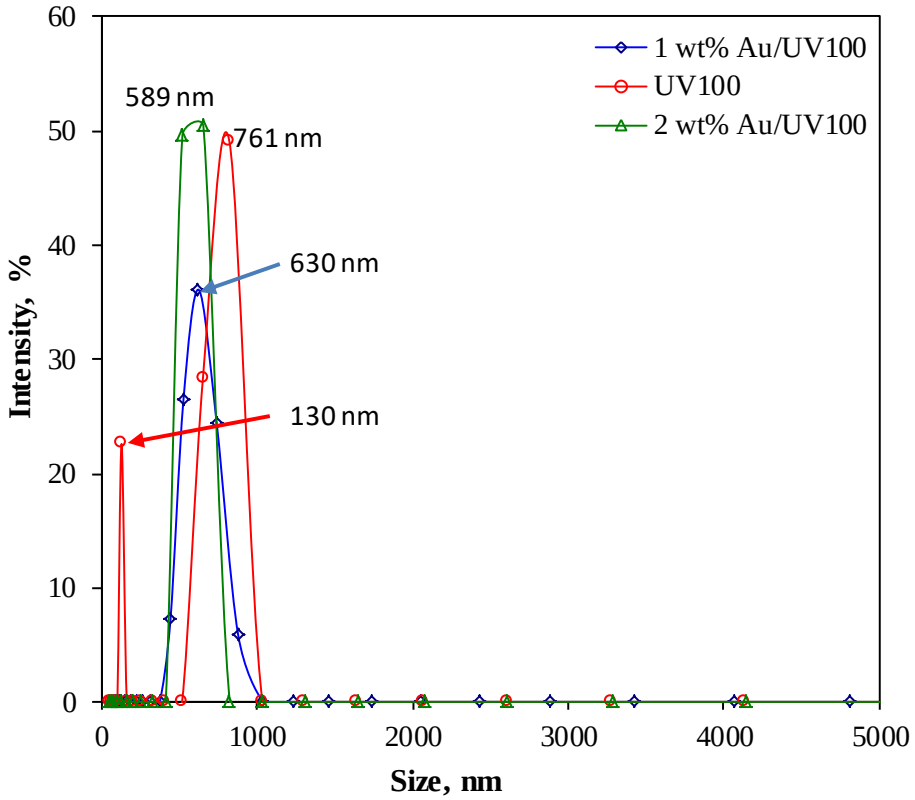

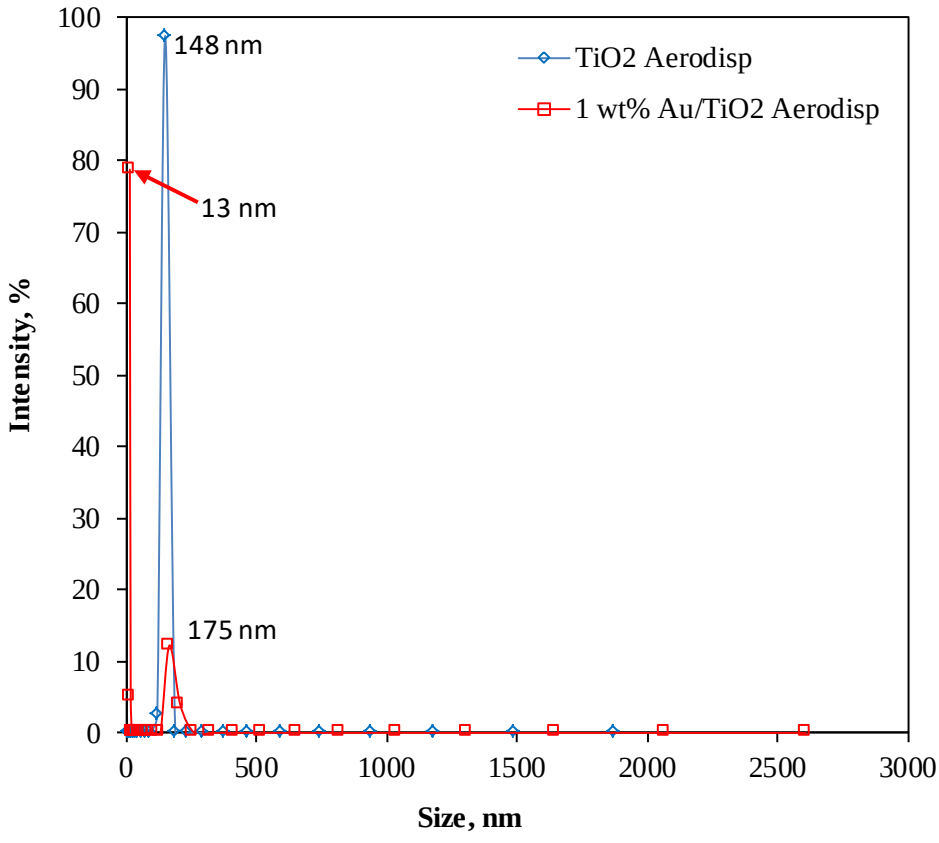

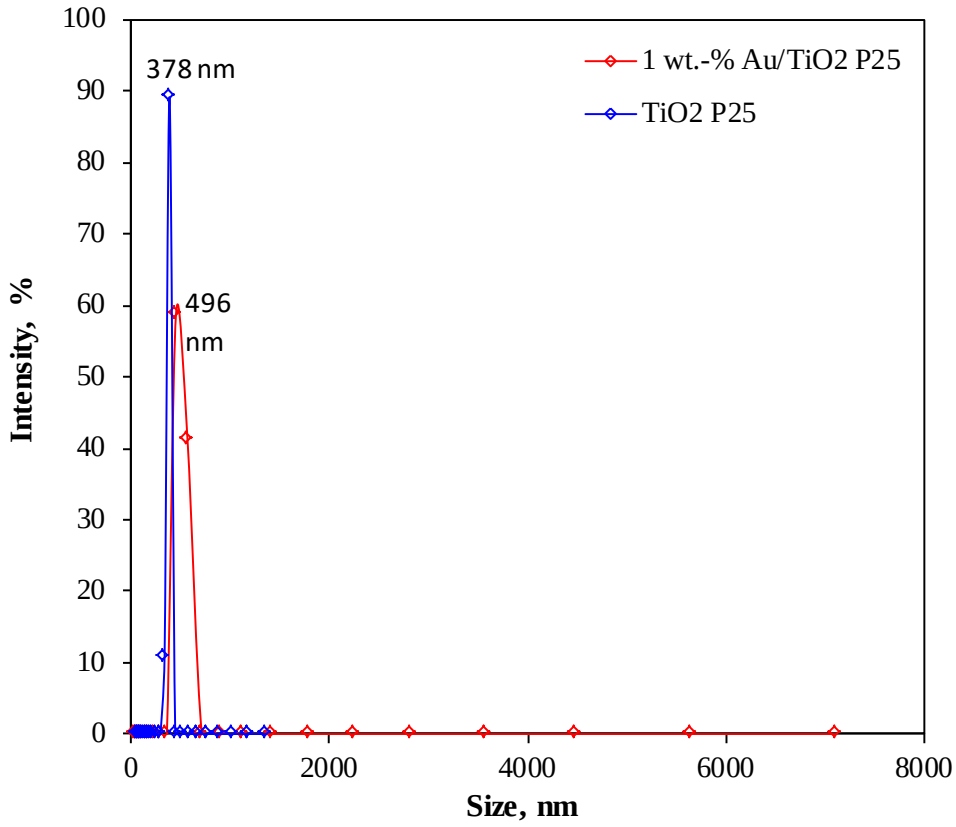
100
90
80
70
60
50
40
30
20
10
0
Intensity, %
0
2000
4000
6000
8000
Size, nm
378 nm
496
nm
1 wt.-% Au/TiO2 P25
TiO2 P25

Appendix 5.6 *Specific geometric surface coverage of SCR-DeNOx substrates with Au/TiO_2 layers in $\mu g\ Au/TiO_2/mm^2$ SCR*

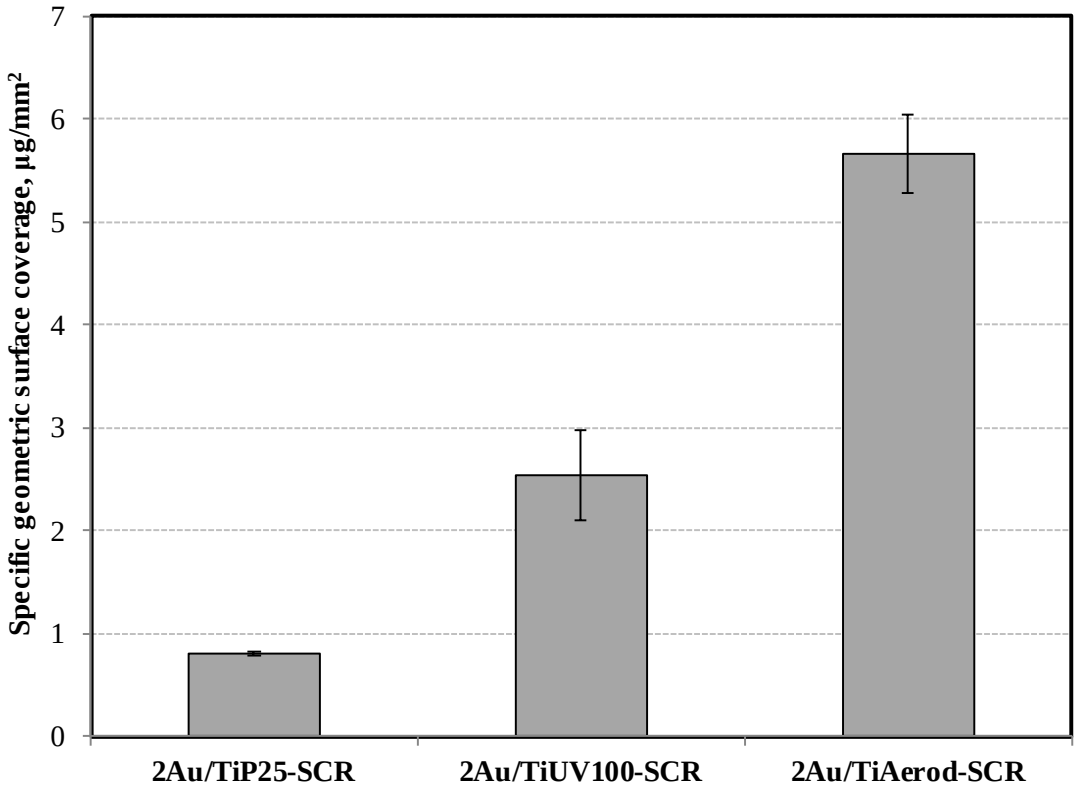

Appendix 5.7 *Elemental composition and distribution at the surface for SCR uncoated catalyst by EDX analysis*

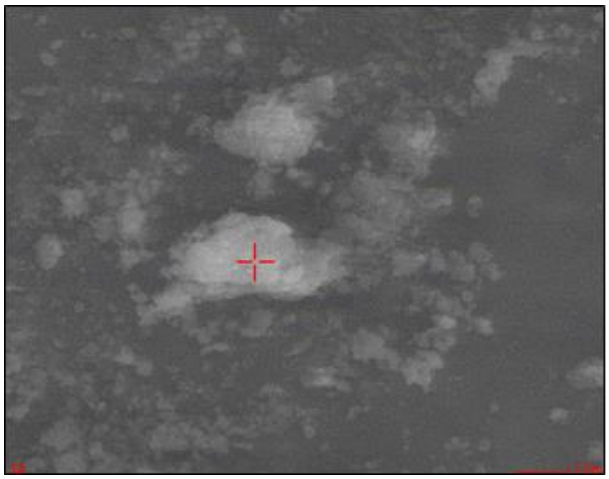

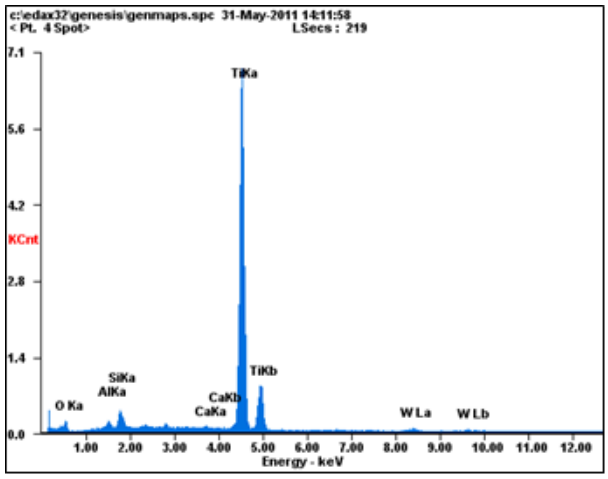

Element	*Wt%*	*At%*
OK	17.65	38.83
AlK	02.22	02.89
SiK	03.40	04.26
CaK	00.35	00.31
TiK	71.93	52.86
WL	04.46	00.85
Matrix	Correction	ZAF

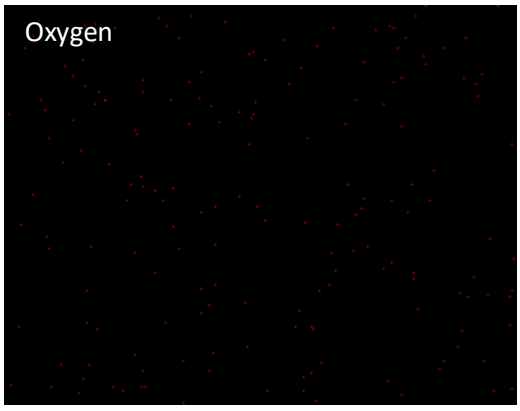

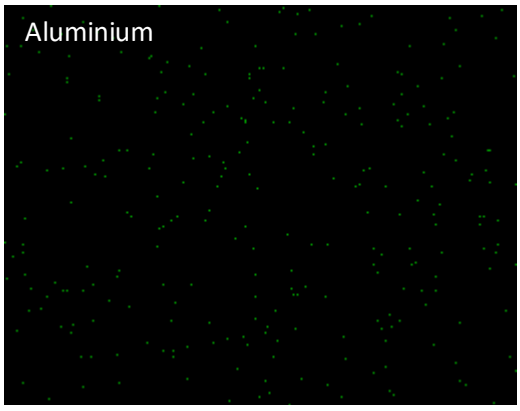

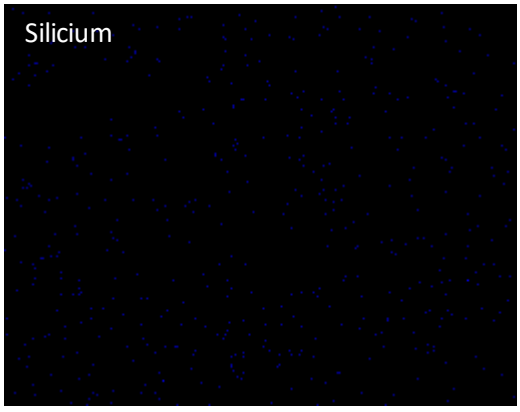

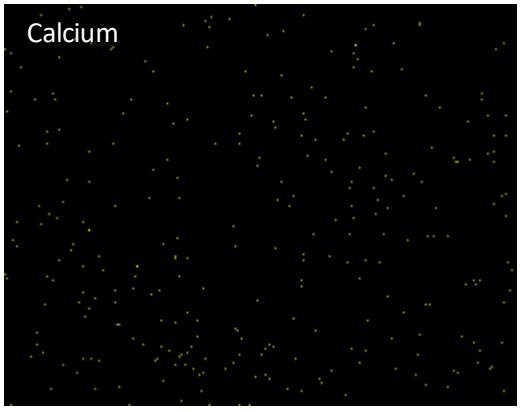

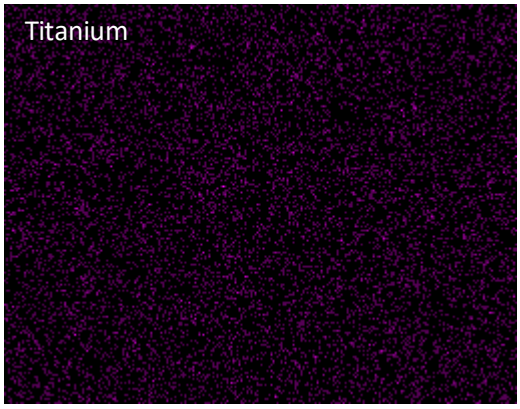
Titanium

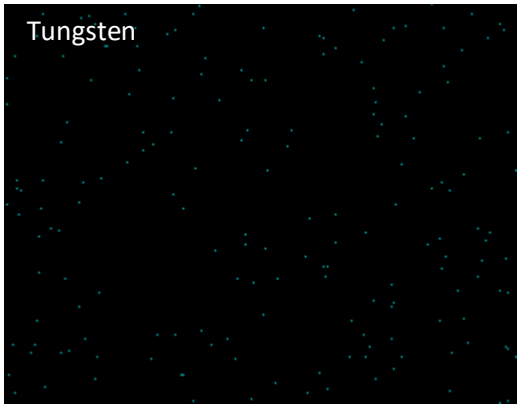
Tungsten

Appendix 5.8 *Elemental composition and distribution at the surface for 1Au/TiAero-SCR catalyst by EDX analysis*

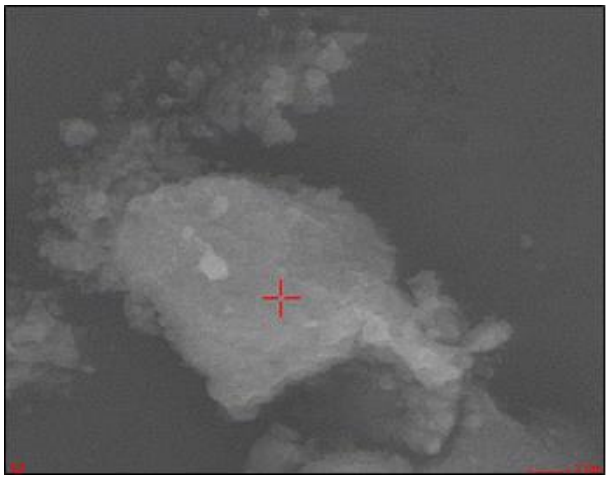

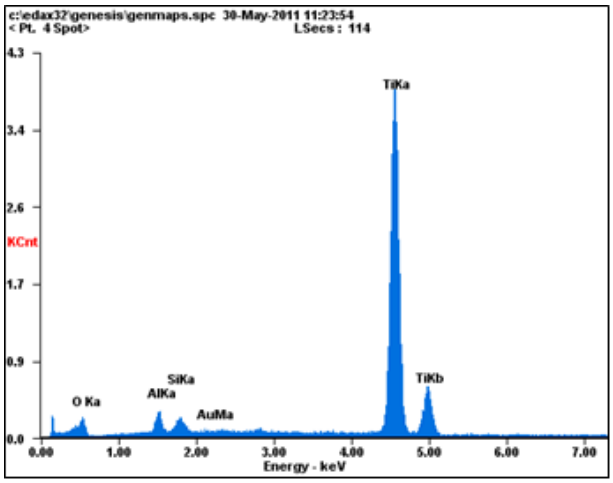

Element	*Wt%*	*At%*
OK	25.80	49.29
AlK	05.26	05.96
SiK	03.04	03.31
AuM	01.29	00.20
TiK	64.61	41.23
Matrix	Correction	ZAF

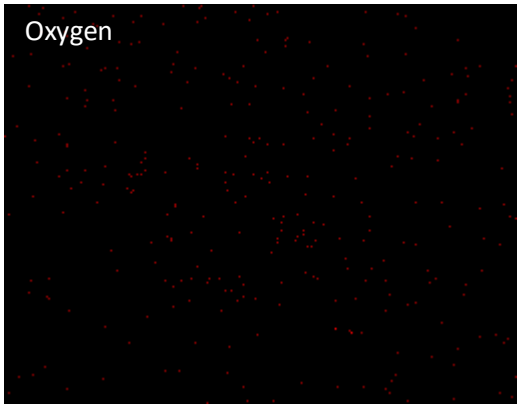

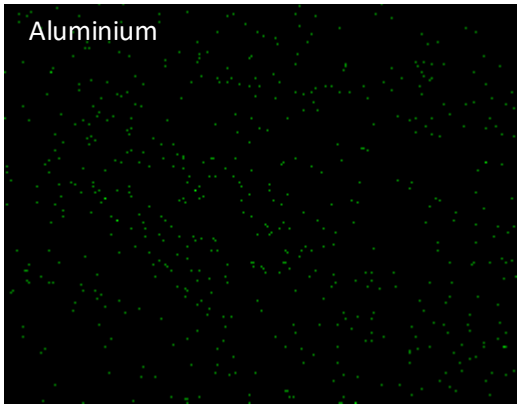

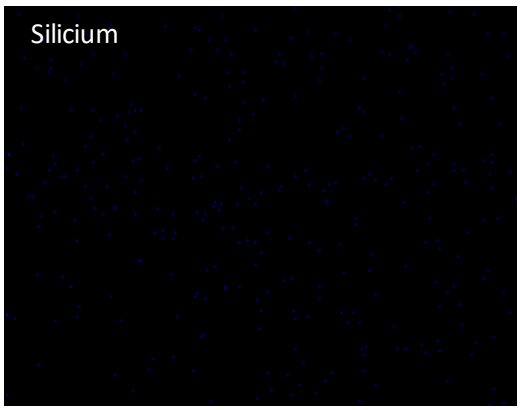

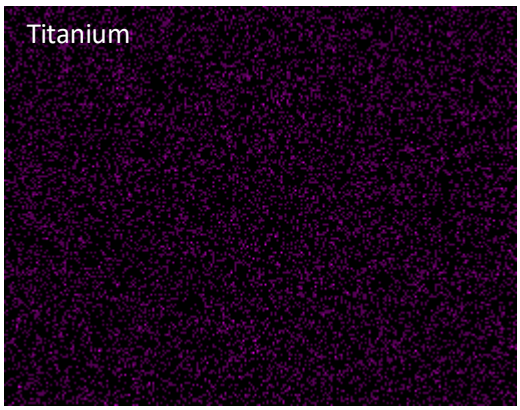

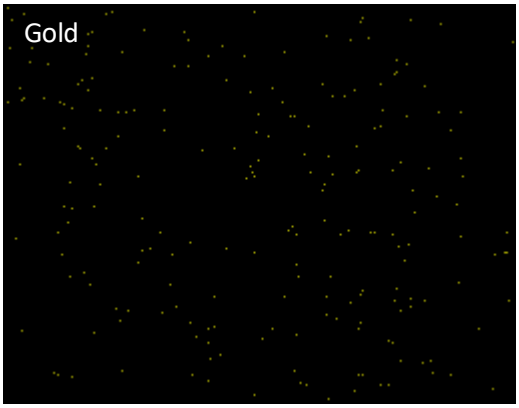
Gold

Appendix 5.9 *Elemental composition and distribution at the surface for 2Au/TiAero-SCR catalyst by EDX analysis*

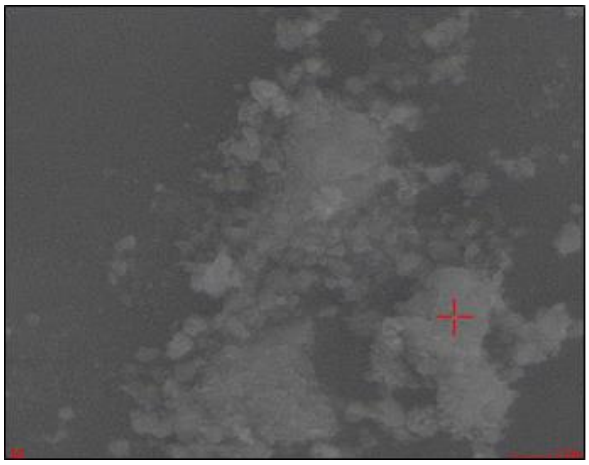

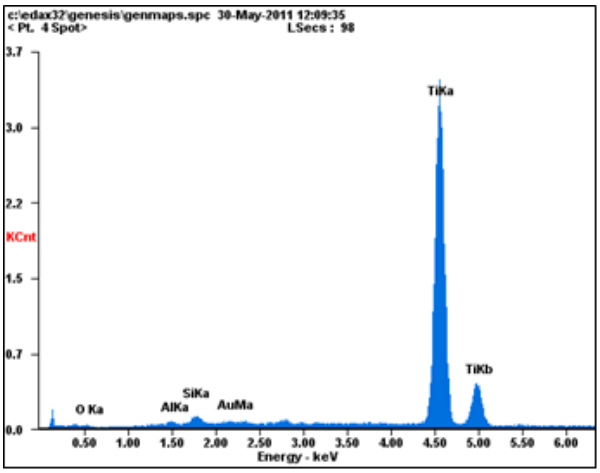

Element	*Wt%*	*At%*
OK	07.41	19.55
SiK	00.54	00.81
AuM	02.17	00.46
TiK	89.88	79.18
Matrix	Correction	ZAF

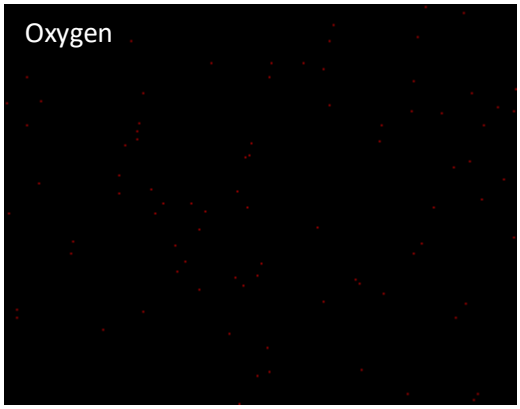

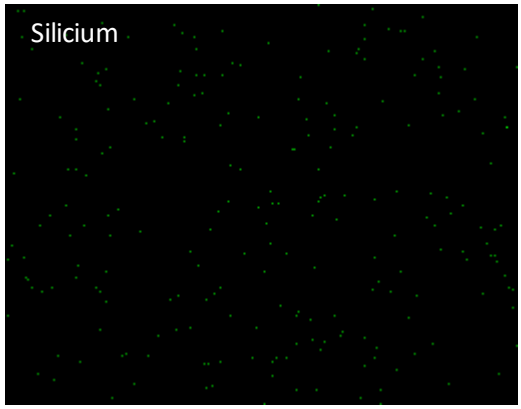

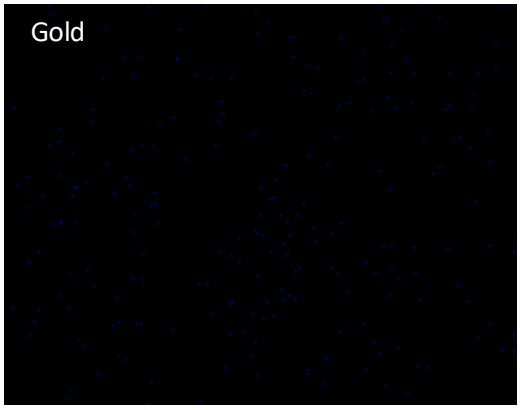

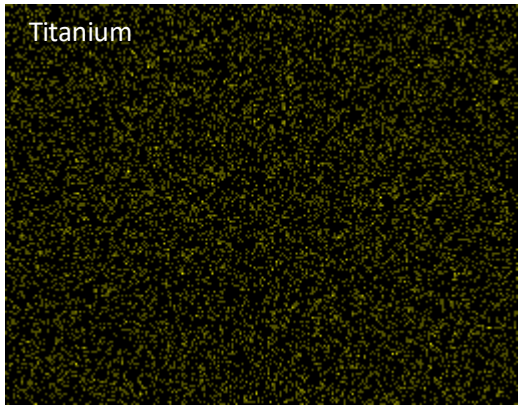

Appendix 6.1 *Likely cost increase of Au-coated SCR catalysts considering only the price of gold*

	Experimental results		
	2Au/TiP25-SCR	2Au/TiUV100-SCR	2Au/TiAerod-SCR
Average geometric surface area of SCR catalyst samples (m^2)	0.0159784	0.01613293	0.01624946
Average mass of Au/TiO_2 coating with 2 wt% Au (mg)	11.49	39.3	85.45
Calculations for a 800 MWel coal fired power plant (1 MWel → 3000 m^3/h flue gas / 1 m^3 SCR catalyst)			
Calculated mass of Au/TiO_2 coating for 376000 m^2 SCR catalyst (kg)*	270.38	915.94	1977.24
Of wich 2 wt% ↓ is Au (kg)	5.407	18.31	39.54
Amount of $HAuCl_4 \cdot 3H_2O$** needed to prepare Au/TiO_2 catalyst powders with 2 wt% Au (kg)	10.83	36.68	79.21
Cost increase considering only the price of $HAuCl_4 \cdot 3H_2O$ *** (€)	877.230	2,971.080	6.416.010
Calculations for a 800 MWel coal fired power plant considering the use of Au/TiO_2-coated SCR catalyst only as a last layer (3rd layer in the SCR-DeNOx reactor)*			
Calculated mass of Au/TiO_2 coating for 125333 m^2 SCR catalyst (kg)	90.13	305.31	659.1
Of wich 2 wt% ↓ is Au (kg)	1.8	6.1	13.18
Amount of $HAuCl_4 \cdot 3H_2O$ needed to prepare Au/TiO_2 catalyst with 2 wt% Au (kg)	3.61	12.23	26.4
Cost increase considering only the price of $HAuCl_4 \cdot 3H_2O$ (€)	292.410	990.360	2,138.670

* 1 m^3 SCR catalyst with 7.1 mm pitch has a geometric surface of ~ 470 m^2/m^3

** $HAuCl_4 \cdot 3H_2O$ of 99.99 % purity contains 49.92 % Au

*** 25 g of $HAuCl_4 \cdot 3H_2O$ salt costs ~ 2025 €

**** due to the DeNOx reaction, mercury oxidation takes place mostly at the outlet of the SCR reactor after NH_3 is consumed. Therefore, Au/TiO_2-coated SCR catalysts with increased mercury oxidation should be used as a last layer in the SCR industrial reactor.

Beatrice-Andreea Dranga (married Esiyok)

PERSONAL DETAILS

E-Mail: beatrice.dranga@iw.uni-halle.de
beatriceandreea@yahoo.com

Nationality: Romanian
TEL: 0312 241 33 43 **Date of birth:** 22.11.1981

EDUCATION

2013- present	**Martin-Luther University Halle-Wittenberg, Germany** **Ph.D student**
2007-2008	**Gheorghe Asachi Technical University of Iasi, Romania** **Master of Science in Clean Process Engineering** Modules included: Fundamentals of Industrial Catalysts Manufacture, Heterogeneous Non-catalytical Processes, Photochemical Processes, and Integrated Environmental Management. **Dissertation: Silica-based porous materials. Synthesis. Characterization. Catalytical applications.**
2002-2007	**Gheorghe Asachi Technical University of Iasi, Romania** **Diploma-engineer in Engineering and Chemistry of Inorganic Substances** Modules included: Inorganic Chemistry, Organic Chemistry, Mathematics, Physical chemistry, Analytical Chemistry, Electrochemistry, Material science, Corrosion Protection in Chemical Industry etc.
1996-2000	**Vasile Adamachi High School, Iasi, Romania**

WORK EXPERIENCE

15.12.2012 – 15.10.2013	**Research assistent at Otto-von-Guericke University, Germany** **Responsabilities**: conducting experimental research, testing of SCR DeNOx catalysts for SO_2/SO_3 conversion, mercury oxidation and DeNOx reaction, testing CaO-based sorbents mercury adsorption capacity.
01.04.2012 – present	**Research stage at Martin-Luther Halle-Wittenberg University**, Zentrum für Ingenieurwissenschaften (ZIW), Germany.

	Responsabilities: conducting experimental research, synthesis of gold-based catalysts, testing of SCR DeNOx catalysts for SO_2/SO_3 conversion, mercury oxidation and DeNOx reaction, doing literature survey.
15.10.2010 – 15.08.2011	**Erasmus Scholarship at Martin-Luther Halle-Wittenberg University**, Zentrum für Ingenieurwissenschaften (ZIW), Germany.
	Responsabilities: conducting experimental research, synthesis of gold-based catalysts, doing literature study, testing of SCR DeNOx catalysts for SO_2/SO_3 conversion, mercury oxidation and DeNOx reaction.
01.02.2010 – 31.08.2010	**Research stage at Martin-Luther Halle-Wittenberg University**, Zentrum für Ingenieurwissenschaften (ZIW), Germany.
	Responsabilities: conducting experimental research, synthesis of gold-based catalysts, testing of SCR DeNOx catalysts for SO_2/SO_3 conversion, mercury oxidation and DeNOx reaction, doing literature study.
01.03.2009 – 31.08.2009	**Erasmus Scholarship at Martin-Luther Halle-Wittenberg University**, Zentrum für Ingenieurwissenschaften (ZIW), Germany.
	Responsabilities: conducting experimental research, synthesis of gold-based catalysts.

RESEARCH INTERESTS

Catalysts synthesis and characterization, gold-based catalysts, catalytical mercury oxidation, reduction of NOx by catalytical means, mercury sorbents.

ADDITIONAL INFORMATION

IT Skills Windows 7, Microsoft Office 2010.

Languages

- Romanian: Mother tongue
- English: Fluent
- Italian: Intermediate
- Spanish: Intermediate
- German: Beginner
- French : Beginner

List of publications

Articles

1. K. Zeng, B.-A. Dranga, J. Krüger, H. Pöllmann, H. Köser. *Trockene Abgasreinigung mit kalkhydrat. Untere Arbeitstemperatur und Hygroskopizität der Halogenidsalze*. (2010), VDI- Berichte Nr. 2110, 225 – 230.
2. Dranga, B.-A.; Lazar, L.; Koeser, H. *Oxidation catalysts for elemental mercury in flue gases – A review*. Catalysts 2012, 2, 139 – 170.
3. Dranga, B.-A.; Koeser, H. *Increased co-oxidation activity for mercury under hot and cold site coal power plant conditions – Preparation and evaluation of Au/TiO_2-coated SCR-DeNOx catalysts*. Applied Catalysis B: Environmental 2015, 166-167, 302 – 312.

Posters

1. Trockene Abgasreinigung mit kalkhydrat. Untere Arbeitstemperatur und Hygroskopizität der Halogenidsalze, K Zeng, **B.-A. Dranga**, J. Krüger, H. Pöllmann, H. Köser, VDI – Fachtagung ″Emissionsminderung 2010″, June 2010, Germany.
2. Nano-Au/TiO_2 suspensions for the preparation of mercury-oxidation catalysts: electro-steric stabilization, particle size and coating efficiency, **Beatrice-Andreea Dranga**, Liliana Lazar, Ion Balasanian, Heinz Koeser, 9th International Symposium of the Romanian Catalysis Society, June 2010, Iasi, Romania.
3. SCR-DeNOx catalysts with increased mercury oxidation activity in flue gases – preparation of Au/nano-TiO_2 coatings, **Beatrice Andreea Dranga**, Katharina Zeng, Heinz Koeser, 44. Jahrestreffen Deutscher Katalytiker und Jahrestreffen Reaktionstechnik, March 16 – 18, 2011, Weimar, Germany.
4. Development of gold-coated SCR-DeNOx catalysts: first results on preparation, characterization and activity towards DeNOx, SO_2/SO_3 conversion and mercury oxidation, **Beatrice Andreea Dranga**, Ioana Fechete, Liliana Lazar, Heinz Koeser, International Symposium of the Romanian Catalysis Society, RomCat 2013, May 29 – 31, Cluj-Napoca, Romania.
5. New vanadium and gold coated SCR-DeNOx catalysts for mercury oxidation in flue gases – first results, K. Zeng, **B.-A. Dranga**, H. Koeser, 7th International Conference on Environmental Catalysis, September 2 – 6, 2012, Lyon, France.
6. Development of Au/TiO_2 coated SCR-DeNOx catalysts with increased mercury oxidation activity, **Beatrice-Andreea Dranga**, Heinz Koeser, ECOSS 30. European Conference on Surface Science, August 31 – September 5, 2014, Antalya, Turkey.

Presentations

1. Indepartarea mercurului din emisiile de la incinerarea deseurilor (Mercury removal from waste incineration emissions), **Beatrice-Andreea Dranga**, Liliana Lazar, Ion Balasanian,Noi frontiere in chimie si inginerie chimica, Editia VI,18 – 20 November, 2009, Iasi, Romania.
2. Hygroskopizität von Erdalkalihalogeniden und untere Arbeitstemperatur von Abreinigungsfiltern in $Ca(OH)_2$ Sorptionverfahren zur Abgasreinigung (Hygroscopicity of alkaline earth halides and lower working temperature of surface filter in $Ca(OH)_2$ sorption processes for cleaning exhaust gas), K. Zeng, **B.-A. Dranga**, J. Krüger, H. Koeser, VGB Chemie im Kraftwerk, October 25 – 27, 2011, München, Germany